2013

Characterization of the mumps virus replicase

Robert Marsden Cox
University of Alabama at Birmingham

CHARACTERIZATION OF THE MUMPS VIRUS REPLICASE COMPLEX

by

Robert Cox

Ming Luo, COMMITTEE CHAIR
Louise Chow
Terje Dokland
Elliot Lefkowitz
Kirill Popov

A DISSERTATION

Submitted to the graduate faculty of The University of Alabama at Birmingham,
in partial fulfillment of the requirements for the degree of
Doctor of Philosophy

BIRMINGHAM, ALABAMA

2013

CHARACTERIZATION OF THE MUMPS VIRUS REPLICASE COMPLEX

Robert Cox

MICROBIOLOGY

ABSTRACT

Negative strand RNA viruses (NSV) are unique because their nucleocapsids are used directly as the template for both transcription and replication. The viral genomic RNA is coated by the nucleoprotein (N) for the entirety of the NSV replication cycle. The viral polymerase, which is composed of the L and P proteins, can only recognize encapsidated RNA as the template for RNA synthesis. Our previous studies have solved the EM structure of the MuV N-RNA complex at 25Å. This structure revealed how the nucleocapsid is assembled and provides an initial model for examining how the viral polymerase may recognize the nucleocapsid as the template for transcription and replication. However, the low resolution of the MuV N-RNA model can only provide a limited amount of information about the MuV nucleocapsid structure. Further experiments are required to address the unique properties of paramyxovirus replication, such as the "rule of six" and post-transcriptional mRNA editing. The structure of the MuV N-RNA ring, along with structural data from several other NSVs, was used to design the experiments in this proposal. The long term goal is to delineate the interactions of the MuV N-P-L-RNA complex. A system was developed to express and purify the N and P proteins of mumps virus. Purified N-RNA complex was further examined using electron microscopy. Systematic studies were conducted to map the different domains of MuV P. Interactions between MuV P and the nucleocapsid were then determined. Additionally, the oligomerization domain of MuV P was defined and its crystal structure

was solved. Next, the three dimensional structure of the authentic MuV NC was solved using cryo-electron microcopy, and the effects of phosphoprotein binding on the MuV NC structure were observed. These studies provided insights into how MuV P associates with NC and what changes are induced by P binding. From these studies, a model of the MuV replicase was created, reflecting the novel features of the mumps N and P proteins discovered in this thesis.

Keywords: mumps, nucleocapsid, phosphoprotein, RNA, virus, replication

ACKNOWLEDGMENTS

I would first like to thank Ming Luo for accepting me into his lab and providing me with the insight and training necessary to become a successful researcher. I am very grateful for all of the great opportunities he has given me, as well as his patience.

I'd like to thank my committee, Louise Chow, Terje Dokland, Elliot Lefkowitz, and Kirill Popov for their support and encouragement.

I would also like to thank everyone in the Luo lab; Shihong Qiu, Jun Tsao, and Michael Rowse. I want to give a special thanks to Todd Green who has always been there to help and advise me on any problem I encountered.

I want to thank my friends and family for all of their support, especially my mother and father.

Finally, I would like to thank my beautiful wife Svetlana Atasheva, whose love and kindness have supported me throughout my graduate career. I am very grateful for all of the things you have done.

TABLE OF CONTENTS

Page

LIST OF TABLES

Tables *Page*

LIST OF FIGURES

Figure *Page*

INTRODUCTION

CHARACTERIZATION OF A MUMPS VIRUS NUCLEOCAPSIDLIKE PARTICLE

STRUCTURAL AND FUNCTIONAL CHARACTERIZATION OF THE MUMPS VIRUS PHOSPHOPROTEIN

STRUCTURAL STUDIES ON THE AUTHENTIC MUMPS VIRUS NUCLEOCAPSID SHOWING UNCOILING BY THE PHOSPHOPROTEIN

LIST OF ABBREVIATIONS

Abbreviations

CTD – C-terminal domain

IHRSR – iterative helical real space refinement NTD – N-terminal domain

MeV – measles virus

MuV – mumps virus

N – nucleocapsid protein

N-arm – N-terminal extension of the VSV N protein

NBD – nucleocapsid binding domain

NC – viral genome encapsidated by N protein subunits

N_{CTD} –C-terminal domain of the nucleocapsid protein

N_{NTD} –N-terminal domain of the nucleocapsid protein

NLP – N protein complex composed of a ring of N subunits encapsidating RNA

NLP_{379} – trypsinized MuV NLP lacking 170 residues from the C-terminus

N^0 – monomeric and RNA –free nucleocapsid protein

N^0-P – complex of phosphoprotein and monomeric and RNA-free nucleocapsid protein

NP – nucleocapsid protein

NSV – non-segmented negative strand RNA virus

NSRV - non-segmented negative strand RNA virus

N-tail – flexible C-terminus of the nucleocapsid protein of paramyxoviruses

N379 – trypsinized MuV NLP lacking 170 residues from the C-terminus

P - phosphoprotein

P_{OD} –oligomerization domain of the phosphoprotein

P_{N^0D} –N^0 chaperoning domain of the phosphoprotein

P_{NTD} –N-terminal domain of the phosphoprotein

P_{CTD} –C-terminal domain of the phosphoprotein

PIV5 – parainfluenza virus type 5

RSV – repiratory syncytial virus

RABV – rabies virus

SeV – Sendai virus

SPR – surface plasmon resonance

vRdRp – viral RNA dependent RNA polymerase

VSV – vesicular stomatitis virus

INTRODUCTION

Non-segmented negative strand RNA viruses (NSV) are grouped into four families within the order *Mononegavirales*; *Bornaviridae*, *Filoviridae*, *Rhabdoviridae*, *and Paramyxoviridae*. NSV include a wide variety of highly significant human and animal pathogens. Members of *Mononegavirales* share many common features, including the arrangement of genes and mode of gene expression. While the number of genes differs between different members of NSV, they share a similar overall scheme for transcription and genome replication.

The *Paramyxoviridae* family includes measles virus (MeV), respiratory syncytial virus (RSV), parainfluenza viruses (PIV), Sendai virus (SeV), and mumps virus (MuV). Other newly emerging paramyxoviruses include Hendra virus, metapneumovirus, and Nipah virus. In developed countries, vaccines have proven effective in providing protection from some paramyxovirus infections, such as measles and mumps. However, outbreaks still occur, even among vaccinated individuals. Unfortunately, no vaccines exist for other paramyxoviruses, such as RSV. Additionally, there are currently no effective antiviral drugs available to treat paramyxovirus infections. The development of new and effective means of controlling these pathogens is critical for treating infections and preventing future outbreaks. Studies on the mechanisms of paramyxovirus replication will provide crucial insights into the synthesis of RNA by the viral polymerase. Knowledge of these mechanisms could provide valuable information necessary for the development of new vaccines or antiviral drugs. The

experiments outlined in this dissertation are aimed at determining the interactions between the MuV nucleocapsid protein (N) and phosphoprotein (P) in order to gain a better understanding of the mechanisms involved in viral RNA synthesis.

CLINICAL DISEASE

MuV was first isolated in 1934 (1). It is a highly contagious pathogen. In humans, MuV causes highly inflammatory, systemic infections (2). Transmission occurs through saliva and respiratory secretions. MuV initiates infection in the upper respiratory tract, where it can then spread to the parotid glands. Viremia circulates MuV throughout the body to different locations including the testes, ovaries, pancreas, and thyroid. Virus is released in respiratory secretions from asymptomatic patients approximately seven days prior to any clinical symptoms. This makes controlling the spread of MuV extremely difficult. Infection is most often associated with acute, painful swelling of the salivary and parotid glands. However, other symptoms include encephalitis, meningitis, myocarditis, nephritis, orchitis, and pancreatitis. The swelling resulting from mumps orchitis can lead to testicular atrophy and in some cases, sterility. MuV is also highly neurotropic and neurovirulent, capable of causing mild meningitis to severe, and sometimes fatal, encephalitis (3). Infection with MuV was the most common cause of viral meningitis and encephalitis prior to the era of mass immunizations (2). Meningoencephalitis can occur in up to fifty percent of individuals infected with MuV (4).

While the number of MuV infections has decreased due to mass vaccination, outbreaks continue to occur (5). The Jeryl Lynn vaccine is highly efficacious and produces

very few adverse side effects. The rate of aseptic meningitis following vaccination with the Jeryl Lynn strain is only 1 in 1.8 million (5). However, much higher incidents of vaccine-associated meningitis have been observed for other MuV vaccines. The Urabe vaccine was estimated to cause meningitis in one out of every 1,000-11,000 doses (5). The Urabe vaccine has since been recalled due to safety concerns. While genomes of clinical isolates and vaccine strains have been sequenced, the molecular biology behind MuV virulence is not well understood (6). No single change in nucleotide or amino acid sequence is completely responsible for the overall level of virulence or attenuation (7, 8). Additionally, no simple pattern of genomic mutations has been found to delineate whether a strain is attenuated or virulent (6, 9, 10).

MUMPS VIRUS GENOME

MuV is an enveloped NSV belonging to the family *Paramyxoviridae*. Like other paramyxoviruses, the MuV genome consists of a single 15.3 kb strand of negative-sense RNA encapsidated by the viral nucleocapsid (N) protein. The MuV genome encodes eight viral proteins (11). Leader (Le) and trailer (Tr) regions flank the 3'- and 5'-termini of the genome, respectively (Figure 1). These regions play multiple roles in transcription, replication, and assembly of progeny virus. Additionally, a series of consensus sequences are located at the beginning and end of each gene. These sequences are involved in transcription initiation, polyadenylation, and transcription termination of individual genes.

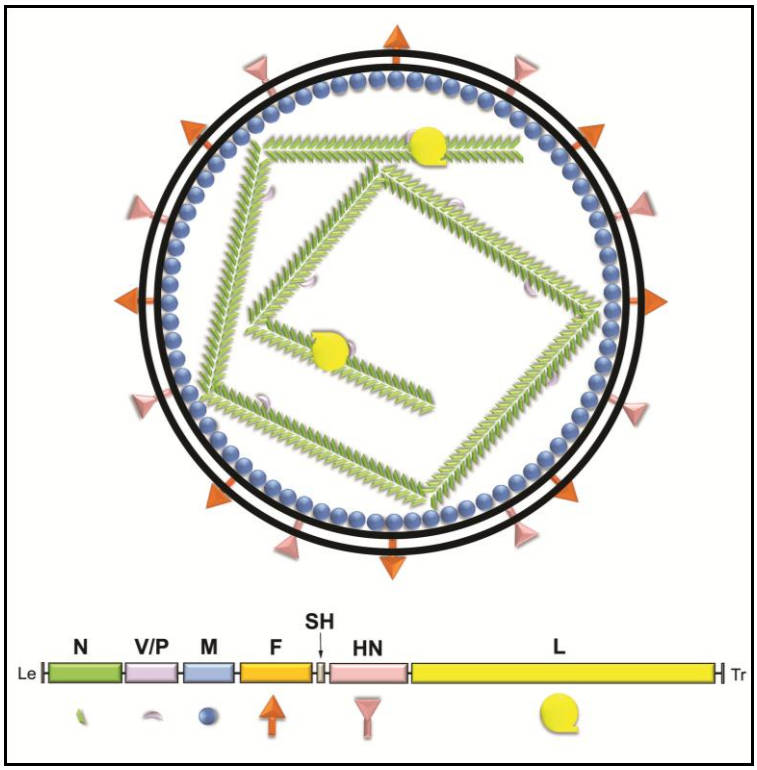

Figure 1: MuV virion and genome. The MuV genome is a single 15.3 kb strand of negative sense RNA. The MuV genome encodes for eight proteins; six structural proteins (N, P, M, F, HN, and L) and two accessory proteins (V and SH). MuV possess a pleiomorphic envelope. The viral membrane is decorated with the HN and F proteins. The M protein coats the interior surface of the viral envelope. Within the virion, the MuV RNA genome is completely encapsidated by the N protein.

POST-TRANSCRIPTIONAL mRNA EDITING

The family *Paramxyoviridae* is divided into two subfamilies: *Paramyxovirinae* and *Pneumovirinae*. Viruses of the *Paramyxovirinae* subfamily are classified into five genera: *Respirovirus*, *Morbillivirus*, *Rubulavirus*, *Avulavirus*, and *Henipavirus*. MuV belongs to the genus *Rubulavirus*. This classification is based in part on the genetic organization and expression of P genes (Figure 2). A unique feature of paramyxoviruses is their ability to post-transcriptionally edit mRNA encoding for the P protein. This unique feature of the paramyxovirus family allows it to stand apart from other NSVs. Post-transcriptional editing

of mRNA does not occur in other NSVs, such as rhabdoviruses. Paramyxovirus P genes contain an mRNA editing site, where pseudotemplated nucleotides are inserted during mRNA synthesis. In SeV, a specific sequence in the P gene is responsible for causing the mRNA transcript to backtrack (Table 1). This allows for three open reading frames downstream to be available for translation, yielding the P, V, and W proteins (Figure 2). This backtracking also occurs in the MuV P gene, and results in the addition of two Gs to

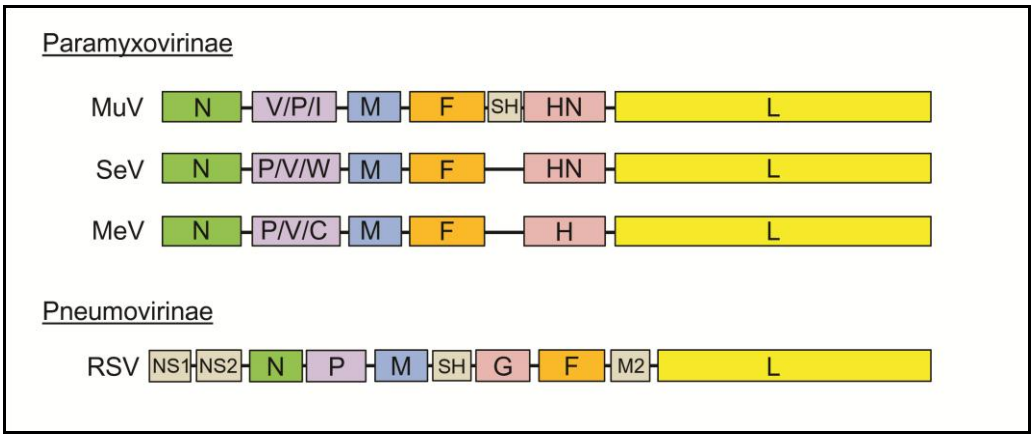

Figure 2: Layout of genes from different paramyxoviruses. MuV, SeV, and MeV all belong to the subfamily *Paramyxovirinae* in the family *Paramyxovirdae*. RSV belongs to the subfamily *Pneumovirinae*.

Species	Genus	P editing signal	Percentage of expression
SeV	*Respirovirus*	3'- GAGUUGUUUUUUC**C** - '5	P = 70%, V = 28%, W = 2%
MuV	*Rubulavirus*	3'- CUUAAAUUCUCCCC - '5	V = 66%, P = 30%, I = 3%

Table 1. Paramyxovirus P gene mRNA editing signals. The various editing signals listed (3′ to 5′; negative sense RNA strand). The SeV P edit site was previously determined and this C is boxed and in bold. The percentage of each P gene product transcribed is shown in the far right column for SeV and MuV. The functions of MuV I are unknown.

the mRNA transcript. Interestingly, this phenomenon does not occur during replication. In contrast to other genera in which the unedited P gene mRNA codes for the P protein, the unedited MuV P gene codes for the V protein. The percentages of SeV and MuV P/V expression are shown in Table 1.

V PROTEIN

Viruses have evolved diverse means to evade innate immune signaling and the antiviral interferon response (12). During infection, paramyxoviruses are subjected to a variety of intracellular antiviral responses, including the interferon (IFN) response. The V protein plays important roles in viral pathogenesis by inhibiting IFN signaling and production. Paramyxovirus V proteins have no cellular homologues. V proteins share their N-terminal domain (NTD) with viral P proteins but contain a distinct, highly conserved C-terminal domain (CTD) that binds two atoms of zinc (13-15). The V protein specifically inhibits IFN-induced antiviral responses through direct inhibition of cellular STAT proteins. The MuV V protein blocks IFN signaling by targeting STAT1 for degradation (16-23). MuV V protein-dependent degradation of STAT proteins involves MuV V, STAT1, STAT2, STAT3, and several other cellular proteins (21).

MATRIX PROTEIN

Similar to other enveloped viruses, paramyxovirus particles are formed by budding from membranes of infected cells. The matrix protein (M) plays a critical role in virus assembly and budding (24, 25). M proteins assembles beneath the host plasma membrane

promotes other viral components to gather at these locations. The paramyxovirus M protein can probably interact with both the cytoplasmic tails of the HN and F glycoproteins (26, 27), as well as the nucleocapsid (28-31), to initiate virus assembly and budding (27).

FUSION PROTEIN

The fusion (F) glycoprotein F is a type I fusion protein (32). The F protein mediates both cell-to-cell and virus-to-cell fusion in a pH-independent manner. For most paramyxoviruses (33-38), interaction of HN with its receptor is essential in order for F to promote membrane fusion during infection

SHORT HYDROPHOBIC PROTEIN

The small hydrophobic (SH) protein is a small hydrophobic integral membrane protein shown to play a role in blocking TNF-alpha mediated apoptosis ((39-42). The SH gene has been identified in all MuV strains. However, SH expression is not required for virus growth *in vitro* (43, 44).

HEMAGGLUTININ-NEURAMINIDASE

The hemagglutinin-neuraminidase (HN) carries out three main functions: receptor binding, fusion activation and virus release (45). HN is essential for activation of the fusion protein. The initial step of viral entry occurs at neutral pH on the host membrane. After attachment, HN activates the viral fusion protein to direct fusion of the viral envelope with the plasma membrane of the cell (45-48).

NUCLEOCAPSID PROTEIN

The nucleocapsid protein (N) encapsidates the viral genome to form the helical nucleocapsid (NC) (Figure 3A). The NC is a highly unique protein-RNA complex, in which the viral RNA (vRNA) is completely encapsidated by the N protein. The NC serves as the sole template for the viral RNA dependent RNA polymerase (vRdRp). In order for the NC to function as a template for RNA synthesis, it must be flexible enough for the vRdRp to gain access the encapsidated RNA. However, the NC must also be sturdy enough to protect the encapsidated genome. The first atomic structures of NSV nucleocapsids were two nucleocapsid-like particles (NLP) belonging to vesicular stomatitis virus (VSV) and rabies

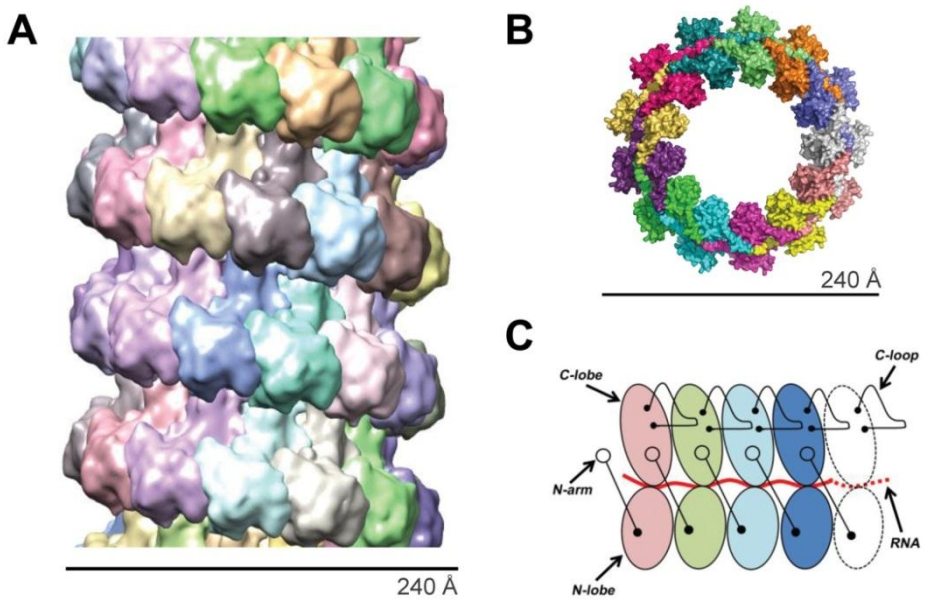

Figure 3. Nucleocapsid protein (N). (**A**) Model of the authentic MuV nucleocapsid. (**B**) Model of a 13 subunit MuV NLP using the crystal structure of the VSV N-RNA complex (49). The MuV NLP consist of 13 N subunits encapsidating 78 bases of RNA (51) (**C**) Schematic diagram of the VSV NLP. Each VSV N subunit is composed of two domains: the N-lobe and the C-lobe. The RNA is encapsidated in a cavity between the two lobes. The N-arm and C-loop connect each N protein to its neighbors (49).

virus (RABV) (49, 50). These NLP consist of a segment of RNA encapsidated by a ring of N protein subunits (Figure 3B). The N proteins assemble side-by-side and parallel to one another along the length of the RNA. Each nucleoprotein subunit can be divided into two distinct regions, the N-terminal lobe and the C-terminal lobe (Figure 3C) (49). Viral RNA is encapsidated inside a large cavity located between the two lobes. In VSV, a N-terminal arm and an extended loop in the C-terminal lobe have been shown to be important for capsid stability (52).

There are several differences between the MuV nucleocapsid and the nucleocapsids of other NSVs. First, the MuV nucleocapsid appears to be relatively flexible compared to the nucleocapsids of other NSVs. Current data also suggests that MuV N is less effective at protecting its encapsidated RNA compared to the other NSVs such as VSV (51). In addition, unlike VSV, the nucleocapsids of paramyxoviruses are capable of forming helical structures in the absence of the matrix protein. Kinks or bends may be present along the length of the nucleocapsid, but the overall helical structure is maintained. The N protein subunits most likely interact with each other through side-by-side and top-and-bottom interactions in order to follow the helical symmetry. The ability of paramyxovirus nucleocapsids to form helical structures may have functional implications, not only for virion assembly, but also for replication (53, 54). Previous mutational studies showed that if the N-terminal arm of the VSV N protein is removed, the ability to retain RNA is lost (52). The N-terminal arm extends to the C-lobe of each neighboring nucleoprotein subunit and positions the two domains of the N protein for proper formation of the RNA binding cavity (Figure 1C). This provides evidence that the N-terminal arm might be capable of exposing the RNA template without affecting the association of the N protein with the encapsidated genome. The L protein or the

L-P complex might be able to induce this conformational change, which would lead to the exposure of the encapsidated genome for RNA synthesis. Upon completion of RNA synthesis, the N-terminal arm could then reposition itself and restore the RNA back into the binding cavity. Translocation of the polymerase along the nucleocapsid during RNA synthesis is thought to involve the repeated attachment and release of the phosphoprotein's nucleocapsid binding domain (55). It has been suggested that P "cartwheels" on the nucleocapsid, by the breaking and reforming contacts between the C-terminus of P, and the nucleocapsid (55). This action may cause the N protein to open, allowing the polymerase access to encapsidated RNA. The RNA template probably temporarily dissociates from the nucleocapsid in order to be read by the viral polymerase.

PHOSPHOPROTEIN

The phosphoprotein (P) is a component of the vRdRp. The P protein is essential for the replication of all NSVs. P performs several roles in the viral cycle. P is required by the L protein for RNA synthesis (56, 57), interacts with the NC template (58-61), and chaperones soluble N protein to the nascent viral RNA during encapsidation (58, 62, 63). The P protein is a modular protein that consists of different functional domains separated by disordered regions (Figure 4) (62, 64-66). Structures for individual domains of several NSV P proteins have been solved (67-72). The structure of a full-length NSV P has yet to be determined.

The N-terminal region of NSV P proteins is responsible for keeping the RNA-free form of N, termed N^0, soluble, as well as chaperoning N^0 to the viral RNA during encapsidation (58, 62, 63). The N-terminal regions for VSV P, RABV P, and SeV P all

contain N^0 binding sites (58, 63, 64, 73). It is logical to suspect that this is also true for the MuV P protein.

All NSV P proteins contain a motif in their central regions known as the oligomerization domain (69, 70). In addition, all NSV P form homo-oligomers, but their

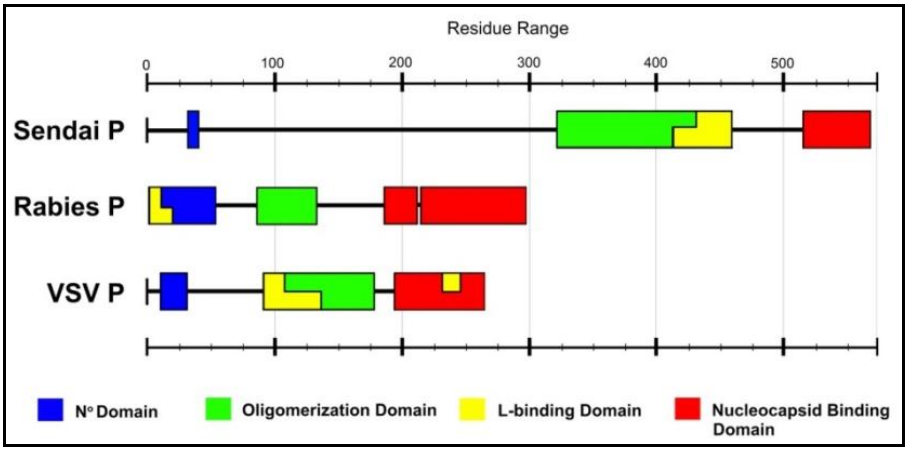

Figure 4. Modular organization of NSV P. Diagram displaying the modular organization of the SeV P, rabies P, and VSV P. P proteins contains four major functional domains; the N^0 chaperoning domain (blue), the oligomerization domain (green), the L binding domain (yellow), and the nucleocapsid binding domain (red).

lengths and oligomerization states vary (74). For example, recombinant, full-length P proteins from VSV and RABV form dimers in solution (75, 76). In contrast, in paramyxoviruses, such as Sendai virus and measles virus, P forms tetramers (62, 71). Additionally, the oligomerization domain of VSV P was shown to be dispensable for transcription and replication (77). However, the oligomerization domain of MeV P and SeV P is required for both transcription and replication (65, 71, 73, 78, 79)

As well as positioning the polymerase on the nucleocapsid template (55), P also interacts with the nucleocapsid itself. A nucleocapsid binding region is located on the C-

terminal end of the MuV P, and its position is well conserved in other NSV (55, 74, 78). Structures of the C-terminal domains of RABV P, VSV P, and MuV P have been solved (72, 80, 81). Recently, the crystal structure of the VSV NLP in complex with the nucleocapsid binding domain (NBD) of VSV P was solved. It revealed that the VSV NLP contains a distinct binding site for P, located between neighboring N subunits (82). In VSV, the P protein binding site on the N protein is formed by residues 352-386 and a portion of the extended loop of the C-lobe (82). The N protein binds P by attaching to it from opposite sides (82). The location of P binding could bring L in close proximity to the encapsidated RNA. Similarly, the MeV P binding site is located on the C-terminus of the N protein (83). However, MuV P has been shown to recognize a sequence in the N-terminal region of N, not the C-terminus (55). Therefore, MuV may utilize a unique mechanism for the attachment of its polymerase to the nucleocapsid compared to other NSVs.

The P protein is phosphorylated at several sites (84). For paramyxoviruses and several NSV, phosphorylated residues are located in a long disordered region on the N-terminus (76, 85-92). Current data suggests that phosphorylation of the P protein plays an important role in viral RNA synthesis. The phosphorylation status of P is thought to be important in regulating the switch from transcription to replication (93). For parainfluenza virus 5 (PIV5), a relative of MuV, the phosphorylation state of P influenced the ability of the polymerase to synthesize viral RNA (84). The transcriptional activity of VSV P is also regulated by phosphorylation (85). In VSV, the phosphorylation sites are located on positions involved in P-N and P-L interactions, which could affect RNA synthesis. Phosphorylation of viral proteins is thought to be carried out by host kinases (84, 87). The role of phosphorylation in MuV replication remains unclear.

LARGE PROTEIN

The large (L) protein is a large multifunctional protein. The L protein contains all of the enzymatic activities necessary for RNA synthesis (67, 94, 95). In addition to RNA synthesis, L is capable of providing a 5' cap structure on viral mRNA and polyadenylation of the 3' end of viral mRNA (95-99). Sequence and phylogenetic analyses have divided NSV L proteins into six different domains connected by variable regions (100-102). However, the roles for all of the different L domains in RNA synthesis are unclear.

In order for efficient transcription and replication, the L protein must be positioned at the mouth of the RNA cavity in order to access the RNA genome. In VSV, the L protein has been shown to interact with two phosphorylation sites on P (82). More importantly, these residues are located next to a solvent-accessible loop above the RNA cavity of the N protein (82). This would allow L to be positioned within 5 nanometers of the encapsidated RNA. Since the RNA is contained within the cavity, the N protein must undergo some conformational changes in order for the L protein to gain access to the genome. The conformational changes that allow the L protein to access the encapsidated genome are still unknown.

VIRAL RNA SYNTHESIS

The life cycle of the virus begins with the binding of the HN protein on the viral membrane to sialic acid on cellular glycolipids or glycoproteins (Figure 5A). The HN protein aids in adsorption of the virus to the host cell. Upon attachment, the F protein promotes fusion of the viral envelope with the plasma membrane in pH independent manner (Figure

5B). Upon entry into the host cell, the virion uncoats and releases the NC along with the viral polymerase into the cytoplasm. Once in the cytoplasm, the vRdRp uses the NC as the

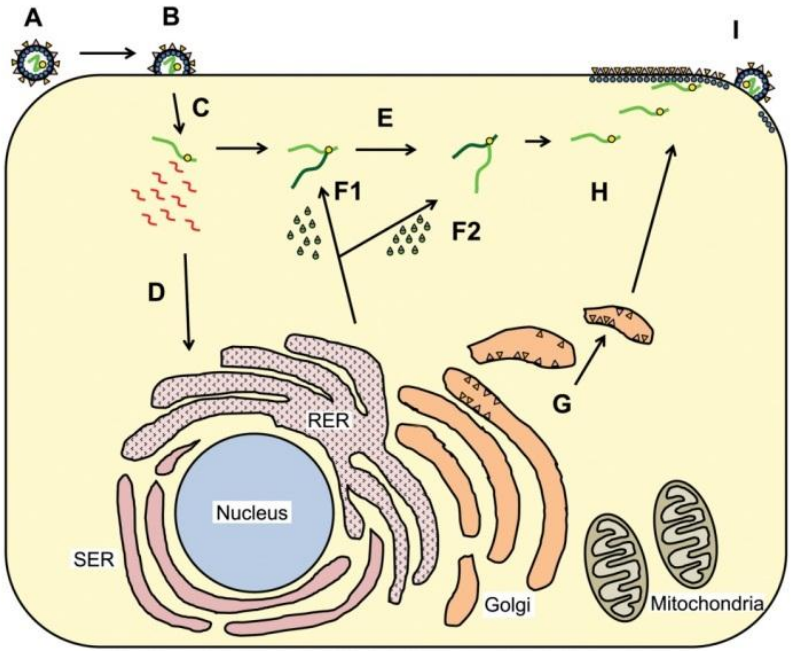

Figure 5: The MuV life cycle. (**A**) The life cycle of the virus begins with the binding of the HN protein on the viral membrane to sialic acid on cellular glycolipids or glycoproteins . The HN protein aids in adsorption of the virus to the host cell. (**B**) Upon attachment, the F protein promotes fusion of the viral envelope with the plasma membrane in pH independent manner. (**C**) Upon entry into the host cell, the virion uncoats and releases the NC along with the viral polymerase into the cytoplasm. (**D**) Once in the cytoplasm, the vRdRp uses the NC as the template for both transcription (**D**), and replication (**E**). Newly synthesized N is chaperoned to replication complexes (**F**) in order to encapsidated newly synthesized antigenomes (**F1**) and genomes (**F2**). After the viral glycoproteins HN and F are processed in the Golgi apparatus (**G**), they are trafficked to the plasma membrane (**H**), along with matrix and newly synthesized genomes. The M protein accumulates on the interior surface of the cell plasma membrane where it plays a role in packaging the NC genomes into mature virions. (**I**) The virus then assembles and is released from the infected cell.

template for both transcription and replication (Figure 5D-E). The vRdRp transcribes the encapsidated genome into 5' capped and 3' polyadenylated mRNAs (95). During transcription, the vRdRp recognizes the 3' end of the nucleocapsid template and begins to

synthesize mRNA. The leader region and the first gene-start sequence provide a promoter element (103-106). The polymerase then caps and methylates the nascent mRNA, and synthesizes the mRNA transcript (107-110). At the end of each gene, the polymerase recognizes a signal to polyadenylate, and after doing so, releases the viral mRNA (Figure 6A) (111-114). Next, the vRdRp either leaves the template, or skips over an intergenic sequence and reinitiates transcription at a downstream start site (115). This continues along the template making progressively less and less of each viral mRNAs (Figure 6B). This mode of transcription is referred to as the "start-stop" model of sequential transcription.

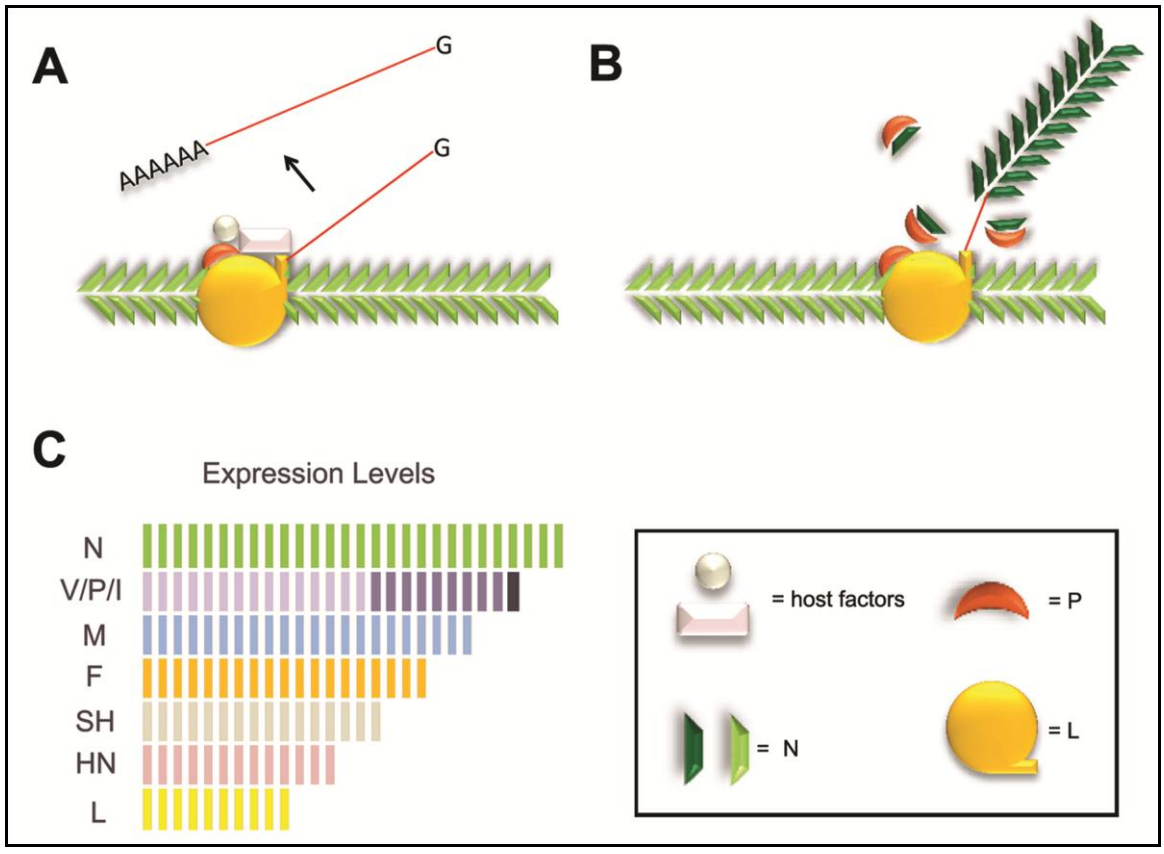

Figure 6. Overview of NSV RNA Synthesis. (**A**) The vRdRp both caps and polyadenylates viral mRNA. The viral transcriptase is composed of the nucleocapsid genome in complex with P, L, and other host factors. (**B**) N-P-L replicase complex. Genome replication requires ongoing N protein synthesis in order to encapsidate newly made antigenomes and genomes. During replication, the vRdRp ignores all cis-acting signals to produce full length genomic RNA. (**C**) Levels of mRNA synthesis due to sequential and polar expression.

The vRdRp also replicates the viral RNA genome (116-119). Despite using the same viral proteins, transcription and replication are distinct processes. Transcription can occur *in vitro*, using only the correct salts and ribonucleotides (120, 121). In contrast, genome replication requires ongoing N protein synthesis. In order to switch from transcription to genome replication, a large amount of N protein must first be translated in order to genomes (Figure 6C). However, while N protein synthesis is required for replication, it might not be the sole determinant between transcription and replication. Additionally, during replication, the vRdRp ignores all cis-acting signals, such as polyadenylation sites, to produce full-length genomic RNA.

REPLICATION AND THE "RULE OF SIX"

Paramyxovirus genome lengths have also been observed to follow a "rule of six" (122). The "rule of six" describes an observation that the genomes of paramyxoviruses can only be read efficiently by the viral polymerase when the length of their genomes is an integer of six (122). Within the virion, the stoichiometry of the helical N-RNA complex is one N protomer for six nucleotides (51). The promoter for replication has been shown to include two specific sequences (122). One sequence is positioned near the 3' end of viral genome and the other is located 13 hexamers downstream. The promoter sequences must be found within a full hexamer block of each other to initiate replication. The 3' promoter can be repositioned downstream as long as the distance between the two sequences is maintained (122). One explanation is that the two sequences may stack on top of each other (Figure 7).

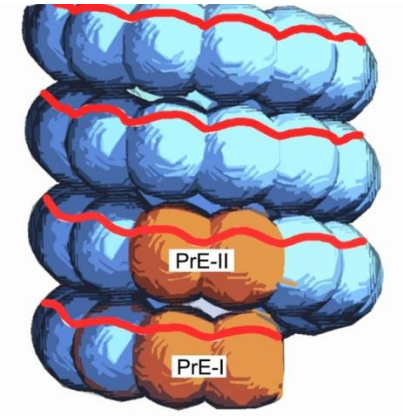

Figure 7: Model of genomic promoters. A cartoon model of of the MuV NC which can allow the two promoter sequences to stack on top of each other. PrE-I is 3' promoter and Pre-II is the second promoter. The positions of PrE-I and PrE-II are shown as the orange N subunits. Encapsidated RNA is depicted in red.

The ability of the two sequences to be located in such close proximity might allow them to form an intitiation site for the viral polymerase. This unique feature adds an extra level of complexity to the nucleocapsids of paramyxoviruses.

Current knowledge about the molecular mechanisms of transcription and replication of paramyxoviruses is incomplete. The NC-P-L replicative complex of MuV possesses several key features that make it an attractive subject for structural characterization. Also, the vRdRp has no known homologue in human or animal tissues, making it an ideal target for antiviral therapies. Structural characterization and the determination of the molecular mechanisms behind the replicative complex of MuV is a critical prerequisite for the discovery and design of new antiviral drugs. The experiments laid out in this dissertation are designed to determine the interactions between components of the MuV replicase complex.

These experiments may offer key insights into the mechanisms behind MuV replication, as well as the replication of other NSVs.

In Chapter I, a system was developed to express and purify the N and P proteins of mumps virus in *Escherichia coli*. Coexpression of the MuV N and P proteins resulted in a soluble complex containing RNA. The P protein was subsequently removed, and the resulting N-RNA complex was examined using electron microscopy. Similar to other NSV, the MuV N-RNA complex appeared as a ring of N subunits encapsidating non-specific RNA.

In Chapter II, systematic studies were conducted to map the different domains of MuV P. By pulldown assays were performed to determine interactions between MuV P and the nucleocapsid. Interactions determined by pulldown assays were further analyzed using surface plasmon resonance. Additionally, the oligomerization domain of MuV P was defined and its crystal structure was solved.

In Chapter III, the three dimensional structure of the authentic MuV NC was solved using cryo-electron microcopy. The effects of phosphoprotein binding on the MuV NC structure were observed. These studies provided insights into how MuV P associates with NC and what changes are induced by P binding. From these studies, a model of the MuV replicase was created, reflecting the novel features of the mumps N and P proteins discovered in this thesis.

CHARACTERIZATION OF A MUMPS VIRUS NUCLEOCAPSIDLIKE PARTICLE

by

ROBERT COX, TODD J. GREEN, SHIHONG QIU, JUNGSOON KANG, JUN TSAO, PETER E. PREVELIGE, BIAO HE AND MING LUO

Journal of Virology Nov. 2013, p. 11402–11406 Vol. 83, No. 21

ABSTRACT

The nucleocapsid protein (NP) of mumps virus (MuV), a paramyxovirus, was coexpressed with the phosphoprotein (P) in *Escherichia coli*. The NP and P proteins form a soluble complex containing RNA. Under a transmission electron microscope, the NP-RNA complex appears as a nucleocapsidlike ring that has a diameter of approximately 20 nm with 13 subunits. There is a piece of single-stranded RNA with a length of 78 nucleotides in the NP-RNA ring. Shorter RNA pieces are also visible. The MuV NP protein may provide weaker protection of the RNA than the NP protein of some other negative-strand RNA viruses, reflecting the degree of NP protein association.

INTRODUCTION

Mumps virus (MuV) is the cause of an acute, but usually non-life-threatening, infection which occurs most frequently in childhood or adolescence. MuV belongs to the family *Paramyxoviridae*, genus *Rubulavirus*. The MuV genome consists of one nonsegmented single-stranded RNA molecule with seven negative-sense genes encoding eight proteins in the following order: the nucleocapsid protein (NP), V protein (V)/phosphoprotein (P), matrix protein (M), fusion protein (F), small hydrophobic protein (SH), hemagglutinin-neuraminidase (HN), and large (L) protein.

The MuV NP protein is 549 amino acids in length and is composed of an N-terminal domain and a reportedly unstructured C-terminal tail (11). The N-terminal domain is suggested to be the part mainly responsible for RNA encapsidation, P protein binding, and formation of the nucleocapsid (10, 11). The primary function of the NP protein of a negative-strand RNA virus (NSRV) is to form the viral nucleocapsid by encapsidating the viral genomic RNA during replication. Crystal structures of nucleocapsidlike NP-RNA complexes have been solved for vesicular stomatitis virus (VSV) and rabies virus (RABV) (1, 7). The crystal structure shows that the NP proteins line up side by side to form a continuous capsidlike structure, with the RNA accommodated in a central tunnel in the capsid. The nonsegmented NSRVs encode their own viral polymerases, a complex composed of the L and P proteins. In order to allow the polymerase to access the RNA template during viral

transcription or replication, the nucleocapsid must undergo some conformational change to expose the RNA. It is expected that MuV NP has some similarity with these previously determined structures; however, differences are expected since the nucleocapsid template of a paramyxovirus follows a strict "rule of six," i.e., the length of the viral genome needs to be an integer of six nucleotides in order to serve as a fully functional template (12).

RESULTS AND DISCUSSION

A single vector was constructed to coexpress the MuV NP and P proteins in Escherichia coli at equal molar ratios by following the approach of Green et al. (6). Soluble N-terminally His-tagged P protein could be copurified with the NP protein by affinity chromatography. When the loaded Ni affinity column was briefly washed with a buffer (20 mM Tris [pH 7.9], 500 mM NaCl, 50 mM imidazole), a portion of the NP protein was found to elute from the column (Fig. 1A, lane 4). However, a significant fraction of the NP protein remained bound in the column. The NP-P complex was found to elute from the Ni affinity column at a concentration of approximately 150 mM imidazole. The fraction eluted by a mild wash was purified by ion-exchange chromatography (HiTrap Q HP; GE Healthcare) (Fig. 1B). Fractions containing the NP protein were further purified by size exclusion chromatography using a Sephacryl S-300 column (GE Healthcare) (Fig. 1E). The NP protein was mostly in fractions corresponding to molecular masses larger than 300,000 Da, suggesting the presence of a complex much larger than the monomeric protein. Recombinant nucleocapsidlike ring structures were previously observed for VSV, RABV, and respiratory syncytial virus (RSV) (1, 2, 6). It is therefore logical to suspect that this fraction of the MuV NP protein is also a nucleocapsidlike ring.

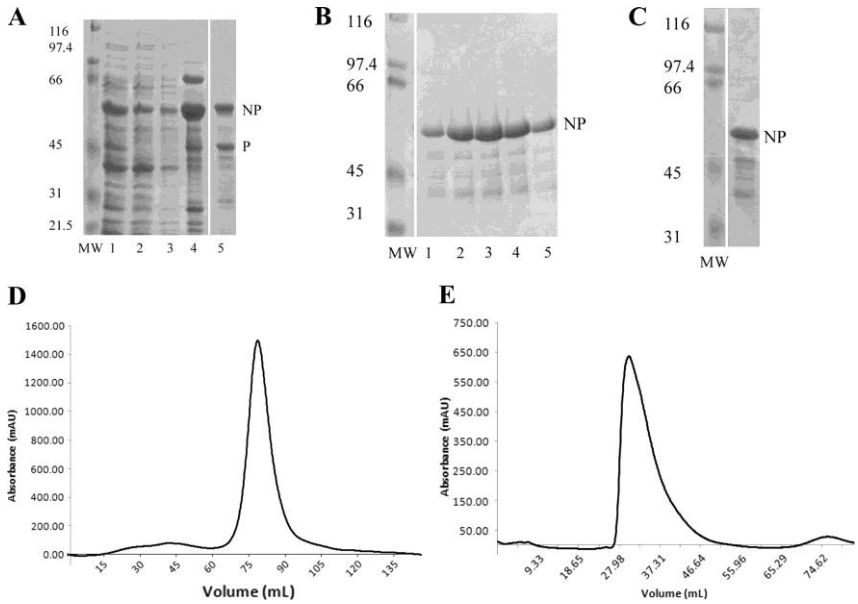

Figure 1. **MuV NLP expression**. MuV NP and P proteins were coexpressed in *E. coli* and purified as described in the text. (A) Lanes 1 to 4 represent total soluble proteins postinduction, in the Ni column flowthrough, in the binding buffer wash, and in the washing buffer wash of the Ni column, respectively. Lane 5 shows a fraction containing the NP-P complex eluted by the linear imidazole gradient from the Ni affinity column. (B) The washing buffer wash contained a large amount of NP protein. It was dialyzed to 200 mM NaCl and further purified on a HiTrap Q HP (GE Healthcare) ion-exchange column. Lanes 1 to 5 contain the MuV NP-RNA complex. (C) Fractions containing the NP-RNA complex from the ion-exchange column were further purified by size exclusion chromatography. Lanes 1 and 2 represent the molecular weight markers (in thousands) and fractions containing the MuV NP-RNA complex, respectively. (D) Profile of MuV NP-RNA eluting from the ion-exchange column. The largest peak represents the NP-RNA complex. (E) Profile of MuV NP-RNA eluting from the size exclusion column. The single large peak represents the NP protein.

The purified MuV NP protein fraction was examined under EM using an FEI Tecnai Spirit electron microscope (EM) at the high-resolution imaging facility at the University of Alabama at Birmingham (Fig. 2). The EM images clearly showed that the majority of the MuV NP protein is in the form of a ring similar to those observed for VSV, RABV, and RSV NP-RNA complexes (6, 9, 15). A collection of isolated ring images were averaged using the program EMAN (14). Since almost all the images were taken down the central axis of the ring structures and no tilt of the grids was applied during imaging, the averaging was carried

out with only two-dimensional images. To build an initial model, 1,173 images were collected and averaged. Among different rotation axes, the 13-fold axis (C13) produced the

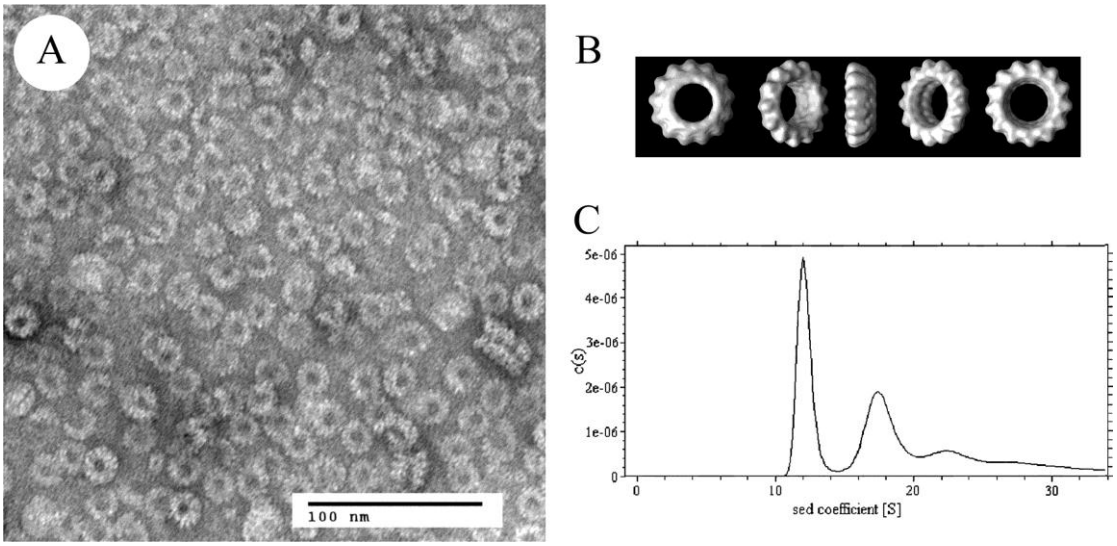

Figure 2. **The MuV NLP.** The number of MuV NP protein subunits per nucleocapsid ring was determined by EM analysis and analytical ultracentrifugation experiments. (A) A typical EM image of negatively stained MuV NP-RNA (50 mM Tris [pH 7.5], 470 mM NaCl). (B) Particles were selected, and a three-dimensional model was generated from 445 views of MuV nucleocapsidlike rings. The average internal and external diameters are 5.6 nm and 20.0 nm, respectively, and the thickness of the ring is 6.7 nm. The number of subunits per nucleocapsidlike ring was determined to be 13. The resolution was determined at a Fourier shell correlation of 0.5 to be 24 Å. The statistics of image reconstruction are as follows: mean = −0.084843; standard deviation = 0.98878; root mean square = 0.99241; contour level = 2.71; subsampling interval = 2 Å. The image was displayed with Chimera (16). (C) The number of molecules per nucleocapsidlike ring was verified by analytical ultracentrifugation. Band profiles suggested a dominant single species, and the sedimentation is consistent with a ring with 13 NP subunits. Sed., sedimentation.

best averaged image. Using this model, a final collection of 445 images was used to generate a three-dimensional model for the MuV NP-RNA ring (Fig. 2B). The outer diameter measured for the averaged ring structure is 20.0 nm, and the inner diameter is 5.6 nm. The thickness of the ring is 6.7 nm. The shape of the ring, with one end narrower than the other, is similar to the shape of rings of other nucleocapsidlike particles. This number of subunits, 13, is consistent with that of the twist in the nucleocapsid of measles virus, another member

of paramyxovirus family; the diameter of the ring and its hollow center are consistent with those of the nucleocapsid of measles virus (3).

To confirm the size determined with the averaged EM image, the sedimentation coefficient (s20,w) was determined to be 32.191 S by ultracentrifugation by using the programs Sednterp and Sedfit (13, 18) (Fig. 2C). The molecular mass calculated from the sedimentation coefficient is 853,000 Da. This molecular mass is within the experimental error when it is compared to the calculated molecular mass of a 13-subunit MuV NP-RNA ring (830,960 Da), assuming that the molecular mass of a MuV NP subunit is 62 kDa and that of six nucleotides per subunit is 1.92 kDa.

Similar structures of other recombinant NSRV NP protein complexes often contain encapsidated RNA. We measured the ratio of the optical density at 260 nm to that at 280 nm for the MuV NP protein complex and found the value to be 1.26, indicating that the MuV NP protein complex has encapsidated RNA. To characterize the encapsidated RNA, materials extracted with Trizol (Invitrogen) from the purified NP protein complex were examined by electrophoresis under denaturing conditions (Fig. 3A, lane 4). The gel clearly showed that RNA is present in the complex. However, the length of RNA is more variable than what has been observed for the VSV, RABV, or RSV NP-RNA complexes (6, 9, 19). Assuming that each NP subunit accommodates six nucleotides, the RNA in a fully occupied 13-subunit ring of the MuV NP-RNA complex should have a length of 78 nucleotides. In fact, a dominant RNA band corresponding to this length was shown in the RNA gel (Fig. 3A, lane 4, band I). Additionally, a large number of RNA pieces smaller than band I were observed (Fig. 3A). The appearance of a dominant band, band II, which was actually part of a population of small RNA pieces, could be an artifact of ethidium bromide or SYBR gold (Invitrogen) staining.

This observation suggests that the RNA piece encapsidated by the MuV NP protein during heterologous expression was not fully protected during purification, which is supported by the observation that the RNA in the MuV N-RNA complex is susceptible to digestion when incubated with RNase A for 1 h at 37°C (Fig. 3A, lane 6).

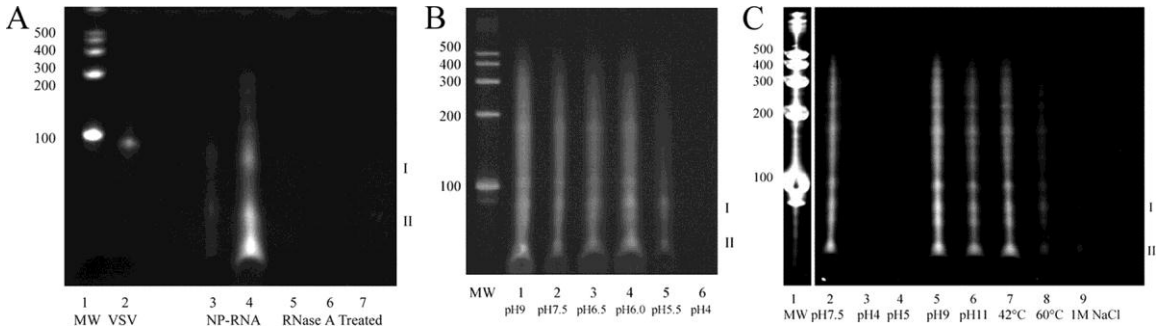

Figure 3. **MuV NLP RNA**. The MuV nucleocapsidlike particles contain RNA. The length of the RNA encapsidated in the MuV NP ring was measured by comparison with the RNA molecular weight marker (Century Marker; Ambion). (A) RNA was extracted from purified VSV NP-RNA complex (lane 2), the MuV NP-RNA complex (lanes 3 and 4), and RNase A-treated MuV NP protein incubated at pH 7.5 (lane 6). The gel was stained with ethidium bromide. Two RNA bands are labeled I and II. (B and C) Purified samples of the MuV NP-RNA complex were incubated for 1 h under different buffer conditions. The samples were then returned to normal buffer conditions (50 mM Tris [pH 7.5], 470 mM NaCl) and allowed to incubate overnight at 8°C. RNA was extracted using Trizol (Invitrogen), and samples were analyzed in a 10% 8 M urea-polyacrylamide gel. Both gels were stained with SYBR gold (Invitrogen). (B) Lanes 1 to 6 correspond to the MuV NP-RNA complex incubated at pH 9, pH 7.5, pH 6.5, pH 6.0, pH 5.5, and pH 4.0, respectively. (C) Lanes 1 to 9 correspond to MW Marker (Century Marker; Ambion) and MuV NP-RNA complex incubated at pH 7.5, pH 4, pH 5, pH 9, pH 11, 42°C, 60°C, and MuV NP-RNA complex in 1 M NaCl (pH 8.3), respectively.

In order to determine the effect of pH, salt, and temperature on the susceptibility of NP-bound RNA, the MuV NP-RNA ring was incubated under a variety of different conditions. The conditions examined included pH 4, pH 4.5, pH 5, pH 5.5, pH 6.0, pH 6.5, pH 7.5, pH 9, pH 11, 1 M NaCl, 2 M NaCl, 42°C, and 60°C. The NP-RNA ring was incubated for 1 h under each condition and then returned to normal buffer conditions (50 mM

Tris [pH 7.5], 470 mM NaCl). The NP-RNA ring was then allowed to incubate overnight at 8°C, and RNA was extracted using Trizol (Fig. 3B and C). It was found that the RNA contained in the MuV NP-RNA complex is highly susceptible to digestion by contaminant nucleases under several of these conditions. After incubation at a pH lower than 5, all RNA pieces were lost. This level of RNA protection is significantly less than that of the VSV NP-RNA ring (6). At a pH above 6, no further loss of RNA was observed, which is similar to findings with the VSV and RABV NP-RNA rings (6, 9). When the MuV NP-RNA ring was subjected to 1 M NaCl, the RNA was also lost, similar to the situation when the nucleocapsid of influenza A virus was treated with high salt concentrations (8). The RNA in the VSV or RABV NP-RNA complex was not affected by high salt concentrations (6, 9). Finally, the RNA was lost when the MuV NP-RNA ring was heated to 60°C for 1 hour. No information on heat treatment of other NSRV NP-RNA rings was available at the time this study was done. The loss of RNA at a pH of less than 5.0 or under high-salt or high-temperature conditions suggested that associations between the MuV NP subunits may be weaker than between the NP subunits of other NSRVs.

EM images were taken of samples that had been subjected to different conditions as described above (Fig. 4). These images (Fig. 4A and B) showed that the loss of RNA from the MuV NP-RNA ring after various treatments was not due to denaturation of the NP protein. The ring structures remained intact after RNA was lost and looked like untreated MuV NP-RNA rings. These ring structures could be considered “empty-capsid”-like structures. One interesting observation is that the MuV empty-capsid-like rings formed rodlike structures after being subjected to pH 4.0 and then reneutralized (Fig. 4C). It seems

that the MuV rings could easily make top-and-bottom interactions as would be present in the superhelical structure of the paramyxovirus nucleocapsid (4, 17).

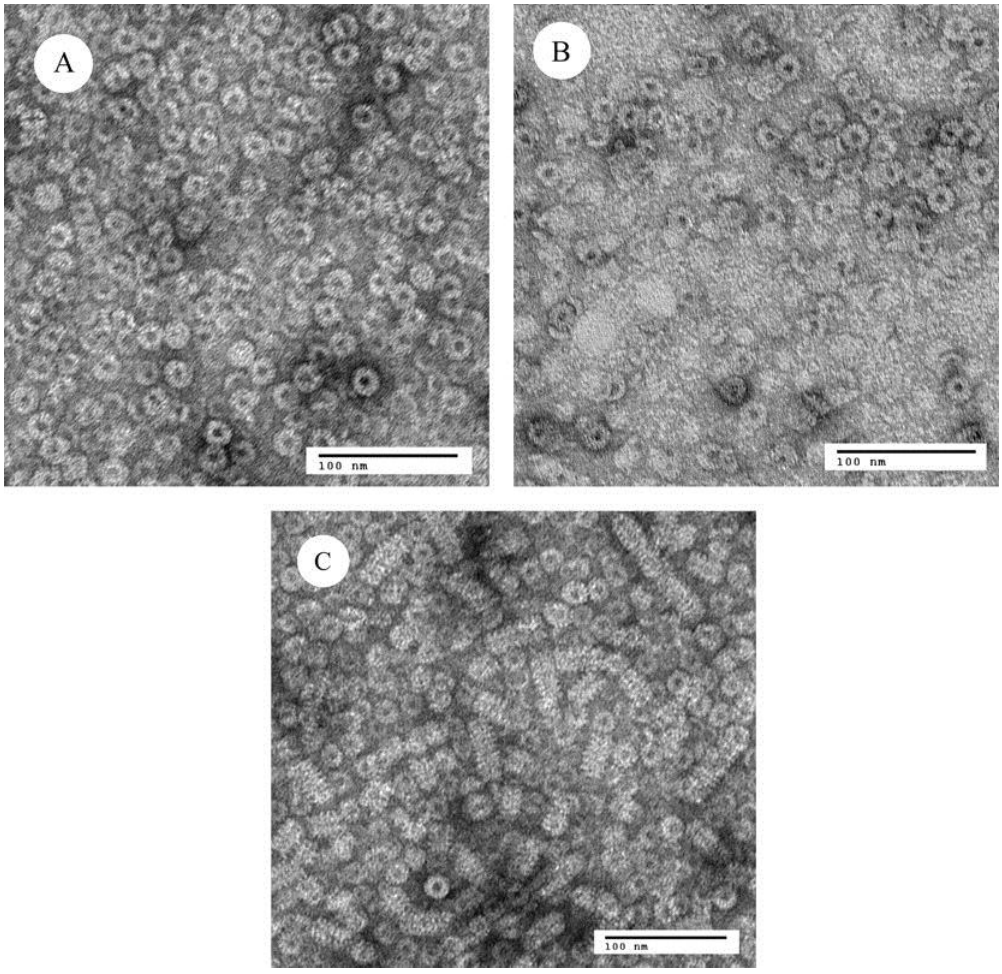

Figure 4. **EM analysis of MuV NLP.** EMs of the MuV NP-RNA complex were negatively stained with 2% uranyl acetate (magnification, ×42,000). (A) The MuV NP-RNA complex incubated in 50 mM Tris pH 8.3 plus 1 M NaCl; (B) the MuV NP-RNA complex as a precipitant in 0.1 M citric acid-sodium citrate (pH 4) plus 470 mM NaCl; (C) the MuV NP-RNA complex incubated at pH 4 and resolubilized by increasing the pH back to approximately 7.5. The ring structures in panels A, B, and C were comparable to that of the untreated MuV NP-RNA ring (Fig. 2A) after the RNA was lost. These ring structures could be considered "empty-capsid"-like structures. The scale bar in the bottom right corner of each micrograph corresponds to 100 nm.

Several NSRV nucleocapsidlike rings have recently been described (2, 7, 9). Coexpression of the MuV NP and P proteins in *E. coli* has resulted in the production of

nucleocapsidlike rings with morphologies similar to those seen in other NSRVs. The MuV NP-RNA ring contains 13 NP subunits and contains RNA. There are multiple sizes of RNA contained within the NP ring, which is not seen with other NSRVs such as the NP-RNA ring of VSV, suggesting that the RNA in the MuV NP ring is less protected (6). The study of the MuV nucleocapsidlike particle will lead to further understanding of the unique features of the paramyxovirus nucleocapsid.

ACKNOWLEDGMENTS

This work is supported in part by National Institutes of Health grant AI050066 to M.L. and grant AI-065795 to B.H.

REFERENCES

1. **Albertini, A. A., A. K. Wernimont, T. Muziol, R. B. Ravelli, C. R. Clapier, G. Schoehn, W. Weissenhorn, and R. W. Ruigrok**. 2006. Crystal structure of the rabies virus nucleoprotein-RNA complex. Science **313**:360-363.
2. **Bourhis, J.M., B. Canard B, and S. Longhi.** 2006. Structural disorder within the replicative complex of measles virus: functional implications. Virology **344**(1):94-110.
3. **Brandling-Bennett, A. D., J. Modlin, and W.A. Orenstein**. 1975. Current status of mumps in the United States. J Infect Dis **132**(1):106-9.
4. **Bhella, D., A. Ralph, L. B. Murphy, and R. P. Yeo**. 2002. Significant differences in nucleocapsid morphology within the Paramyxoviridae. J Gen Virol **83**:1831-1839.
5. **Bhella D, A. Ralph, and R.P. Yeo.** 2004. Conformational flexibility in recombinant measles virus nucleocapsids visualised by cryo-negative stain electron microscopy and real-space helical reconstruction. J Mol Biol **340**(2):319-331.
6. **Green, T. J., S. Macpherson, S. Qiu, J. Lebowitz, G. W. Wertz, and M. Luo**. 2000. Study of the assembly of vesicular stomatitis virus N protein: role of the P protein. J Virol **74**:9515-9524
7. **Green, T.J., X. Zhang, G.W. Wertz, and M. Luo.** 2006. Structure of the vesicular stomatitis virus nucleoprotein-RNA complex. Science **313**:357-360.
8. **Heggeness, M.H., P.R. Smith, I. Ulmanen, R.M. Krug, P.W. Choppin**. 1982. Studies on the helical nucleocapsid of influenza virus. Virology. **118**(2):466–470.
9. **Iseni, F., A. Barge, F. Baudin, D. Blondel, and R. W. Ruigrok.** 1998. Characterization of rabies virus nucleocapsids and recombinant nucleocapsid-like structures. J Gen Virol **79**:2909-2919
10. **Kingston, R. L., W. A. Baase, and L. S. Gay**. 2004. Characterization of nucleocapsid binding by the measles virus and mumps virus phosphoproteins. J Virol **78**:8630-8640.
11. **Kingston, R. L., L. S. Gay, W. S. Baase, and B. W. Matthews**. 2008. Structure of the Nucleocapsid-Binding Domain from the Mumps Virus Polymerase; an Example of Protein Folding Induced by Crystallization. J Mol Biol **379**:(4) 719-731
12. **Kolakofsky, D., L. Roux, D. Garcin, and R. W. Ruigrok**. 2005. Paramyxovirus mRNA editing, the "rule of six" and error catastrophe: a hypothesis. J Gen Virol **86**:1869–1877
13. **Laue, T.M., B.D. Shah, T.M. Ridgeway, and S.L. Pelletier**. 1992. *Analytical Ultracentrifugation in Biochemistry and Polymer Science* (Harding, S. E., Rowe, A. J., and Horton, J. C., Eds.) pp 90-125, Royal Society of Chemistry, Cambridge, U.K

14. **Ludtke, S. J., P. R. Baldwin, and W. Chiu**. 1999. EMAN: semiautomated software for high-resolution single-particle reconstructions. J Struct Biol **128**:82-97.
15. **Maclellan K., C. Loney, R.P. Yeo, and D. Bhella.** 2007. The 24-angstrom structure of respiratory syncytial virus nucleocapsid protein-RNA decameric rings. J Virol **81**(17):9519-24.
16. **Pettersen, E. F., T. D. Goddard, C. C. Huang, G. S. Couch, D. M. Greenblatt, E. C. Meng, and T. E. Ferrin.** 2004. UCSF Chimera: a visualization system for exploratory research and analysis. J. Comput. Chem. **25**:1605-12.
17. **Schoehn, G., M. Mavrakis, A. Albertini, R. Wade, A. Hoenger, and R. W. Ruigrok.** 2004. The 12 A structure of trypsin-treated measles virus N-RNA. J Mol Biol **339:**301-12.
18. **Schuck, P.** 2000. Size distribution analysis of macromolecules by sedimentation velocity ultracentrifugation and Lamm equation modeling. Biophysical Journal **78:**1606-1619.
19. **Tran, T. L., N. Castagne, D. Bhella, P. F. Varela, J. Bernard, S. Chilmonczyk, S. Berkenkamp, V. Benhamo, K. Grznarova, J. Grosclaude, C. Nespoulos, F. A. Rey, and J. F. Eleouet.** 2007. The nine C-terminal amino acids of the respiratory syncytial virus protein P are necessary and sufficient for binding to ribonucleoprotein complexes in which six ribonucleotides are contacted per N protein protomer. J Gen. Virol **88:**196-206

STRUCTURAL AND FUNCTIONAL CHARACTERIZATION OF THE MUMPS VIRUS PHOSPHOPROTEIN

by

ROBERT COX, TODD J. GREEN, SANGEETHA PURUSHOTHAM, CHAMPION DEIVANAYAGAM, GREGORY J. BEDWELL, PETER E. PREVELIGE, MING LUO

Journal of Virology July 2013, p. 7558-7568 Vol. 87, No. 13

ABSTRACT

The phosphoprotein (P) is virally encoded by the *Rhabdoviridae* and *Paramyxoviridae* in the order *Mononegavirales*. P is a self-associated oligomer and forms complexes with the large viral polymerase protein (L), the nucleocapsid protein (N), and the assembled nucleocapsid. P from different viruses has shown structural diversities even though their essential functions are the same. We systematically mapped the domains in mumps virus (MuV) P and investigated their interactions with nucleocapsid-like particles (NLPs). Similar to other P proteins, MuV P contains N-terminal, central, and C-terminal domains with flexible linkers between neighboring domains. By pulldown assays, we discovered that in addition to the previously proposed nucleocapsid binding domain (residues 343-391), the N-terminal region of MuV P (residues 1-194) could also bind NLP. Further analysis of binding kinetics was conducted using surface plasmon resonance. This is the first observation that both the N- and C-terminal regions of a negative strand RNA virus P are involved in binding the nucleocapsid. Additionally, we defined the oligomerization domain (P_{OD}) of MuV P as residues 213-277 and determined its crystal structure. The tetrameric MuV P_{OD} is formed by one pair of long parallel α-helices with another pair in opposite orientation. Unlike the parallel orientation of each α-helix in the tetramer of Sendai virus P_{OD}, this represents a novel orientation of a P_{OD} where both the N- and C-terminal domains are at either end of the tetramer. This is consistent with the observation that both the N- and C-terminal domains are involved in binding the nucleocapsid.

INTRODUCTION

The phosphoprotein (P) is a multi-functional protein encoded in the genomes of negative strand RNA viruses (NSVs) of the *Rhabdoviridae* and *Paramyxoviridae* in the order *Mononegavirales*. P performs several essential functions in virus replication. It is the cofactor in the viral RNA-dependent-RNA-polymerase (RdRp), a complex that also includes the virally encoded large (L) protein. L harbors the catalytic functions for RNA synthesis and mRNA capping. P also directly binds the nucleocapsid, the active template for viral RNA synthesis. Through this interaction, P delivers the RdRp to the nucleocapsid. In the absence of P, the RdRp cannot recognize the nucleocapsid or gain access to the viral genome. The domain responsible for P to bind the nucleocapsid, P_{NBD}, has been mapped to the C-terminal region for a number of NSVs, including vesicular stomatitis virus (VSV), rabies virus (RABV), measles virus (MeV), Sendai virus (SeV), Mokola virus (MOKV), and mumps virus (MuV) (1-5). Three-dimensional structures of this domain revealed a certain degree of structural homology among different viruses (5-9). The crystal structure of VSV P_{NBD} in complex with a nucleocapsid-like particle (NLP) clearly showed that the P binding site in the nucleocapsid is formed by two neighboring nucleocapsid protein (N) subunits (10). The large extended loop in the C-lobe and a single α–helix (α13) of one N subunit and the same extended loop in an adjacent N subunit make up the U shaped P binding site with α13 at the bottom of the cleft. This high-affinity P binding site could only be created by N subunits that

are assembled together in the nucleocapsid. By this mechanism, the cofactor P can dock the RdRp specifically to the nucleocapsid in order to use it as the template for viral RNA synthesis. In addition, P forms a stable complex with N that is free of RNA, termed N^0-P. This encapsidation-competent complex of N and P exists prior to incorporation of N into the nucleocapsid (11). During virus replication, the N subunit in the N^0-P complex is used to concomitantly encapsidate the newly synthesized viral RNA (12). The domain essential for keeping N free of RNA in the N^0-P complex has been mapped to the N-terminal region ($P_{N°D}$) of P for several NSVs (11, 13-15). A crystal structure of VSV $P_{N°D}$ in complex with a VSV N mutant showed that $P_{N°D}$ sits in the cavity where the viral RNA would be accommodated in the nucleocapsid (16). Occupation of the cavity may be instrumental in allowing P to keep N free of RNA in the N^0-P complex.

Another important feature of P is that its functional form is a self-associated oligomer. Self-association is required for supporting viral RNA synthesis (17), but is not necessary for the association of P with other viral proteins such as L or N. The domain responsible for P oligomerization (P_{OD}) is located in the central region of P. $P_{N°D}$ and P_{NBD} are linked to P_{OD} through flexible loops, which appears to be a common modular structure for all NSV P proteins. The length of P differs greatly among NSVs, and there is no homology for P_{OD}. Furthermore, the structure and the mode of self-association also vary considerably from one P to another. In the case of SeV P (568 amino acids), P_{OD} corresponds to residues 320-433. Each SeV P_{OD} subunit donates a single long helix to form a tetrameric coiled-coil, with all helices being parallel to one another. Short helices at the N-terminal end of SeV P_{OD} contribute to additional tetrameric interactions. For VSV P (265 amino acids), P_{OD} comprises residues 107-177 (18, 19). VSV P_{OD} dimerizes by domain swapping of a β-

hairpin from each subunit that participates in collating a β-sheet of four anti-parallel strands on each side. Two parallel α–helices held together by a number of hydrophobic interactions form the core of the VSV P dimer. By comparison, the oligomerization mode of RABV P_{OD} is quite different from that of VSV P_{OD}, despite the two viruses being closely related members of the Rhabdovirus family. RABV P_{OD} spans residues 92 to 131 in P (297 amino acids), and forms a dimer (20). However, each polypeptide contains two anti-parallel helices linked by a loop. The dimer of RABV P_{OD} involves a four-helix bundle between two parallel subunits. This particular orientation places $P_{N°D}$ and P_{NBD} at the same end of RABV P, in contrast to other P proteins in which the two domains are at distant opposite ends of the oligomer (19-21). In VSV, it has been shown that a chimeric P dimer with one P mutant lacking $P_{N°D}$ and another mutant lacking P_{NBD} can fully support VSV RNA synthesis (17). In the case of the RABV P dimer, it is not clear what the functional implications are when all $P_{N°D}$ and P_{NBD} domains are at the same end.

For this report, we carried out systematic studies of the domains of MuV P and their possible interactions with the nucleocapsid. Previously, MuV P expressed as a recombinant GST-fusion protein was shown to bind a truncated N (N_{398}) that was described as capable of assembling into NLP (4). In addition, deletion of the last 49 residues in MuV P abolished NLP binding, and the C-terminal domain (C343-391) alone was shown to be capable of binding NLP (4). In contrast, nucleocapsid binding by the P protein from other paramyxoviruses reportedly requires interactions with the C-terminal tail region of N (22-25). The previous report appears to suggest that MuV P contains a P_{NBD} that is similar to other paramyxoviruses, but its binding site on the nucleocapsid may be located in a different region of N. The crystal structure of the C-terminal domain of MuV P showed that it contains

three packed α–helices that may be induced to fold when P binds the nucleocapsid (7). We expanded the study of nucleocapsid-binding to include all domains in MuV P. Our structural and functional characterization of MuV P is discussed here with comparison to other NSV Ps.

MATERIALS AND METHODS

MATERIALS

Restriction enzymes and T4 DNA ligase were purchased from New England BioLabs. pET28b and BL21(DE3) were purchased from Novagen. Primers for PCR were purchased from Invitrogen and Integrated DNA Technologies.

PLASMID CONSTRUCTION

The P genes were amplified from a cDNA clone of MuV strain 88-1961 (GenBank: AF467767.2) by PCR. Primers for amplification on the 5' end of the gene fragments contained NheI restriction sites while 3' primers contained XhoI sites. Sequences of the primers can be sent upon request. The P gene or gene fragments and the pET-28b plasmid were each digested with restriction enzymes NheI and XhoI and gel purified. The purified digested P genes were individually ligated in frame with the N-terminal polyhistidine tag, resulting in the vector MuV P-pET28b, or MuV (P clone ID)-pET28b.

PROTEIN EXPRESSION AND PURIFICATION

Expression vectors were transformed into *E. coli* strain BL21(DE3). Bacteria were cultured in LB broth at 37 °C until OD_{600} reached 0.6. Protein expression was induced with 1 mM IPTG for 18 hours at 18 °C. The cells were harvested by centrifugation and resuspended in binding Buffer A containing 20 mM Tris (pH 7.9), 500 mM NaCl and 5 mM imidazole. The cells were disrupted by sonication, and then centrifuged for 1hr at 18,000rpm. Soluble fractions were collected and passed through a Ni-Affinity column (Chelating Sepharose Fast Flow, GE Healthcare). The loaded Ni-affinity column was washed with 5 column volume (CV) of binding Buffer A. The loaded column was washed with 5 CV of wash Buffer A containing 20 mM Tris (pH 7.9), 500 mM NaCl, and 50 mM Imidazole. Samples were eluted with elution Buffer A containing 20 mM Tris (pH 7.9), 500 mM Imidazole, and 500 mM NaCl. Proteins were further purified by size exclusion chromatography (Sephacryl S-75 or S-200, GE Healthcare) in size exclusion buffer containing 20 mM Tris pH 7.5 and 500 mM NaCl.

PURIFICATION OF TRYPSINIZED MUV NLP

The MuV N protein was expressed and NLP was purified as previously reported (26). NLP has a ring structure composed of 13 N subunits and a single strand of random RNA. The purified NLP was allowed to incubate overnight at room temperature with trypsin at a 1 mg:100 mg ratio (trypsin:N). Trypsin was then inactivated by the addition of PMSF (1 mM). The digested NLP (NLP_{379}) was concentrated to 8 mg/ml and purified by size exclusion chromatography using a S-400 column (HiPrep Sephacryl S-400, GE Healthcare). The

identity of the digested N was confirmed by N-terminal amino acid sequencing and mass spectrometry analysis. The size of the NLP_{379} was consistent with that of a ring structure similar to the full-length NLP.

IDENTIFICATION OF PROTEASE RESISTANT FRAGMENTS OF THE MUV P PROTEIN

The full-length P protein was digested using three different proteases: trypsin (TPCK treated, Worthington), α-chymotrypsin (Sigma), and proteinase K (Fisher). The amounts of enzymes used per mg of the P protein were 0.2 U, 0.1 U, 0.2 μg for trypsin, chymotrypsin, and proteinase K, respectively. The P protein was digested with each protease for a maximum of 2 hrs at 37°C. During this time course, aliquots of each digestion mixture were taken at five minute intervals and denatured for analysis in SDS-PAGE gels. SDS-PAGE gels of digestion reactions were electroblotted onto PVDF membranes and stained with coomassie blue. Bands corresponding to stable P fragments were cut out and sent to the Protein Analysis Core at UTMB (Galveston, TX) for N-terminal amino acid sequencing. Products at optimal time-points from the limited digestions of P were purified using a Gelfree 8100 Fractionation System (Protein Discovery), in accordance with the manufacturer's protocol. Fractions containing pure digestion products were subjected to mass spectrometry analysis at the Protein Analysis Core at UTMB (Galveston, TX).

BIOINFORMATICS ANALYSIS

The secondary structure of MuV P protein was predicted using Jpred3 (27). PIV5 V protein (Accession #AAA47882) was used in the Jpred3 homologue search.

CRYSTALLIZATION AND DATA COLLECTION OF MUV P_{OD}

P161-277 was expressed and purified as described above and concentrated to 5-7 mg/mL. Crystallization conditions at 20°C were screened using Crystal Screen 1 & 2 (Hampton). An initial crystal hit was found in the handing drop set-up with a reservoir solution containing 0.1 M NaAc (pH 4.6) and 2 M NaCl. Typical crystals appeared in hanging drops after 10-14 days at 20°C. Crystals were cryo-protected in a cryosolution containing the reservoir solution supplemented with 25 % glycerol. For preparation of uranyl acetate derivatives, crystals were soaked stepwise in the reservoir solution containing 0.5, 1.0, 1.5 and 2.5 mM uranyl acetate at approximately 10 minute intervals. Uranyl acetate soaked crystals were cryo-protected by the same protocol as native crystals, except for the addition of 2.5 mM uranyl acetate to the cryosolution. Native crystals diffracted X-rays to a resolution of 2.2 Å when exposed to synchrotron X-rays at SER-CAT beamline BL-22 BM at APS.

STRUCTURE DETERMINATION AND REFINEMENT

The phases of X-ray diffraction data were determined by SIRAS using the program CNS (28). The uranium atom in the uranyl acetate derivative was used as an anomalous

scatterer. An initial model was manually built into solvent flattened maps. The model was then subjected to several rounds of the Autobuild routine in PHENIX (29). The resulting model was subjected to several cycles of manual rebuilding using COOT (30) and refinement with PHENIX (29). TLS refinement was performed using the PHENIX program (31, 32)]. The structure has been deposited in the Protein Data Bank under the code 4EIJ. Solvent accessible surfaces were calculated using CNS (28). Structure figures were created using PyMOL (33). Data collection and refinement statistics are shown in Table 1.

CONTACT AREA BETWEEN THE HELICES

In order to estimate how tight the interactions are between the different helices, calculations of the buried surface areas were performed in CNS (28) (Table 2). The total buried surface area is similar for each of the inter-chain interactions. Among the three possible pairs of contacts, Chain A-B proved to have the highest percentage of buried surface. However, the negligible differences among the three pairs strongly suggest that the oligomeric state of MuV P_{OD} is a tetramer.

Table 1. Crystal X-ray data, phasing, and refinement statistics

Parameter[a]	**BL-22 BM**[b]	
	Native crystal	**Uranyl derivative**
Data collection statistics		
X-ray source	SER-CAT, APS, IL	SER-CAT, APS, IL
Wavelength (Å)	1.0	1.0
Space group	R32	R32
Cell dimensions		
a, *b*, *c* (Å)	80.348, 80.348, 165.17	78.919, 78.919, 165.447
α, β, γ (°)	90, 90, 120	90, 90, 120
Resolution (Å)	50–2.2 (2.24–2.2)	50–2.9 (2.96–2.9)
R_{sym}	0.062 (0.38)	0.081 (0.47)
Avg $I/\sigma(I)$	26.695 (4.145)	23.11 (3.0)
Completeness (%)	99.9 (100)	99.6 (97.6)
Redundancy	4.6 (4.7)	3.5 (3.7)
No. of reflections	49,262	16,324
No. of unique reflections	10,717 (528)	4,601 (233)
Phasing statistics		
Heavy atom sites		$3\times U(O)_2$
Resolution range (Å)		50–2.56 (2.76–2.56)
Figure of merit, acentric/centric		0.6566/0.3542 (0.6584/0.3531)
Phasing power, iso/ano		1.3471/1.3104 (1.2658/1.4415)
R_{cullis}, iso/ano		0.599/0.7606 (0.6059/0.9150)
Refinement statistics		
Molecules (ASU)	2	
Resolution (Å)	26.6–2.2 (2.31–2.2)	
Avg B-factor (Å^2), protein/water	43.05/46.52	
Coordinate error (maximum likelihood based)	0.26	
No. of reflections used	10,308	
R_{work}/R_{free}	0.1814/0.2302	
Completeness (%)	96.15	
No. of atoms		
Protein	942	
Water	58	
Glycerol	1	
RMSD		
Bond length (Å)	0.006	
Bond angle (°)	0.887	
Ramachandran plot (%), favored regions	98.3	

- a $R_{sym} = \Sigma|(I - \langle I \rangle)|/\Sigma \langle I \rangle$, where $\langle I \rangle$ is the observed intensity; $R_{work} = \Sigma(||F_{obs}| - k|F_{model}||)/\Sigma(|F_{obs}|)$. R_{free} was obtained for a test set of reflections (9.98%).
- b Values for the highest-resolution shell are indicated in parentheses.

Table 2. Surface area calculations

	Surface (Å^2)		
Chain	**Buried**	**Total**	**% Buried**
Chain A		6,382	
Chain B		5,824	
A-B	2,771	9,436	29.3
A-A′	2,570	10,193	25.2
B-B′	2,601	9,050	28.7
Tetramer	5,065	13,809	36.7

GLUTARALDEHYDE CROSSLINKING

Protein crosslinking studies were carried out with the addition of 0.1% glutaraldehyde stock solution diluted in PBS. Increasing concentrations of glutaraldehyde were added to 50 μl of P161-277 (3 mg/ml) and allowed to incubate for 4 hours or overnight on ice. The reactions were quenched by addition of 18 μl of SDS-PAGE sample buffer. Samples were denatured and analyzed by SDS-PAGE.

SEDIMENTATION VELOCITY ANALYSIS

Sedimentation velocity experiments were performed in an XL-A analytical ultracentrifuge (Beckman Coulter) in two channel epon centerpieces. The data were collected at 280 nm**,** and a speed of 40,000 rpm in an An60Ti 4-hole rotor at 20˚C. The concentration of protein loaded was ~1 mg/mL. The data (Table 3) were analyzed with the program SEDFIT using both the c(s) and c(s,ff0) models

(http://www.analyticalultracentrifugation.com/default.htm). The c(s,ff0) model was used for molecular weight estimation of the sedimenting species. The buffer density, buffer viscosity, and protein partial specific volume used in these calculations were estimated with the program SEDNTERP (http://bitcwiki.sr.unh.edu/index.php/Main_Page).

Table 3. Sedimentation velocity statistics

Sample	S value	RMSD	f/f0	Mol mass (kDa)
P161-277	2.6	0.009049	1.8525	57.8
P full	3.8	0.01062	2.6522	165.5

PULLDOWN ASSAY

In order to map N-P interactions, a pulldown assay was performed. A small column containing 50 µl of charged Chelating Sepharose Fast Flow beads was first saturated with the P protein or a P fragment. After allowing the sample to flow through the column, the beads were washed with 10 CV of binding Buffer B, containing 20 mM Tris (pH 7.9), 50 mM NaCl, and 5 mM Imidazole. NLP, or NLP_{379}, in binding Buffer B was added to the loaded column at a 1:1 molar ratio (N:P) and incubated at room temperature for 15 minutes. The NLP or NLP_{379} solution was allowed to flow through. Next, the loaded column was washed with 10 CV of binding Buffer B, followed by wash with 5 CV of wash Buffer B containing 20 mM Tris (pH 7.9), 50 mM NaCl, and 50 mM Imidazole. The protein was eluted with 5 CV of elution Buffer B containing 20 mM Tris (pH 7.9), 50 mM NaCl, and 500 mM Imidazole. The eluate was denatured in SDS-PAGE sample buffer and electrophoresed in a 12% SDS-PAGE gel. Gels were stained with 1% Coomassie Brilliant blue dye. The full-length MuV P protein was used as a positive control for binding NLP. The purified NLP or NLP_{379} in the absence of any P fragments was used as a negative control.

BIACORE 2000 ANALYSIS

Real time binding analysis of the MuV P protein to the MuV NLP and its truncated form NLP_{379} were analyzed using surface plasmon resonance on a BIAcore 2000 instrument (GE Healthcare). Purified NLP or N_{379} ligands were immobilized on the carboxylated surface of a CM5 sensor chip using an amine-coupling kit. Analytes full-length MuV P and P fragments P1-194, P161-277, and P286-391 were flowed over the immobilized NLP or NLP_{379} CM5 chip at a flow rate of 20 μL/min at 25˚C. Regeneration of the chip surface after each cycle was performed using (0.015 M HEPES in 0.5 M NaCl). The change in the surface plasmon resonance angle is displayed as response units, where 1,000 response units (RU) is equal to 1 ng of analyte bound per nm^2 on the sensor surface. The experiments were carried out in triplicates and kinetic association (K_A) and dissociation (K_D) rate constants were deduced using the 1:1 Langmuir kinetic model with BIA evaluation software.

RESULTS

DIGESTION STUDIES OF MUV P

In order to study the structure and function of the MuV P protein, a single vector was constructed to express the MuV P protein in *E. coli*. Following expression, his-tagged recombinant P was purified from the soluble fraction of the lysate. The P protein was further purified by size exclusion chromatography and was analyzed by SDS-PAGE. Purified P migrates to a position consistent with that observed in previous publications, approximately 5 kDa higher than the calculated molecular weight of 41.5 kDa (26). Slow migration has also been observed for VSV P (34), suggesting that NSV P proteins appear to migrate slower in SDS PAGE

The full-length P protein was shown to be susceptible to digestion by residual impurities over a brief time period following purification. In order to define domains within MuV P, limited proteolytic digestion studies were performed. Purified full-length P protein was digested using three different proteases: trypsin, chymotrypsin, and proteinase K. Digestion products were examined by SDS-PAGE, which showed that each protease had a different digestion pattern (Figure 1A-C). In order to identify the N- and C-termini of the stable fragments, individual bands corresponding to digested products were isolated and analyzed by N-terminal amino acid sequencing and mass spectrometry. The results for the

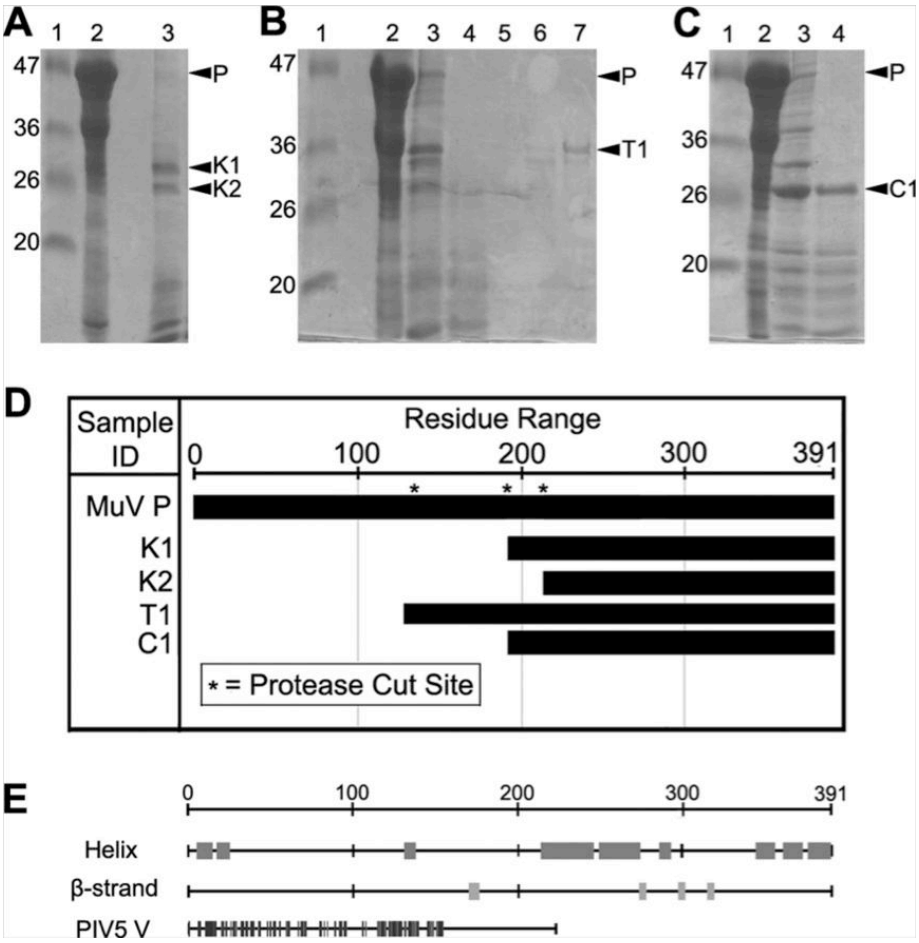

Fig 1. Limited digestion of MuV P by different proteases. In panels A to C, lanes 1, 2, and 3 correspond to the molecular mass ladder, undigested P protein, and digested P protein, respectively. (A) Proteinase K digestion resulted in two stable fragments (K1, residues 194 to 391; K2, residues 214 to 391) (lane 3). (B) Trypsin digestion resulted in a major stable fragment (T1, residues 135 to 391) (lane 3). Lanes 4 to 7 correspond to the different fractions separated using the Gelfree 8100 fractionation system. (C) Chymotrypsin digestion resulted in a major stable fragment (C1, residues 194 to 391) (lane 4). The identity of the major stable fragments was revealed by N-terminal amino acid sequencing and molecular weight determination, and is summarized in panel D. The molecular masses for fragments T1 and C1 were determined through mass spectrometry. The molecular masses of fragments K1 and K2 were approximated from their position on SDS-PAGE gels. Protease cut sites (*) represent the sequences identified using N-terminal sequencing. (E) Summary of bioinformatics analysis using Jpred3. Predicted helical regions are shown in the schematic to the right of "Helix". Predicted beta-strand regions are shown in the schematic to the right of "β-strand". Homology to PIV5 V protein is shown in the schematic to the right of "PIV5 V".

limited digestion studies are summarized in Figure 1D. Trypsin digestion resulted in a major stable fragment corresponding to residues 135-391 with an N-terminal sequence of MINRF and a molecular weight of 27.7 kDa. Chymotrypsin digestion resulted in a major stable fragment corresponding to residues 194-391 with an N-terminal sequence of AHPSP and a molecular weight of 21.7 kDa. While bands corresponding to other partially digested products were seen on SDS-PAGE gels for both trypsin and chymotrypsin digestions, the molecular weight of these fragments could not be determined by mass spectrometry. Proteinase K digestion resulted in two stable fragments. Identification of mass by mass spectrometry was not successful. The residue numbers for the two K fragments (K1 and K2), therefore, were designated based on their N-terminal sequence, and the molecular weight approximated from their position on SDS-PAGE. The N-terminal sequence for K2 was SVISA and likely corresponds to residues 214-391. The N-terminal sequence for K1 was somewhat ambiguous, but the sequence in cycles 3 thru 5 was PSP. This sequence with the size observed on SDS-PAGE of approximately 22 kDa is consistent with a fragment encompassing residues 194-391. The chymotrypsin and K1 fragments are thus the same, and consistent with the cleavage pattern of each enzyme where each cleaves adjacent to the carboxyl group of bulky or aromatic amino acids. The sequence at this cleavage site of P is Y/AHPSP.

BIOINFORMATICS ANALYSIS

Secondary structure prediction by Jpred3 identified nine different regions as probable helical regions (Figure 1E). The prediction also identified four different regions that were likely to have β-strand conformation. In addition, the Jpred3 search identified PIV5 V as a

homologue of MuV P. PIV5 V has a 37% identity to MuV P, located within the first 155 residues and 164 residues of MuV P and PIV5 V, respectively. These data were used along with the results of protease digestion to design a clone library of MuV P fragments. These protein fragments were expressed and purified by the same methods used for the full-length P. The yield of purified protein per liter varied for each fragment. A list of cloned P fragments and a summary of protein expression results are shown in Figure 2. P fragments

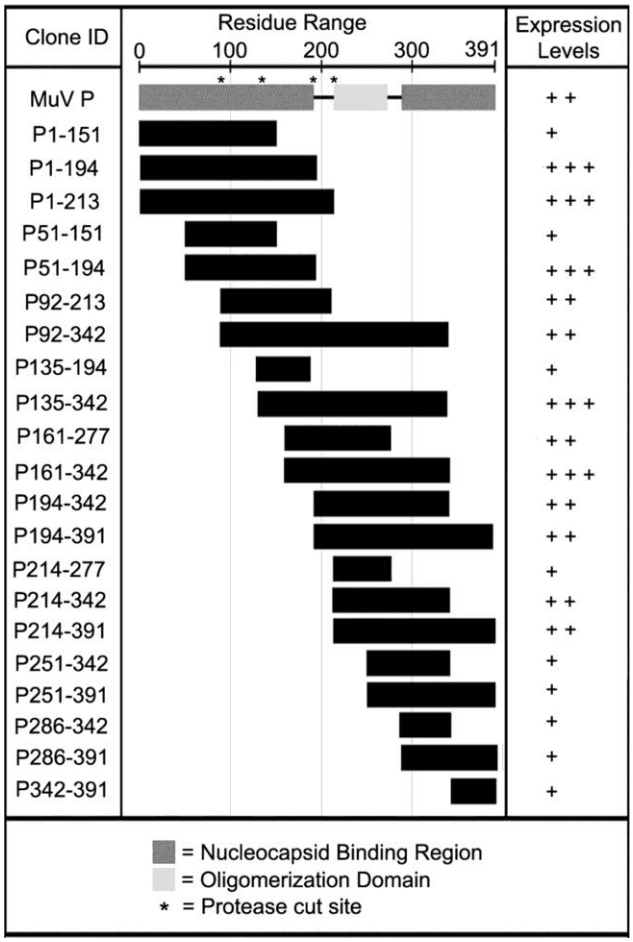

Fig 2. Summary of MuV P fragments. A schematic representation of MuV P modules is shown at the top. For expression levels, "+" indicates <15 mg/liter, "++" indicates 15 to 25 mg/liter, and "+++" indicates >25 mg/liter of purified recombinant protein. Fragments were derived from a combination of protease digestion and bioinformatics analysis.

that were consistent with the results of the protease digestion have a better expression level in the soluble fraction

STRUCTURE OF THE P OLIGOMERIZATION DOMAIN

Several fragments were subjected to crystal screens. Crystals were grown with fragment P161-277 and the crystal structure was determined to 2.2 Å resolution. Only residues 213-277 could be fit correctly into the electron density maps. The traced polypeptide represented an appropriate protein volume for the unit cell with a solvent content of 60.04%, assuming a partial specific volume of 0.74 cc/g. Composite omit maps were created to confirm that modeling was carried out correctly. The lack of residues 161-212 is likely due to digestion *in situ* during crystallization as crystal formation only occurred after two weeks. The asymmetric unit contains two chains (A and B) that cover residues 213-273 and 215-277, respectively (Figure 3A). Both chains are composed of a single long α-helix. However, Chain A, unlike Chain B, contains a kink at Gly 246. Chain A also contains a stretch of amino acids with extended conformation at the C-terminal end (residues 272-277) of its long helix.

The crystallized MuV P fragment forms a tightly packed tetramer through non-crystallographic and crystallographic symmetry contacts (Figure 3B). We therefore define this tetramer as MuV P_{OD}. This tetrameric coiled-coil structure is reminiscent of SeV P_{OD} (Figure 3C). However, the tetramer formed by SeV P_{OD} is composed of four parallel helices, whereas the tetramer formed by MuV P_{OD} is composed of two sets of parallel helices that are

in opposite orientation (Figure 3B). In the MuV P_{OD} tetramer that is primarily formed with hydrophobic interactions (Table 3), there are two zippers of charged sidechain interactions at

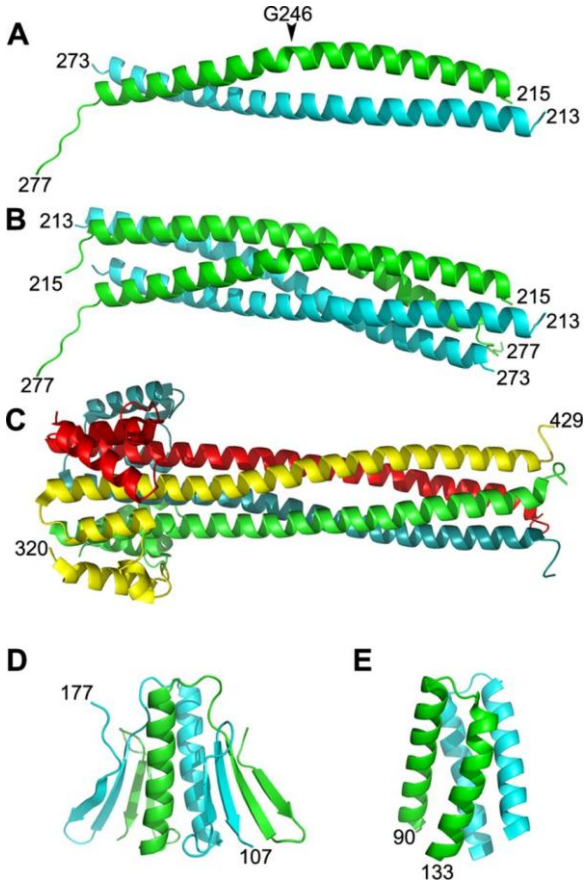

Fig 3. Structure of MuV P_{OD}. (A) Crystal structure of two parallel extended α-helices (chain A in green and chain B in cyan). Chain A contains residues 215 to 277, and a kink at Gly246 is noted. Chain B contains residues 213 to 273. (B) P_{OD} tetramer as found in the crystal. The crystal structures of P_{OD}s from SeV (C), VSV (D), and RABV (E) are shown for comparison. The range of residues for each P_{OD} is labeled. In panels C to E, each independent polypeptide chain is a different color.

Table 3. Sedimentation velocity statistics

Sample	S value	RMSD	f/f0	Mol mass (kDa)
P161-277	2.6	0.009049	1.8525	57.8
P full	3.8	0.01062	2.6522	165.5

each end in addition to hydrophobic surface contacts among the helices. Between the parallel pair of helices, the zipper is formed by Asp229, Glu236 and Asp240 (Chain A) and Arg231 and Lys238 (Chain B) as mentioned above (Figure 4A; inset A). Between the antiparallel pair of helices, the zipper is formed by Lys253 and Lys260 (Chain B) and Asp229, Glu236 and Asp240 (Chain B') (Figure 4B; inset B). The helices wrap around each other and seem to clamp one another through these charge zippers at both ends of the tetrad.

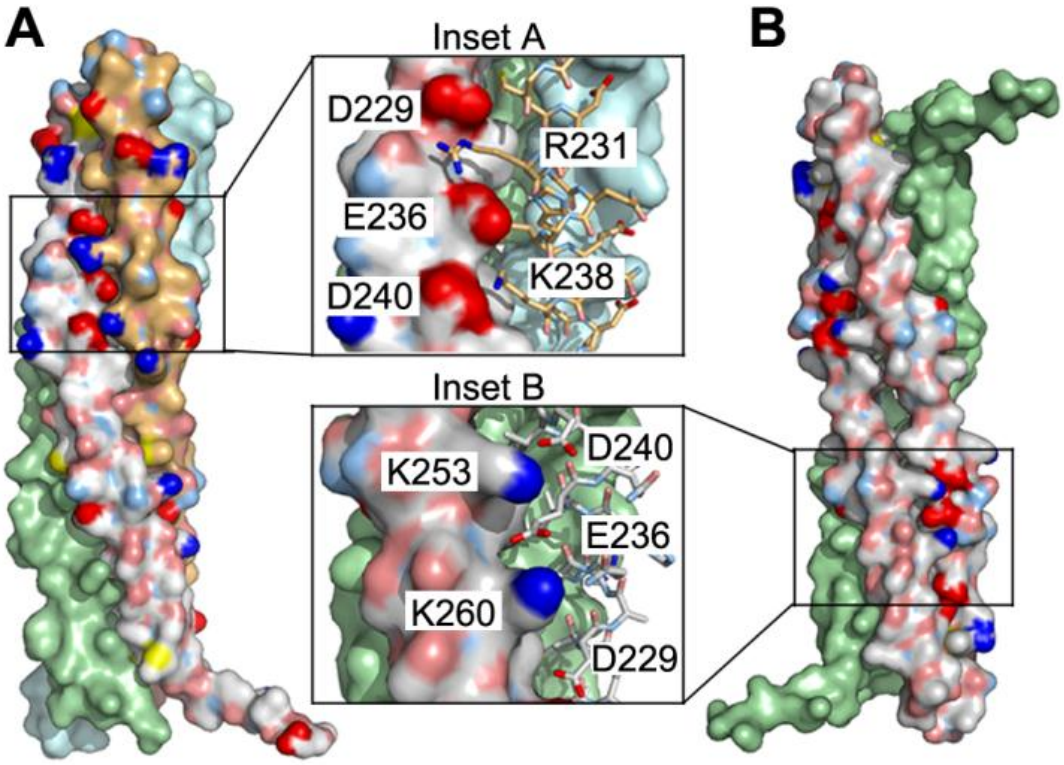

Fig 4. Tetrameric interactions. (A) Chain A-B interactions. In addition to extensive surface contacts, the main interactions between chains A and B also include a zipper of charged residues: Asp229, Glu236, and Asp240 (chain A) and Arg231 and Lys238 (chain B). In panel A, chain A is on the left, and chain B is on the right. The other two chains in the tetramer are monocolored. (B) Chain B-B′ interactions. Residues Lys253 and Lys260 from chain B (left) also form a zipper of charged residues—Asp229, Glu236, and Asp 240—from the antiparallel chain B′ (right). This clamping by the zippers occurs on both ends of the tetramer. The tetramer in panel B is rotated left-handed by 90° compared to the tetramer in panel A.

GLUTARALDEHYDE CROSSLINKING

In order to verify the tetrameric state of the MuV P protein, crosslinking reactions were performed using glutaraldehyde. Initially, full-length P was used in crosslinking experiments. However, because MuV P is highly susceptible to nonspecific digestion (35), the resulting crosslinked products were composed of a mixture of different P fragments, and no clear data could be discerned (data not shown). Since the majority of the known protease sensitive sites are contained within the terminal regions, P161-277 was used in place of the full-length P protein and the resulting crosslinked products were much easier to identify. Following analysis in SDS-PAGE gels, bands representing monomers, dimers, trimers, and tetramers could be clearly discerned (Figure 5A).

SEDIMENTATION VELOCITY ANALYSIS

To further confirm the oligomeric state determined by the P_{OD} crystal structure, we carried out ultracentrifugation analyses to measure the sedimentation coefficient of the purified P protein and fragment P161-277. For both P161-277 and full-length P, the data revealed a single dominant species (Figure 5). The molecular weight derived from sedimentation coefficient is 57.8 kDa for P161-277, which corresponds to the theoretical weight of a P161-277 tetramer (57.6 kDa). Furthermore, the molecular weight derived from sedimentation coefficient is 165.5 kDa for full-length P, very close to the theoretical

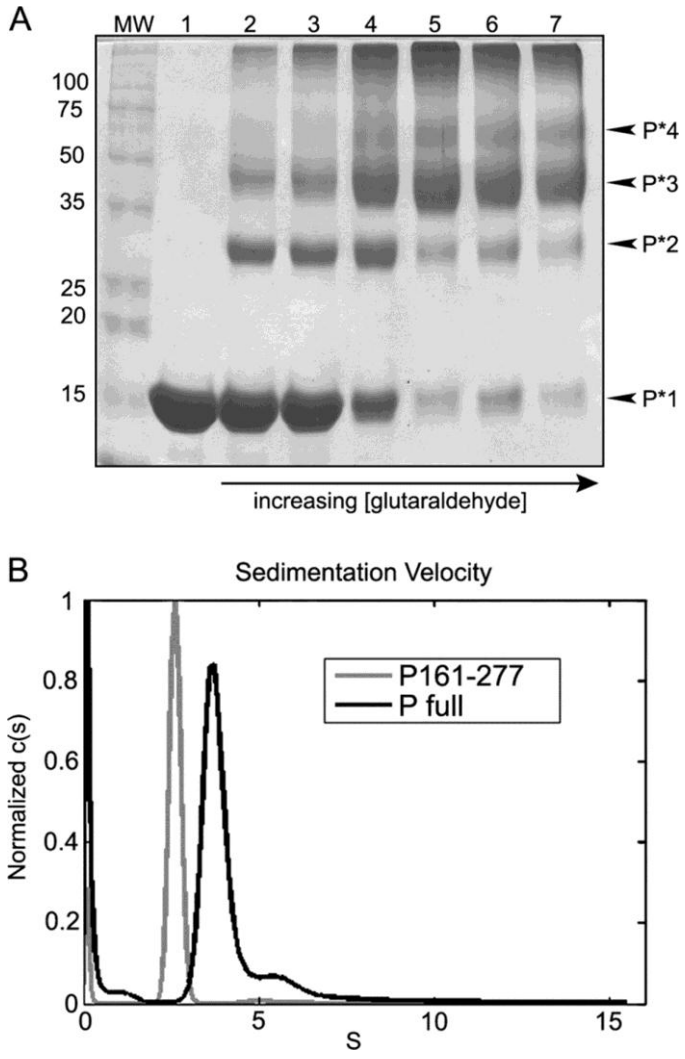

Fig 5. Oligomerization state of MuV P. (A) Cross-linking with glutaraldehyde. MuV P161-277 was cross-linked using glutaraldehyde in order to assess the oligomerization state. Cross-linking products were analyzed in SDS-PAGE gels. Lanes 1 to 5 correspond to 4 h of incubation with glutaraldehyde at the following concentrations: 0, 0.05, 0.06, 0.1, and 0.2%. Lanes 6 and 7 correspond to overnight incubation with 0.2 and 0.3% glutaraldehyde, respectively. Bands representing P161-277 monomers (P*1), dimers (P*2), trimers (P*3), and tetramers (P*4) can be seen at ~15, ~30, ~45, and ~60 kDa, respectively, and are noted to the right of the gel. (B) Sedimentation velocity analysis. Sedimentation coefficients were determined, and molecular masses were derived for P161-277 and full-length P (Table 3). The distribution plots showed a single species for each sample. The derived molecular mass for P161-277 (57.8 kDa) corresponded to the theoretical mass of a P161-277 tetramer (57.6 kDa). Furthermore, the molecular mass derived for full-length P (165.5 kDa) was very close to the theoretical molecular mass for a MuV P tetramer (168 kDa).

molecular weight for a MuV P tetramer (168 kDa). We therefore concluded that the purified MuV P protein or P161-277 is a tetramer, concurring with the results from the crystal structure.

NUCLEOCAPSID BINDING

A number of recombinant P fragments were expressed and purified (Figures 1 and 2). In order to determine which parts of the MuV P protein interact with the nucleocapsid, a pulldown assay was developed. Purified P fragments were first added to a small Ni-affinity column in saturating amounts. After allowing the supernatant to flow through, the beads were washed once to remove any unbound protein. NLP of MuV prepared as previously reported (26) was added to the loaded column at a 1:1 molar ratio (N:P) and allowed to incubate at room temperature for 15 minutes. The NLP solution was then allowed to flow through. The loaded column was washed to remove any unbound protein. The proteins were then eluted from the column, and the products were denatured and electrophoresed in SDS-PAGE gels. A summary of the results from the pulldown assays is shown in Figure 6. These assays confirmed that the extreme C-terminal domain, P342-391, is a nucleocapsid binding domain as previously reported (4). Other C-terminal fragments including residues 251-391, 286-391 and 342-391 each bound NLP (Figure 6). Unexpectedly, the results showed that the N-terminal region of MuV P (P_{1-194}) was also capable of binding NLP. This has not been reported previously for a NSV P protein and suggests that the functional domains of MuV P may be different from those of other NSVs.

In addition to using NLP formed by the full-length NLP (540 amino acids), binding assays were also conducted using a trypsin digested form of the MuV NLP (NLP_{379}). The digested NLP_{379} was used to determine if P binding could be abolished in NLP lacking the C-terminal region of N. Similar to the full-length NLP, NLP_{379} was also bound by both the N-terminal (1-194, 51-194) and C-terminal (251-391, 286-391, and 342-391) regions of MuV P (Figure 6D,E).

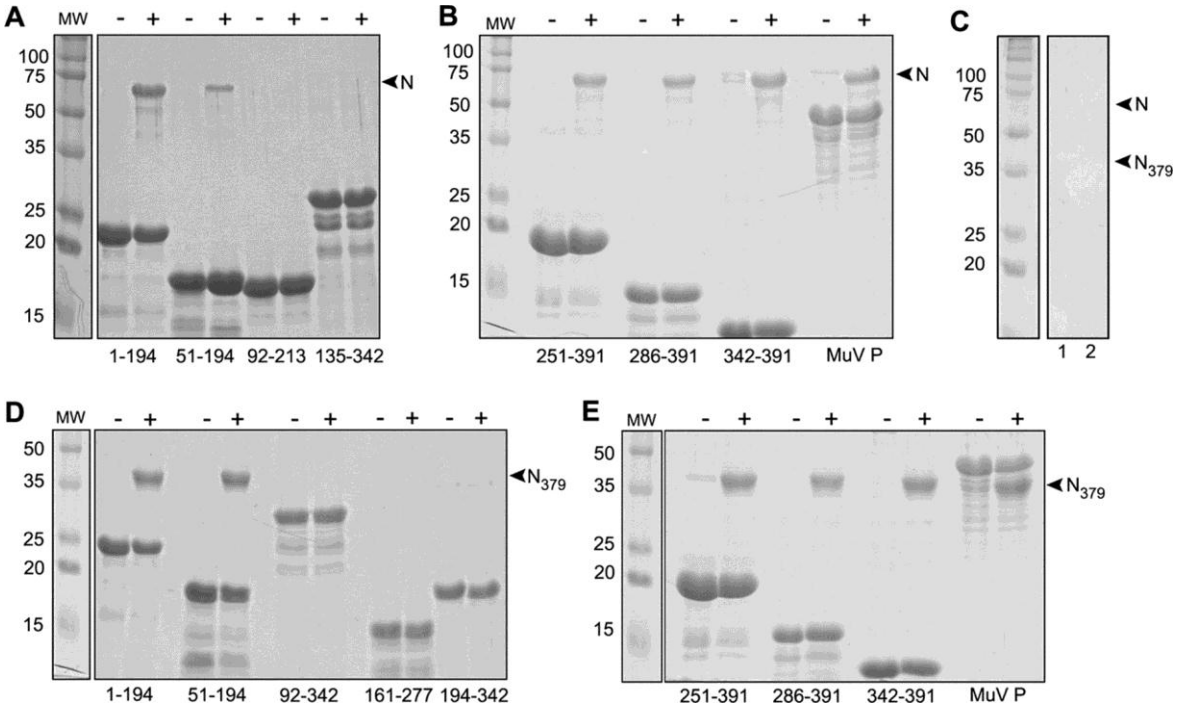

Fig 6. NLP pulldown assays. In order to determine which P fragments could interact with NLP, pulldown assays were performed. The headers of the gels in panels A, B, D, and E indicate whether the P protein (or P fragments) saturated column was incubated with NLP (+) or NLP379 or not (−). Amino acid numbers corresponding to individual P fragments are labeled on the footer of the gels. The positions for N protein (labeled "N" in panels A and B) and trypsinized N (labeled "N_{379}" in panels D and E) are noted (A and B), and trypsinized NLP (N379) are noted by arrows on the right sides of each gel (D and E). (C) Negative controls. Lanes 1 and 2 show the results for negative controls for NLP and trypsinized N379, respectively, with no P fragments added to the column.

AFFINITY OF P FRAGMENTS BINDING NLP

Based upon pulldown experiments, we concluded that MuV P contains two separate nucleocapsid binding domains: the N-terminal domain (P1-194) and the C-terminal domain (P286-391). In order to further characterize the interactions between the two separate nucleocapsid binding domains and NLP, surface plasmon resonance analysis was conducted. The recombinant full-length P, P1-194, P161-277, and P286-391 were investigated for their ability to interact with immobilized NLPs or NLP_{379}. All analytes, except for P161-277 as a negative control, exhibited measurable binding (Figure 7; Table 4). Kinetics experiments were conducted at multiple concentrations (Figure 7). Modeling the association and dissociation of the P analytes with NLP using the 1:1 Langmuir binding model led to estimated K_A values of 2.02×10^5 M^{-1} for N1-194, 2.35×10^6 M^{-1} for P286-391, 2.23×10^6 M^{-1} for the full-length P (Table 4). Using K_D calculations, P286-391 also exhibited a relatively higher affinity for NLP with an estimated dissociation constant of 4.26×10^{-7} M as compared with N1-194 (4.95×10^{-6} M). Next we tested the ability of P to bind immobilized NLP_{379} (Figure 7, E-H). Modeling the association and dissociation of the P analytes with NLP_{379} using the 1:1 Langmuir binding model led to estimated K_A values of 2.17×10^6 M^{-1} for P1-194, 1.01×10^5 M^{-1} for P286-391, 1.61×10^6 M^{-1} for the full-length P (Table 4). The estimated K_A and K_D values, P1-194 exhibited a relatively higher affinity for NLP_{379} with an estimated dissociation constant (K_D) of 4.6×10^{-7} M as compared with P286-391, which has a K_D value of 9.88×10^{-6} M. Control SPR experiments with P161-277, which contains the OD domain, did not show measurable interactions with full length NLP or NLP_{379}. The SPR data indicate a 1.3-fold higher affinity in P binding the full length NLP versus NLP_{379}, but shows a slower dissociation rate (Fig. 7A, E). The curves of Fig. 7F, G show that there are

very fast on and off rates for both P1-194 and P286-391 to NLP_{379} as compared to the full length NLP.

Table 4. Binding kinetics

Sample	K_A **(M^{-1})**	K_D **(M)**
P1-194 + N full	2.02×10^5	4.95×10^{-6}
P286-391 + N full	2.35×10^6	4.26×10^{-7}
P full + N full	2.23×10^6	4.48×10^{-7}
P1-194 + NLP_{379}	2.17×10^6	4.60×10^{-7}
P286-391 + NLP_{379}	1.01×10^5	9.88×10^{-6}
P full + NLP_{379}	1.61×10^6	8.65×10^{-7}

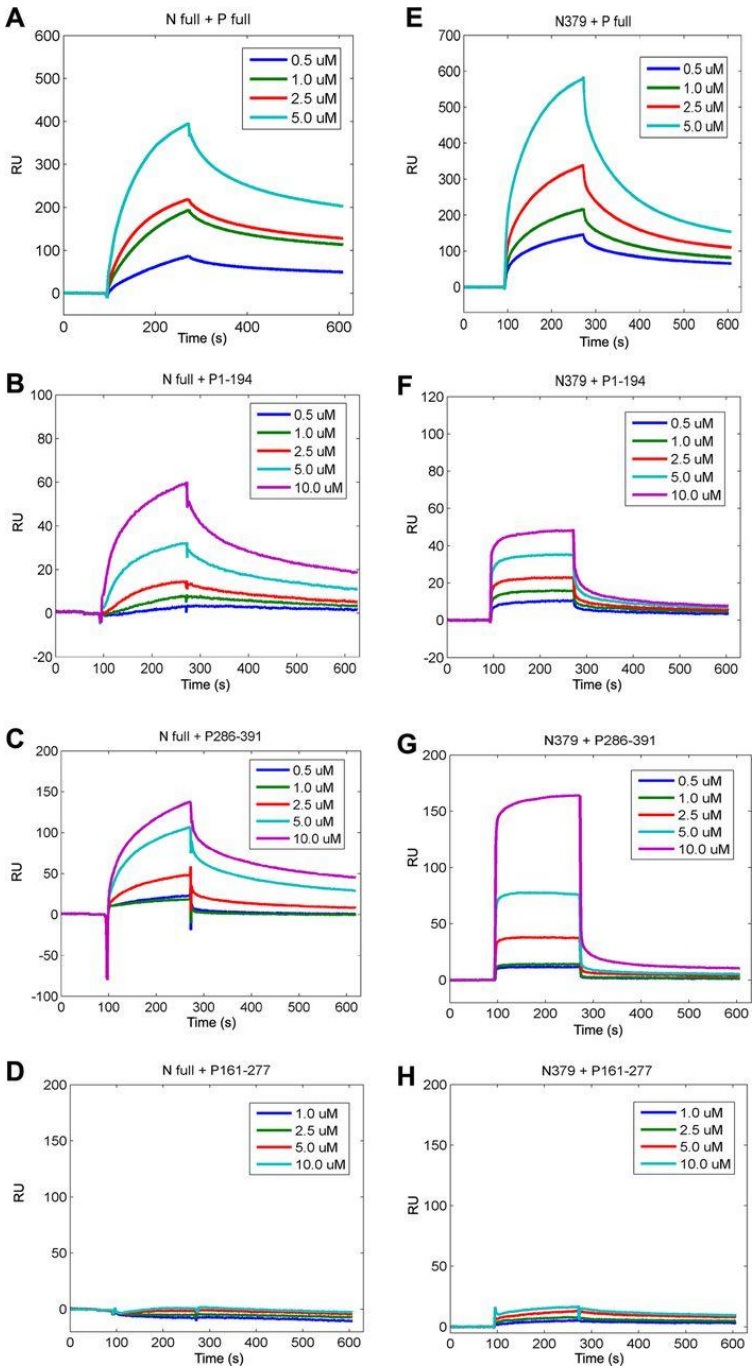

Fig 7. Evaluation of N-P interactions using surface plasmon resonance. (A to D) Full-length NLP was immobilized, and P protein analytes (full-length P, P1-194, P286-391, and P161-277, respectively) were injected over the CM5 chip surface. All analytes displayed a measurable binding response (1 RU = 1 pg/mm2). (E to H) N379 was immobilized, and P protein analytes (full-length P, P1-194, P286-391, and P161-277, respectively) were injected over the CM5 chip surface. All analytes displayed a measurable binding response. All experiments were carried out in triplicate. K_A and K_D values are listed in Table 4.

DISCUSSION

It has been anticipated that MuV P has a modular structure composed of separated functional domains. Here, we present an experimental approach to more accurately map the functional domains of MuV P. In our proteolytic studies, the N-terminal region of P preceding residue 194 appeared to be less stable than the region that follows since more cleavage sites were found here. This is consistent with observations of other NSV Ps in which the N-terminal region is more disordered compared to the middle and C-terminal regions of P (11, 23, 36, 37). A previous study determined the structure of an extreme C-terminal segment (residues 343-391) of MuV P (7). Our proteolytic digestion study did not identify this smaller region of P as a stable fragment. A possible explanation for not being able to map P343-391 in the current study is that this C-terminal region is part of a larger C-terminal domain. The P343-391 region was previously proposed to be MuV P_{NBD} by analogy to other P proteins. P343-391 may be a molten globule since its crystallization required the addition of stabilizing agents (7). On the other hand, the protein expression data did point to a potential linker between P_{OD} and the C-terminal domain to be from residue 277 to 286. This could suggest that the C-terminal domain of MuV P is larger than previously thought. P proteins of other NSVs were reported to contain flexible regions between $P_{N°D}$, P_{OD}, and P_{NBD} (1, 21, 36, 38-43).

Crystallization studies clearly defined that MuV P_{OD} comprises residues 213-277 when P161-277 was used in crystal growth. The structure of MuV P_{OD} was determined and

shows a stable tetramer containing one pair of long parallel α-helices (64 residues) and a second pair of parallel helices in opposite orientation. The presence of P tetramers in solution was confirmed by analytical ultracentrifugation and crosslinking with glutaraldehyde (Figure 5). The unique organization of this tetrameric coiled-coil where parallel helices are joined with antiparallel helices has not been reported for a native protein before. In this distinctive assembly, interactions between the parallel helices are different from those between the antiparallel helices. By contrast, interactions between any neighboring pair of helices are identical in an all parallel or all antiparallel coiled-coil. The helices in the MuV P_{OD} tetramer are held together by a large hydrophobic contact area between each monomer (Table 2) and two zippers of charged sidechain interactions (Figure 4). This interesting orientation of antiparallel helices places the N-terminal and the C-terminal regions at both ends of MuV P_{OD}. This particular structure may well suit the functional requirements of MuV P as discussed below.

We have shown that P binds the full length MuV NLP and truncated NLP_{379}. These observations confirm that the P binding site in the MuV nucleocapsid does not fully require the N-tail, same as previously reported (4). In lieu of the apparent dispensability of this N-tail, nucleocapsid binding by MuV P may involve several regions of both N and P. Given this and the novel structure of MuV Pod, P may well be different from other NSV Ps in binding the nucleocapsid. With this open-minded approach, His-tagged fragments covering the full range of MuV P were tested for binding a well prepared NLP composed of 13 N subunits and a piece of random RNA as previously described (26). In the His-tag pulldown assays, full-length MuV P and the previously identified C-terminal domain, P343-391, were shown to bind NLP as expected. What was unexpected is that the N-terminal region of MuV P from

residues 1 to 194 could also bind NLP. This indicates that specific nucleocapsid binding may require both the N-terminal and the C-terminal regions of MuV P, a binding mode that is different from all other known NSV Ps. The NLP binding by the N-terminal and C-terminal regions was confirmed by surface plasmon resonance experiments. This analysis showed that the C-terminal region of P has a higher affinity for NLP. When the N-tail was removed by trypsin digestion (NLP_{379}), the C-terminal region of P still binds NLP_{379} with a lower affinity. The affinity of binding NLP_{379} by the C-terminal region of P is similar as that of the N-terminal region of P binding to the full length NLP. These observations suggest that the C-terminal region of P interacts with the N-tail and additional regions of N, and the N-terminal region of P interacts with regions of N not including the N-tail. However, there is a 10.7-fold increase in binding NLP_{379} by the N-terminal region of P versus the full length NLP. This increase could point to the accessibility of the N^0 binding site for P upon removal of the N-tail. Evidence shows that this site is located in the RNA cavity for other N proteins (11, 36, 37). The N^0 binding motif of P could potentially bind in this site if encapsidated RNA was displaced from NLP_{379}. The overall affinity of the full length P for NLP is lower than that of the individual domains. The affinity values for the full length tetrameric P may be underestimated because the NLP is representative of a single turn of the helical nucleocapsid and thus does not have the multiple binding sites available in the helical nucleocapsid (described below). In addition, the full length P was not very stable in solution.

Comparisons of known structures of P uncovered three modes of P oligomerization (Figure 3B-E). In the SeV P tetramer, oligomerization results in a coiled-coil structure of four long parallel α–helices (21). Similarly, the subunits in the VSV P dimer are also parallel to each other even though the β–sheet on each side is formed by domain swapping (19). The

parallel orientation of P subunits in the oligomers places the N-terminal regions on one end and the C-terminal regions on the other. Since specific nucleocapsid binding in these viruses requires only the C-terminal region of P, the N-terminal region may be placed far away from the C-terminal region. In the RABV P dimer, however, the N-terminal and C-terminal regions are each positioned at the same end due to the U-shaped structure that links two antiparallel helices in each P_{OD} subunit (20). There is no indication that the N-terminal region of RABV P is involved in binding the nucleocapsid. It is not clear what functional implications this particular orientation of RABV P has. MuV P represents a third mode of oligomerization in which parallel and antiparallel P subunits are associated together to form a tetramer. In the MuV P tetramer, the dimensions of the helix bundle are similar to those of the coiled-coil structure of the SeV P tetramer, but the orientations of the helices is different. The antiparallel orientation of the MuV P subunits places two N terminal regions and two C-terminal regions on each end of the tetramer. This organization may be functionally required because both the N-terminal and C-terminal regions of P are involved in binding the nucleocapsid as shown in this report. The two terminal regions should be in close proximity to each other in order to effectively bind the nucleocapsid. The full P binding sites for each terminal regions in the nucleocapsid remain to be identified for MuV. The results shown in Figure 6 and 7 suggest that there are P binding sites within residues 1-379 in addition to the C-terminal tail of N. This mode of binding requires that P bind at least two or more N subunits either in the same turn or in successive turns in the helical nucleocapsid. Since the conserved sequences for initiation of replication (PrE I and II) are located in two successive turns of the nucleocapsid (44) it is possible that P plays a role in recognition of the two sites by the viral RdRp. Our results again demonstrated that NSV P proteins all have a modular

structure with separated functional domains and are present as oligomers (Figure 8). While NSV P proteins harbor analogous functions, each may have very different domain organization, and can interact with other viral proteins, especially the nucleocapsid, in a very different manner.

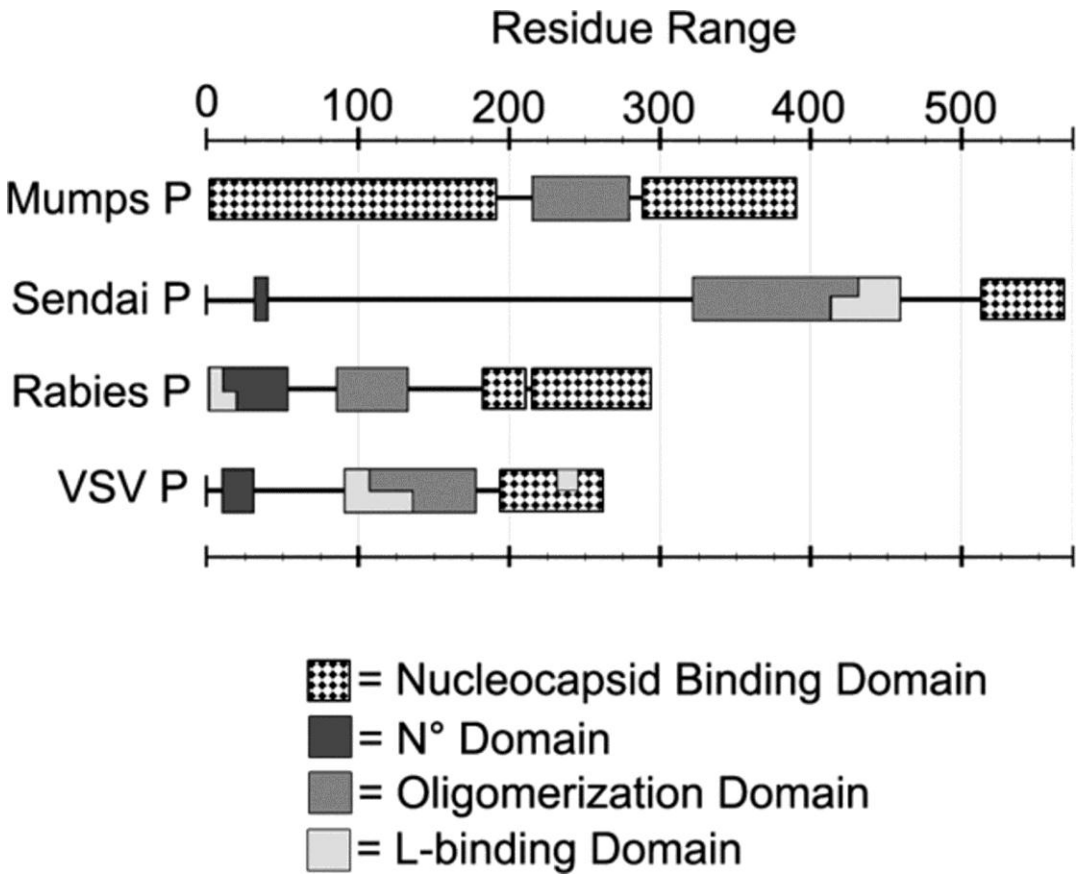

Fig 8. Diagram of the domain organization for four different NSV Ps. P_{OD} is typically located in the central region of P. PN°D and P_{NBD} are linked to P_{OD} through flexible loops. This appears to be a common modular structure for all NSV P proteins.

ACKNOWLEDGMENTS

We thank the staff of the South East Regional Collaborative Access Team (SER-CAT) at the Advanced Photon Source (APS), Argonne National Laboratory, for their assistance in data collection. Use of the Advanced Photon Source was supported by the U. S. Department of Energy, Office of Science, Office of Basic Energy Sciences, under Contract No. W-31-109-Eng-38. SER-CAT supporting institutions may be found at www.ser-cat.org/members.html.

We thank the generosity of the staff at the Stanford Synchrotron Radiation Lightsource (SSRL). "Portions of this research were carried out at the SSRL, a national user facility operated by Stanford University on behalf of the U.S. Department of Energy, Office of Basic Energy Sciences. The SSRL Structural Molecular Biology Program is supported by the Department of Energy, Office of Biological and Environmental Research and by the National Institutes of Health, National Center for Research Resources, Biomedical Technology Program, and the National Institute of General Medical Sciences." The work is supported in part by a NIH grant to ML (AI050066).

REFERENCES

1. **Takacs AM, Das T, Banerjee AK.** 1993. Mapping of interacting domains between the nucleocapsid protein and the phosphoprotein of vesicular stomatitis virus by using a two-hybrid system. Proc Natl Acad Sci U S A **90:**10375-10379.
2. **Toriumi H, Honda Y, Morimoto K, Tochikura TS, Kawai A.** 2002. Structural relationship between nucleocapsid-binding activity of the rabies virus phosphoprotein (P) and exposure of epitope 402-13 located at the C terminus. J Gen Virol **83:**3035-3043.
3. **Ryan KW, Portner A.** 1990. Separate domains of Sendai virus P protein are required for binding to viral nucleocapsids. Virology **174:**515-521.
4. **Kingston RL, Baase WA, Gay LS.** 2004. Characterization of nucleocapsid binding by the measles virus and mumps virus phosphoproteins. J Virol **78:**8630-8640.
5. **Assenberg R, Delmas O, Ren J, Vidalain PO, Verma A, Larrous F, Graham SC, Tangy F, Grimes JM, Bourhy H.** 2010. Structure of the nucleoprotein binding domain of Mokola virus phosphoprotein. J Virol **84:**1089-1096.
6. **Gely S, Lowry DF, Bernard C, Jensen MR, Blackledge M, Costanzo S, Bourhis JM, Darbon H, Daughdrill G, Longhi S.** 2010. Solution structure of the C-terminal X domain of the measles virus phosphoprotein and interaction with the intrinsically disordered C-terminal domain of the nucleoprotein. J Mol Recognit **23:**435-447.
7. **Kingston RL, Gay LS, Baase WS, Matthews BW.** 2008. Structure of the nucleocapsid-binding domain from the mumps virus polymerase; an example of protein folding induced by crystallization. J Mol Biol **379:**719-731.
8. **Ribeiro EA, Jr., Favier A, Gerard FC, Leyrat C, Brutscher B, Blondel D, Ruigrok RW, Blackledge M, Jamin M.** 2008. Solution structure of the C-terminal nucleoprotein-RNA binding domain of the vesicular stomatitis virus phosphoprotein. J Mol Biol **382:**525-538.
9. **Blanchard L, Tarbouriech N, Blackledge M, Timmins P, Burmeister WP, Ruigrok RW, Marion D.** 2004. Structure and dynamics of the nucleocapsid-binding domain of the Sendai virus phosphoprotein in solution. Virology **319:**201-211.
10. **Green TJ, Luo M.** 2009. Structure of the vesicular stomatitis virus nucleocapsid in complex with the nucleocapsid-binding domain of the small polymerase cofactor, P. Proc Natl Acad Sci U S A **106:**11713-11718.
11. **Chen M, Ogino T, Banerjee AK.** 2007. Interaction of vesicular stomatitis virus P and N proteins: identification of two overlapping domains at the N terminus of P that

are involved in N0-P complex formation and encapsidation of viral genome RNA. J Virol **81:**13478-13485.
12. **Qanungo KR, Shaji D, Mathur M, Banerjee AK.** 2004. Two RNA polymerase complexes from vesicular stomatitis virus-infected cells that carry out transcription and replication of genome RNA. Proc Natl Acad Sci U S A **101:**5952-5957.
13. **Mavrakis M, Mehouas S, Real E, Iseni F, Blondel D, Tordo N, Ruigrok RW.** 2006. Rabies virus chaperone: identification of the phosphoprotein peptide that keeps nucleoprotein soluble and free from non-specific RNA. Virology **349:**422-429.
14. **Majumdar A, Bhattacharya R, Basak S, Shaila MS, Chattopadhyay D, Roy S.** 2004. P-protein of Chandipura virus is an N-protein-specific chaperone that acts at the nucleation stage. Biochemistry **43:**2863-2870.
15. **Mir MA, Panganiban AT.** 2006. Characterization of the RNA chaperone activity of hantavirus nucleocapsid protein. J Virol **80:**6276-6285.
16. **Leyrat C, Yabukarski F, Tarbouriech N, Ribeiro EA, Jr., Jensen MR, Blackledge M, Ruigrok RW, Jamin M.** 2011. Structure of the vesicular stomatitis virus N-P complex. PLoS Pathog **7:**e1002248.
17. **Chen M, Ogino T, Banerjee AK.** 2006. Mapping and functional role of the self-association domain of vesicular stomatitis virus phosphoprotein. J Virol **80:**9511-9518.
18. **Ding H, Green TJ, Luo M.** 2004. Crystallization and preliminary X-ray analysis of a proteinase-K-resistant domain within the phosphoprotein of vesicular stomatitis virus (Indiana). Acta Crystallogr D Biol Crystallogr **60:**2087-2090.
19. **Ding H, Green TJ, Lu S, Luo M.** 2006. Crystal structure of the oligomerization domain of the phosphoprotein of vesicular stomatitis virus. J Virol **80:**2808-2814.
20. **Ivanov I, Crepin T, Jamin M, Ruigrok RW.** 2010. Structure of the dimerization domain of the rabies virus phosphoprotein. J Virol **84:**3707-3710.
21. **Tarbouriech N, Curran J, Ruigrok RW, Burmeister WP.** 2000. Tetrameric coiled coil domain of Sendai virus phosphoprotein. Nat Struct Biol **7:**777-781.
22. **Curran J, Homann H, Buchholz C, Rochat S, Neubert W, Kolakofsky D.** 1993. The hypervariable C-terminal tail of the Sendai paramyxovirus nucleocapsid protein is required for template function but not for RNA encapsidation. J Virol **67:**4358-4364.
23. **Longhi S, Receveur-Brechot V, Karlin D, Johansson K, Darbon H, Bhella D, Yeo R, Finet S, Canard B.** 2003. The C-terminal domain of the measles virus nucleoprotein is intrinsically disordered and folds upon binding to the C-terminal moiety of the phosphoprotein. J Biol Chem **278:**18638-18648.
24. **Houben K, Marion D, Tarbouriech N, Ruigrok RW, Blanchard L.** 2007. Interaction of the C-terminal domains of sendai virus N and P proteins: comparison of polymerase-nucleocapsid interactions within the paramyxovirus family. J Virol **81:**6807-6816.
25. **Mavrakis M, McCarthy AA, Roche S, Blondel D, Ruigrok RW.** 2004. Structure and function of the C-terminal domain of the polymerase cofactor of rabies virus. J Mol Biol **343:**819-831.
26. **Cox R, Green TJ, Qiu S, Kang J, Tsao J, Prevelige PE, He B, Luo M.** 2009. Characterization of a mumps virus nucleocapsidlike particle. J Virol **83:**11402-11406.

27. **Cole C, Barber JD, Barton GJ.** 2008. The Jpred 3 secondary structure prediction server. Nucleic Acids Res **36:**W197-201.
28. **Brunger AT, Adams PD, Clore GM, DeLano WL, Gros P, Grosse-Kunstleve RW, Jiang JS, Kuszewski J, Nilges M, Pannu NS, Read RJ, Rice LM, Simonson T, Warren GL.** 1998. Crystallography & NMR system: A new software suite for macromolecular structure determination. Acta Crystallogr D Biol Crystallogr **54:**905-921.
29. **Adams PD, Afonine PV, Bunkoczi G, Chen VB, Davis IW, Echols N, Headd JJ, Hung LW, Kapral GJ, Grosse-Kunstleve RW, McCoy AJ, Moriarty NW, Oeffner R, Read RJ, Richardson DC, Richardson JS, Terwilliger TC, Zwart PH.** 2010. PHENIX: a comprehensive Python-based system for macromolecular structure solution. Acta Crystallogr D Biol Crystallogr **66:**213-221.
30. **Emsley P, Lohkamp B, Scott WG, Cowtan K.** 2010. Features and development of Coot. Acta Crystallogr D Biol Crystallogr **66:**486-501.
31. **Painter J, Merritt EA.** 2005. A molecular viewer for the analysis of TLS rigid-body motion in macromolecules. Acta Crystallogr D Biol Crystallogr **61:**465-471.
32. **Painter J, Merritt EA.** 2006. Optimal description of a protein structure in terms of multiple groups undergoing TLS motion. Acta Crystallogr D Biol Crystallogr **62:**439-450.
33. **Schrodinger, LLC.** 2010. The PyMOL Molecular Graphics System, Version 1.3r1.
34. **Green TJ, Macpherson S, Qiu S, Lebowitz J, Wertz GW, Luo M.** 2000. Study of the assembly of vesicular stomatitis virus N protein: role of the P protein. J Virol **74:**9515-9524.
35. **Karlin D, Ferron F, Canard B, Longhi S.** 2003. Structural disorder and modular organization in Paramyxovirinae N and P. J Gen Virol **84:**3239-3252.
36. **Karlin D, Longhi S, Receveur V, Canard B.** 2002. The N-terminal domain of the phosphoprotein of Morbilliviruses belongs to the natively unfolded class of proteins. Virology **296:**251-262.
37. **Leyrat C, Jensen MR, Ribeiro EA, Jr., Gerard FC, Ruigrok RW, Blackledge M, Jamin M.** 2011. The N(0)-binding region of the vesicular stomatitis virus phosphoprotein is globally disordered but contains transient alpha-helices. Protein Sci **20:**542-556.
38. **Tarbouriech N, Curran J, Ebel C, Ruigrok RW, Burmeister WP.** 2000. On the domain structure and the polymerization state of the sendai virus P protein. Virology **266:**99-109.
39. **Choudhary SK, Malur AG, Huo Y, De BP, Banerjee AK.** 2002. Characterization of the oligomerization domain of the phosphoprotein of human parainfluenza virus type 3. Virology **302:**373-382.
40. **Rahaman A, Srinivasan N, Shamala N, Shaila MS.** 2004. Phosphoprotein of the rinderpest virus forms a tetramer through a coiled coil region important for biological function. A structural insight. J Biol Chem **279:**23606-23614.
41. **Llorente MT, Garcia-Barreno B, Calero M, Camafeita E, Lopez JA, Longhi S, Ferron F, Varela PF, Melero JA.** 2006. Structural analysis of the human respiratory syncytial virus phosphoprotein: characterization of an alpha-helical domain involved in oligomerization. J Gen Virol **87:**159-169.

42. **Gerard FC, Ribeiro Ede A, Jr., Albertini AA, Gutsche I, Zaccai G, Ruigrok RW, Jamin M.** 2007. Unphosphorylated rhabdoviridae phosphoproteins form elongated dimers in solution. Biochemistry **46:**10328-10338.
43. **Gerard FC, Ribeiro Ede A, Jr., Leyrat C, Ivanov I, Blondel D, Longhi S, Ruigrok RW, Jamin M.** 2009. Modular organization of rabies virus phosphoprotein. J Mol Biol **388:**978-996.
44. **Kolakofsky D, Roux L, Garcin D, Ruigrok RW.** 2005. Paramyxovirus mRNA editing, the "rule of six" and error catastrophe: a hypothesis. J Gen Virol **86:**1869-1877.

STRUCTURAL STUDIES ON THE AUTHENTIC MUMPS VIRUS NUCLEOCAPSID SHOWING UNCOILING BY THE PHOSPHOPROTEIN

by

ROBERT COX, SHIHONG QIU, JUN TSAO, CYNTHIA M. RODENBURG, TERJE DOKLAND, BIAO HE, AND MING LUO

In preparation for *Journal of Virology*

Format adapted for dissertation

ABSTRACT

Mumps virus (MuV) is a highly contagious pathogen, and despite massive vaccinations, outbreaks continue to occur worldwide. The virus has a negative-sense, single-stranded RNA genome that is encapsidated by the nucleocapsid protein (N) to form the nucleocapsid (NC). NC serves as the template for both transcription and replication. In this report we solved a 18.5 Å resolution structure of the authentic MuV NC using cryo-electron microcopy. We observed the effects of phosphoprotein (P) binding on the MuV NC structure. The N-terminal domain of P (P_{NTD}) has been shown to bind NC as well and appeared to induce uncoiling of the helical NC. The location of the encapsidated viral genomic RNA was defined by modeling crystal structures of homologous N in NC. These results provide critical insights on the structure-function of the MuV NC and the structural alterations that occur through its interactions with P.

INTRODUCTION

Paramyxoviruses are enveloped non-segmented negative-strand RNA viruses (NSV) belonging to the order *Mononegavirales*. *Mononegavirales* also includes the *Bornaviridae*, *Filoviridae*, and *Rhabdoviridae* families. The *Paramyxoviridae* family includes several important human pathogens such as measles virus (MeV), respiratory syncytial virus (RSV), and mumps virus (MuV). While vaccines exist for some paramyxoviruses, they are not available for others, such as RSV. In addition, no effective antiviral treatments have been developed.

The MuV genome encodes 8 proteins, three of which are required for replication of the MuV genome; the nucleocapsid protein (N), phosphoprotein (P), and the large protein (L). N, P, and L have orthologs in a number of NSV. Studies on the roles of N, P, and L in viral RNA synthesis have shown that each can individually and differentially affect the processes of mRNA transcription and genome replication (1-10).

Throughout the virus replication cycle, the genome of NSV always exists in the nucleocapsid (NC), a unique protein-RNA complex in which the viral RNA (viral genomic RNA (vRNA) or complementary genomic RNA (cRNA)) is completely sequestered by the N protein. NC is used as the functional template for RNA synthesis by the viral RNA dependent RNA polymerase (vRdRp), which includes L and P. The L protein contains all the enzymatic activities needed for viral RNA synthesis, such as the ability to cap and

polyadenylate mRNA transcripts. P acts as a cofactor to home vRdRp onto the NC template for RNA synthesis. In addition, the P protein chaperones N to encapsidate newly synthesized viral genomes during replication. The encapsidation of RNA by N is concomitant with the replication process.

How the sequestered genomic RNA is accessed by vRdRp is not clearly known. Structures of NSV nucleocapsids and nucleocapsid-like particles (NLPs) have been solved previously (11-16). Paramyxovirus NC forms a left-handed helix even though the helical symmetry is not strictly followed due to the flexibility in NC (15, 17, 18). Based on the crystal structure of a RSV NLP, it was shown that the genomic RNA was completely sequestered between two domains (NTD and CTD) of the N protein (15, 16). Fitting the crystal structure in the cryoEM structure of RSV NC revealed that the access to the genomic RNA is blocked by the stacking of layers in the NC helix (15). The vRdRp must be able to unwind the NC helix in order to gain access to the protected genomic RNA. The viral protein that plays this role is P. In vesicular stomatitis virus (VSV) of the *Rhabdoviridae* family that is closely related to paramyxoviruses, NC also forms a left-handed helix when packaged in the virion (19). In the infected cell, however, VSV NC does not retain a helical structure, although the genomic RNA is still sequestered in the nucleocapsid, according to the crystal structure (12). It has been shown that the C-terminal domain of VSV P (P_{CTD}) binds at the interface of two CTDs from neighboring parallel N subunits (20). Binding of P_{CTD} allows vRdRp to specifically recognize NC and to be positioned directly at the gate to the sequestered genomic RNA. Binding between the extreme domain of MeV/Sendai virus (SeV) P, PX, and a helix in the N-terminal region of MeV/SeV N has also been demonstrated (21, 22). This interaction may represent a portion of the overall contact area between N and P_{CTD},

but nevertheless it supports the notion that paramyxovirus P_{CTD} also plays a role in bringing vRdRp to the gate of the sequestered genomic RNA. At the same time, it is likely that additional interactions may be required to unwind the helical NC of paramyxoviruses for efficient viral RNA synthesis. The L protein in vRdRp may play such a role once it is brought to NC by P_{CTD}, or it is possible that other regions in P can help to unwind NC. In our recent studies, it was shown that the N-terminal domain of MuV P (P_{NTD}) also binds NC (23). MuV P forms a unique tetramer in which two P molecules are associated with two P molecules that have the opposite orientation, placing two P_{NTD} and two P_{CTD} at each end of the P tetramer. This novel orientation of P molecules allows P_{NTD} and P_{CTD} to bind NC simultaneously, a unique observation not reported for other paramyxoviruses.

In this report, we determined the three dimensional structure of the authentic MuV NC alone, and observed the effects of different modes of MuV P binding. More importantly, we showed that NC binding by MuV P_{NTD} uncoils NC. These studies have provided insights into how MuV P associates with NC and what changes are induced by P binding.

MATERIALS AND METHODS

VIRUS AND CELLS

Vero cells were grown in complete media (CM), (DMEM supplemented with 10% fetal bovine serum (FBS), 1X glutamine, and 1% penicillin-streptomycin). Cells were cultured at 37 °C with 5% CO_2. MuV strain Iowa (MuV-IA) was used in our studies.

VIRUS PROPAGATION

For infections, MuV-IA stock was diluted in PBS with 10% CM. Cells of approximately 70% confluence were infected with MuV-IA at an MOI=0.01. At 96 hours post infection, or when maximum syncytia formation occurred, the supernatant containing MuV virions was collected.

PLAQUE ASSAYS

Vero cells were grown to approximately 70% confluent. Media was removed and cells were inoculated with serial dilutions of MuV. After incubation at 37 °C for 1 hour, media was removed and a 1:1:1 mixture of 2X DMEM, CM, and 1.5% agarose was added to

monolayers and allowed to solidify. Six days later, cells were fixed with 4% formaldehyde and stained with 1% crystal violet.

PURIFICATION OF NC FROM INFECTED CELLS

Vero cells were infected at 37 °C with MuV-IA at MOI=0.01. At 24 hours post infection, media was changed and the temperature was decreased from 37 °C to 30 °C. At 96 hours post infection, or when maximum syncytia formation occurred, cells were harvested and lysed by freezing-thawing. The cell lysate was then centrifuged in a SW 41 rotor on a continuous 20-40% CsCl gradient for 18 hrs at 32,000 rpm. Following centrifugation, the gradients were fractioned and analyzed using SDS-PAGE.

PURIFICATION OF AUTHENTIC NC FROM VIRIONS

MuV-IA harvest was centrifuged over a 20% sucrose cushion in a SW28 rotor at 28,000rpm for 1.5 hours. The pellet was then resuspended in TNE (10 mM Tris; 200 mM NaCl; 1 mM EDTA; pH 7.4) with 1% Triton X-100 in order to disrupt the virions. The preparation was then centrifuged in a SW 41 rotor on a continuous 20-40% CsCl gradient for 18 hours at 32,000 rpm. Fractions containing purified nucleocapsids were analyzed by SDS-PAGE.

PROTEIN EXPRESSION AND PURIFICATION

Expression vectors were transformed into *Escherichia coli* strain BL21(DE3). The P fragments P_{CTD} (residues 286-391) and P_{NTD} (residues 1-194) were expressed and purified using Ni-affinity chromatography as previously reported (23). Proteins were further purified by size-exclusion chromatography (Sephacryl S-75 or S-200; GE Healthcare) in TNE.

ELECTRON MICROSCOPY OF AUTHENTIC MUV NUCLEOCAPSIDS

The purified nucleocapsids (1 mg/ml) were placed on carbon coated mesh grids and stained with 2% uranyl acetate or 2% phosphotungstic acid. In order to image NC-P complexes, NC was allowed to incubate with excess amounts of either P_{CTD} or P_{NTD} prior to collecting images. Images were taken on a FEI Tecnai F20 electron microscope with a Gatan Ultrascan 4000 digital camera. For frozen hydrated images, the NC sample was added to a freshly glow-discharged quantifoil holey carbon grid (R2/2; Quantifoil Micro Tools GmbH, Germany). Grids were then blotted and plunged into liquid ethane using a VitroBot (FEI). CryoEM was done on an FEI Tecnai F20 electron microscope equipped with a Gatan 626 cryo-sample holder and images were collected under low-dose conditions.

RNASE TREATMENT

Purified MuV NC was incubated with and without RNase A (0.5 mg/ml) at 37 °C overnight. Absorbance measurements were carried out at 260nm and 280nm using a NanoDrop 2000 (ThermoScientific).

IMAGE ANALYSIS

Micrographs were selected for image processing based on optimal defocus, ice thickness and astigmatism. CTF correction and three-dimensional reconstructions were performed using the iterative helical real space reconstruction approach (IHRSR) using the SPARX/EMAN2 package (24-26). Resolution was determined by splitting the data into two equal sets and comparing unsymmetrized reconstructions with a Fourier shell correlation of 0.5.

RESULTS

PREPARATION OF MUV NUCLEOCAPSID

It has been previously reported that a significant amount of NC remains in the infected cells (27). In order to obtain cell-associated NC, infected cells were scraped and lysed by freezing and thawing. The cell lysate was then purified on a continuous 20-40% CsCl gradient. A clear band was visible in the gradient after centrifugation. Fractions containing the presumed NC were analyzed by SDS-PAGE. The N protein in this preparation appeared smaller than that in NC isolated from virions (Figure 1, lane 2). Interestingly, it was approximately the same size as the N fragment in the truncated NLP, NLP_{379}, from our previous report (23). This sample was not used in any further studies.

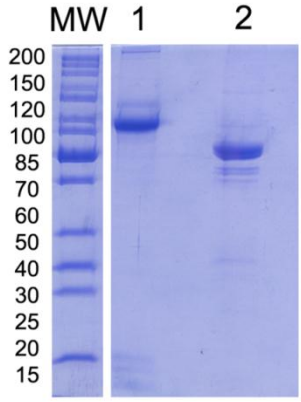

Figure 1. SDS-PAGE of MuV NC preparations. SDS-PAGE analysis of MuV derived NC is shown in Lane 1. The NC isolated from infected cells is shown in Lane 2. The cell derived nucleocapsid migrated at a lower molecular weight than NC derived from virus. The molecular weight ladder is shown in the MW lane.

NC was also purified from detergent treated MuV virions. SDS-PAGE analysis of the material that banded in the CsCl gradient showed a single protein component with a molecular mass corresponding to that of MuV N (60 kDa; Figure 1, lane 1). Unlike the sample purified from infected cells, the virion associated NC has the correct molecular mass and did not suffer from any degradation. The purified sample had a ratio of the absorbance at 260 nm over 280 nm equal to 1.6 (Table 1), and was presumed to be the MuV NC. Fractions containing the purified NC were then concentrated and imaged using negative stain electron microscopy (EM) and cryo-EM.

Table 1. 260/280 Ratios

Sample ID	**260/280**
No RNase A; O/N incubation 37°C	1.17
No RNase A on ice (just purified NC)	1.6
RNase A Treated at time=0	1.37
RNase A treated at time= O/N incubation at 37°C	0.73

RNASE A TREATMENT

Purified NC was incubated with RNase A overnight at 37 °C. 260/280 ratios were recorded before and after incubation. The 260/280 ratios are shown in Table 1. Overnight incubation with RNase A was sufficient to significantly lower the 260/280 ratio, indicating the generation of an empty NC by removal of the encapsidated RNA. This is in agreement with previous observations using MuV NLP (28).

IMAGING OF AUTHENTIC VIRAL NUCLEOCAPSIDS

Images of purified MuV NC by negative stain electron microscopy and cryo-EM showed the classic "herringbone" structure of the typical paramyxovirus NC (Figure 2a). Average diameter and pitch values are listed in Table 2. Images were also taken of MuV NC in the

Table 2. Average Measurements of MuV NC.

Sample	**Stain**	**Pitch**	**Diameter**
NC	cryo	Average: 64.8 Å	Average: 240 Å
		Range: 55-73 Å	Range: 233-249 Å
NC	negative	Average: 58.7 Å	Average: 240 Å
		Range: 53-69 Å	Range: 226-262
NC- P_{CTD}	negative	Average: 70 Å	Average: 294 Å
		Range: 60-83 Å	Range: 276-311
Emtpy NC	negative	Average: 68 Å	Average: 242 Å
		Range: 59-75 Å	Range: 230-257 Å

presence of two different P fragments, each containing a different NBD (23). P_{NTD} appeared to induce the helical NC to uncoil. A large number of unwound NC was observed in negatively stained images (Figure 2b). P_{CTD} did not induce obvious uncoiling of NC. However, there was a clear difference between NC with and without P_{CTD} (Figure 2c). In the presence of P_{CTD}, NC appeared wider and to be decorated by densities presumed to correspond to P_{CTD}. Additionally, negatively stained images of the empty NC showed that the empty NC appeared more flexible than NC containing RNA (Figure 2d). However, due to the

higher flexibility of NC-P_{CTD} the empty NC, no high quality reconstructions could be resolved.

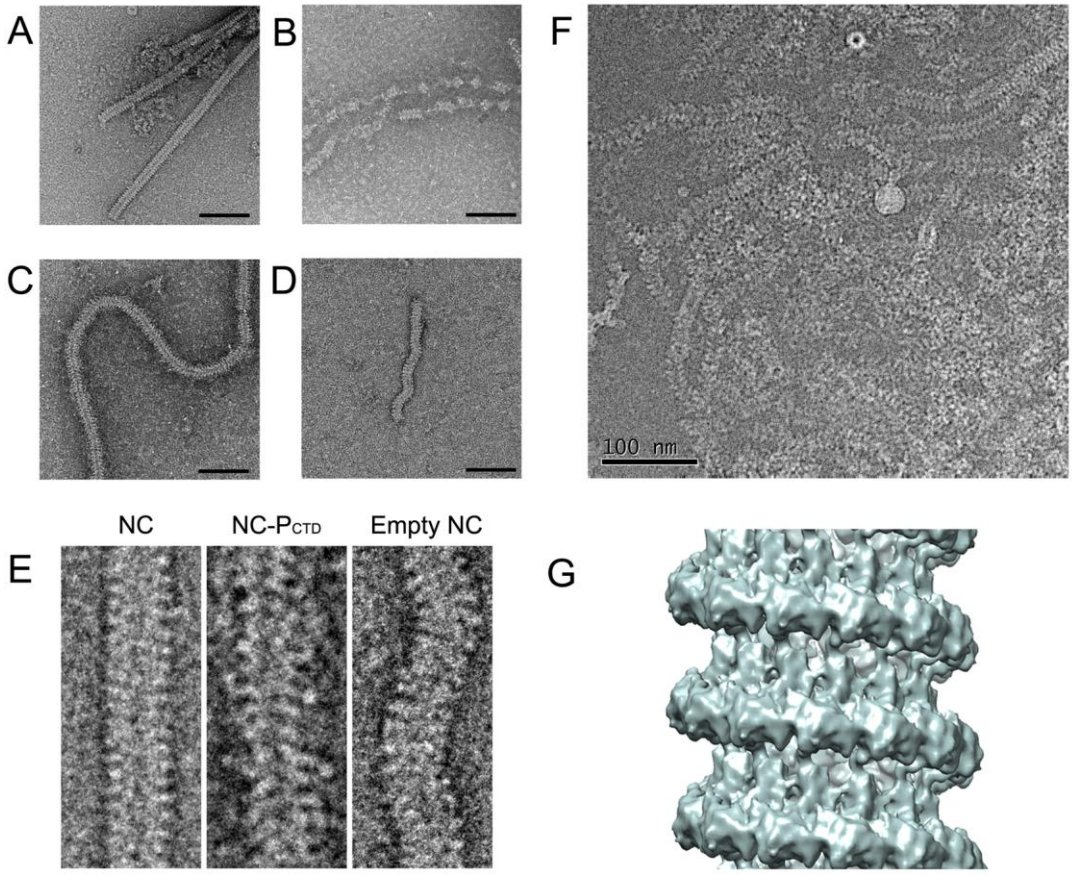

Figure 2. Negatively stained images. Negatively stained images of the MuV NC were taken under several conditions. (A) Purified MuV NC. (B) MuV NC in the presence of P1-194. The N-terminal domain of P appeared to induce uncoiling of the helical NC. (C) MuV NC in association with P_{CTD}. The presence of the C-terminal domain of P did not induce uncoiling of the helical nucleocapsid. However, based upon negatively stained images, the average diameter of NC increased, as did the range and variability of pitch values. (D) RNase A treated "empty" NC appeared more flexible than NC containing RNA. (E) Closer views of the NC helices from purified NC (left), NC with the C-terminus of P (center), and RNase A treated NC (right). (F) CryoEM image of the MuV NC. (G) CryoEM reconstruction of the MuV NC. The structure of the MuV NC is presented at sigma level = 2.2 (29).The helical reconstruction of the MuV NC is a left handed helix with 12.67 N subunits per turn. Each N subunit has a rise of 5.32 Å and an azimuthal angle of -28.42°. Resolution was estimated to be 18.5 Å using FSC = 0.5.

THREE DIMENSIONAL RECONSTRUCTIONS

For the cryoEM reconstruction, a total of 682 images of MuV NC helices were boxed from micrographs. CTF correction and class averaging were performed using the EMAN2 package. The IHRSR method was used to create three dimensional reconstructions of the MuV NC. Class averages of NC were used to determine initial symmetry values such as rise per subunit and azimuthal angle of N. After 50 rounds of helical refinement, symmetry values stabilized. The resulting structure of the MuV NC revealed a typical left handed helix with 12.67 N subunits per helical turn and a rise of 5.32 Å per N subunit (Figure 2g). Resolution was determined to be 18.5 Å using FSC=0.5. Atomic models of VSV N (PDB Code: 2GIC) and RSV N (PDB Code: 2wj8) were then fit into the MuV NC using Chimera (Figure 3a-d) (29).These models confirmed that MuV N possesses the typical NSV N architecture consisting of two core domains, the N-terminal domain (NTD) and the C-terminal domain (CTD). The location of the encapsidated RNA was approximated by fitting the structures of RSV and VSV into the MuV NC (Figure 3e).

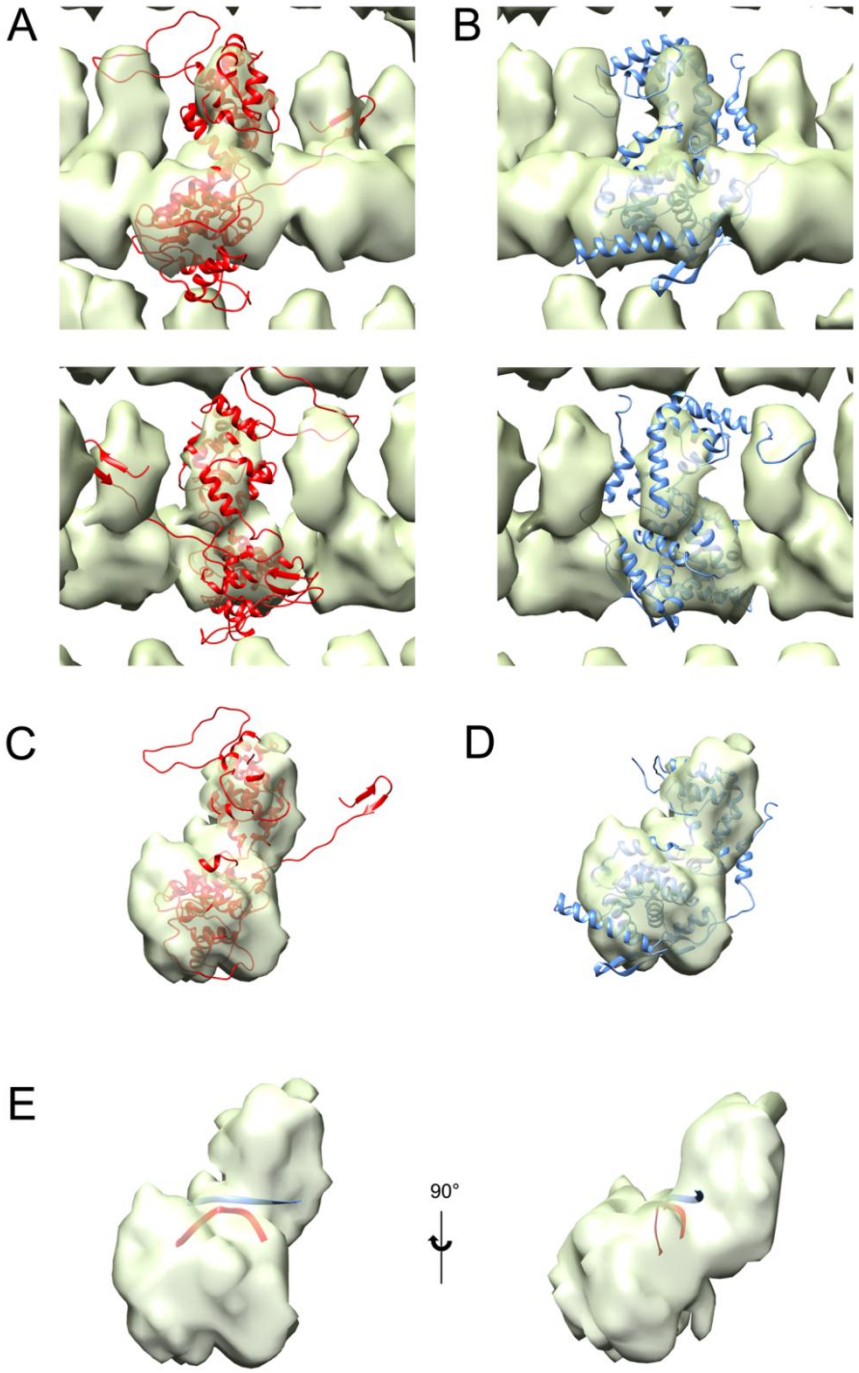

Figure 3. Comparison of MuV NC to other NSV N. Comparisons of MuV N to other NSV N was made by fitting the atomic models of VSV N (A) and RSV N (B) into the MuV NC structure. The crystal structures were drawn as ribbons (30). MuV N appears to share the typical structure as other NSV N, consisting of two core domains; NTD (bottom) and CTD (top). The structure of the MuV NC is presented at a sigma level of 2.28 and 1.82 for A-B and C-E, respectively (29) (C) The approximate location of the encapsidated RNA was determined by fitting the structures of RSV N (blue string) and VSV N (red string) into the MuV NC. The viral RNA is sequestered between NTD and CTD.

DISCUSSION

Currently, the only available structures of authentic paramyxovirus NCs are low-resolution 3D reconstructions due to their flexibility. On the other hand, the atomic structures of several NSV NLPs (N-RNA complexes) have been solved using x-ray crystallography. These include VSV N, Rabies Virus (RABV) N, and RSV N (12, 14, 16). N monomers are composed of two main domains, NTD and CTD. When the crystal structures of the RSV N-RNA complex is fitted in the cryoEM structure of RSV NC, it is shown that the encapsidated RNA runs along a cavity formed at the NTD/CTD interface throughout NC. Both NTD and CTD make lateral interactions with adjacent N subunits. Additionally, each NTD/CTD core has N- and/or C-terminal extensions, termed N-arm and C-loop (or C-arm), respectively, that stabilize NC.

Similar to the MuV NC, structural studies on the NCs of MeV and Sendai virus (SeV) revealed a left handed helical structure with about 13 subunits of N per helical turn, but with high variablility (11, 13, 17). This flexibility may be due to a lack of top-bottom interactions between successive helical turns and a variable nonintegral number of N subunits per turn. The strong lateral interactions between the N subunits maintain the linear integrity of NC. The extent of these interactions varies from virus to virus (12). Similar to other paramyxovirus NCs, MuV NC displayed a considerable amount of flexibility. Average pitch values for MuV NC were 65 Å and 58 Å for frozen hydrated and negatively stained NC,

respectively. Pitch measurements for RSV NC range from 68 Å to 74 Å (15, 16). Similar variability in pitch was also observed for MeV NC and SeV NC (11, 13, 17). With the association of P_{CTD}, average MuV NC pitch measurements increased (Table 2), as did the range and variability of values. The average diameter of MuV NC was 240 Å for both frozen hydrated and negatively stained NC. RSV NC seems to be narrower than MuV NC, measuring between 140 Å and 160 Å in diameter. Moreover, the diameters of SeV NC and MeV are approximately 200 Å, making MuV NC larger than previously studied paramyxovirus NCs. MuV NC- P_{CTD} helices had an average diameter of 287 Å and 294 Å for frozen hydrated and negatively stained NC, respectively. The images of MuV NC-P_{CTD} provide insightful details into the structural changes that accompany P_{CTD} binding to NC. NC- P_{CTD} helices were significantly wider than NC alone, but NC still maintains the helical symmetry. Interestingly, RSV P was shown to bind the C-arm of N (31, 32) In NLP structures, the C-loop/-arm is located in what would be between consecutive turns of the helical NC. The C-loop/-arm may play a role in top-bottom interactions between N subunits on consecutive layers in the helical NC. The interaction between P_{CTD} and NC may allow vRdRp to distort the helical conformation of the NC during RNA synthesis.

The most revealing result of this study is the observation that MuV P_{NTD} appeared to induce the helical NC to uncoil. Prior to being incorporated into the NC, N exists as a monomeric protein (N^0). For VSV and RABV, N^0 is kept monomeric and RNA-free by P, forming a stable complex composed of a single N subunit and a dimer of P (33, 34). The N-terminus of VSV P interacts with the back of the C-lobe of N and the RNA cavity. The N-terminus of RSV P is also required for N^0-P binding (35). P binding can block the lateral contacts between N subunits to prevent NC oligomerization. Once encapsidation occurs the

N^0 oligomerizes and P is free to chaperone another N^0. The N-terminus of P has not been shown to bind NC previously. In our previous studies, we showed that MuV P forms a tetramer with one pair of P molecules associated with each other in a parallel manner, and another pair of parallel P molecules in the opposite orientation. The novel mode of MuV P tetramer association places both P_{NTD} and P_{CTD} at each end of the P tetramer. We hypothesize that P_{NTD} and P_{CTD} act in concert to induce changes in NC for viral RNA synthesis by vRdRp (Figure 4). The primary role of P_{CTD} is to allow vRdRp to specifically recognize NC, similar as P_{CTD} in other P proteins. On the other hand, P_{NTD} primarily uncoils MuV NC to expose the "gate" to the sequestered genomic RNA. The two functions position vRdRp perfectly at the site in NC for viral RNA synthesis. To uncoil NC, P_{NTD} binding may alter the curvature of N-N interactions within the NC so the helical symmetry is completely disrupted.

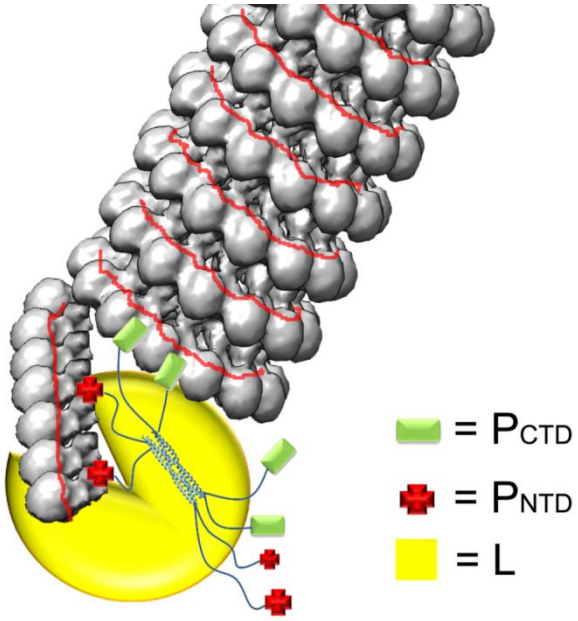

Figure 4. Illustration of the NC-P-L replication complex. The unique orientation of the MuV P tetramer places both P_{NTD} and P_{CTD} at each end of the P tetramer. We hypothesize that P_{NTD} and P_{CTD} act together to induce changes in NC for viral RNA synthesis by vRdRp. The primary role of P_{CTD} is to target the vRdRp specifically to the NC. P_{NTD} acts primarily to uncoil the MuV NC and allow vRdRp to gain access to the sequestered genomic RNA.

The encapsidated RNA also seems to play a role in the stability of the MuV NC. Empty NC in negatively stained images appeared to be considerably more flexible than NC with RNA (Figure 2d). In previous structures, bases in the sequestered viral RNA could stack inside the cavity of the NTD and CTD core (16, 36, 37). Some of the bases stack with the aromatic sidechains of N residues. It is likely that such base stacking also exists in MuV NC, which stabilizes the structure of NC.

Major questions remain about how the polymerase complex assembles and gains access to the encapsidated RNA. The genomic RNA must be released from NC in order to be read by vRdRp. During viral RNA synthesis, NC does not completely disassemble to free the genomic RNA. vRdRp must induce a conformational change in the N subunits in order to access the encapsidated RNA. Most likely, vRdRp only exposes the sequestered RNA in a localized region in NC. After the viral polymerase complex passes, the RNA template returns to its position between the NTD and CTD cores, and the helical symmetry of NC is reestablished. In this report, we have clearly shown that significant structural changes of MuV NC occur upon P binding. These changes in NC could lead exposure of the sequestered RNA to facilitate viral RNA synthesis. P_{NTD} and P_{CTD} appear to play an important role in altering the NC during this process.

ACKNOWLEDGMENTS

This study was supported in part by a NIH grant to Ming Luo (AI050066). CryoEM was carried out at the UAB cryo-electron microscopy facility.

REFERENCES

1. **Chen JL, Das T, Banerjee AK.** 1997. Phosphorylated states of vesicular stomatitis virus P protein in vitro and in vivo. Virology **228:**200-212.
2. **Spadafora D, Canter DM, Jackson RL, Perrault J.** 1996. Constitutive phosphorylation of the vesicular stomatitis virus P protein modulates polymerase complex formation but is not essential for transcription or replication. J Virol **70:**4538-4548.
3. **Pringle CR.** 1970. Genetic characteristics of conditional lethal mutants of vesicular stomatitis virus induced by 5-fluorouracil, 5-azacytidine, and ethyl methane sulfonate. J Virol **5:**559-567.
4. **Perlman SM, Huang AS.** 1973. RNA synthesis of vesicular stomatitis virus. V. Interactions between transcription and replication. J Virol **12:**1395-1400.
5. **Wertz GW.** 1978. Isolation of possible replicative intermediate structures from vesicular stomatitis virus-infected cells. Virology **85:**271-285.
6. **Galloway SE, Wertz GW.** 2009. A temperature sensitive VSV identifies L protein residues that affect transcription but not replication. Virology **388:**286-293.
7. **Galloway SE, Wertz GW.** 2008. S-adenosyl homocysteine-induced hyperpolyadenylation of vesicular stomatitis virus mRNA requires the methyltransferase activity of L protein. J Virol **82:**12280-12290.
8. **Gao Y, Lenard J.** 1995. Cooperative binding of multimeric phosphoprotein (P) of vesicular stomatitis virus to polymerase (L) and template: pathways of assembly. J Virol **69:**7718-7723.
9. **Hwang LN, Englund N, Das T, Banerjee AK, Pattnaik AK.** 1999. Optimal replication activity of vesicular stomatitis virus RNA polymerase requires phosphorylation of a residue(s) at carboxy-terminal domain II of its accessory subunit, phosphoprotein P. J Virol **73:**5613-5620.
10. **Harouaka D, Wertz GW.** 2009. Mutations in the C-terminal loop of the nucleocapsid protein affect vesicular stomatitis virus RNA replication and transcription differentially. J Virol **83:**11429-11439.
11. **Egelman EH, Wu SS, Amrein M, Portner A, Murti G.** 1989. The Sendai virus nucleocapsid exists in at least four different helical states. J Virol **63:**2233-2243.
12. **Green TJ, Zhang X, Wertz GW, Luo M.** 2006. Structure of the vesicular stomatitis virus nucleoprotein-RNA complex. Science **313:**357-360.
13. **Schoehn G, Mavrakis M, Albertini A, Wade R, Hoenger A, Ruigrok RW.** 2004. The 12 A structure of trypsin-treated measles virus N-RNA. J Mol Biol **339:**301-312.

14. **Albertini AA, Wernimont AK, Muziol T, Ravelli RB, Clapier CR, Schoehn G, Weissenhorn W, Ruigrok RW.** 2006. Crystal structure of the rabies virus nucleoprotein-RNA complex. Science **313:**360-363.
15. **Bakker SE, Duquerroy S, Galloux M, Loney C, Conner E, Eleouet JF, Rey FA, Bhella D.** 2013. The respiratory syncytial virus nucleoprotein-RNA complex forms a left-handed helical nucleocapsid. J Gen Virol **94:**1734-1738.
16. **Tawar RG, Duquerroy S, Vonrhein C, Varela PF, Damier-Piolle L, Castagne N, MacLellan K, Bedouelle H, Bricogne G, Bhella D, Eleouet JF, Rey FA.** 2009. Crystal structure of a nucleocapsid-like nucleoprotein-RNA complex of respiratory syncytial virus. Science **326:**1279-1283.
17. **Bhella D, Ralph A, Yeo RP.** 2004. Conformational flexibility in recombinant measles virus nucleocapsids visualised by cryo-negative stain electron microscopy and real-space helical reconstruction. J Mol Biol **340:**319-331.
18. **Desfosses A, Goret G, Farias Estrozi L, Ruigrok RW, Gutsche I.** 2011. Nucleoprotein-RNA orientation in the measles virus nucleocapsid by three-dimensional electron microscopy. J Virol **85:**1391-1395.
19. **Ge P, Tsao J, Schein S, Green TJ, Luo M, Zhou ZH.** 2010. Cryo-EM model of the bullet-shaped vesicular stomatitis virus. Science **327:**689-693.
20. **Green TJ, Luo M.** 2009. Structure of the vesicular stomatitis virus nucleocapsid in complex with the nucleocapsid-binding domain of the small polymerase cofactor, P. Proc Natl Acad Sci U S A **106:**11713-11718.
21. **Longhi S, Receveur-Brechot V, Karlin D, Johansson K, Darbon H, Bhella D, Yeo R, Finet S, Canard B.** 2003. The C-terminal domain of the measles virus nucleoprotein is intrinsically disordered and folds upon binding to the C-terminal moiety of the phosphoprotein. J Biol Chem **278:**18638-18648.
22. **Houben K, Marion D, Tarbouriech N, Ruigrok RW, Blanchard L.** 2007. Interaction of the C-terminal domains of sendai virus N and P proteins: comparison of polymerase-nucleocapsid interactions within the paramyxovirus family. J Virol **81:**6807-6816.
23. **Cox R, Green TJ, Purushotham S, Deivanayagam C, Bedwell GJ, Prevelige PE, Luo M.** 2013. Structural and functional characterization of the mumps virus phosphoprotein. J Virol **87:**7558-7568.
24. **Behrmann E, Tao G, Stokes DL, Egelman EH, Raunser S, Penczek PA.** 2012. Real-space processing of helical filaments in SPARX. J Struct Biol **177:**302-313.
25. **Hohn M, Tang G, Goodyear G, Baldwin PR, Huang Z, Penczek PA, Yang C, Glaeser RM, Adams PD, Ludtke SJ.** 2007. SPARX, a new environment for Cryo-EM image processing. J Struct Biol **157:**47-55.
26. **Egelman EH.** 2007. Single-particle reconstruction from EM images of helical filaments. Curr Opin Struct Biol **17:**556-561.
27. **Moore PM, Hayes EC, Miller SE, Wright LL, Machamer CE, Zweerink HJ.** 1978. Measles virus nucleocapsids: large-scale purification and use in radioimmunoassays. Infect Immun **20:**842-846.
28. **Cox R, Green TJ, Qiu S, Kang J, Tsao J, Prevelige PE, He B, Luo M.** 2009. Characterization of a mumps virus nucleocapsidlike particle. J Virol **83:**11402-11406.

29. **Pettersen EF, Goddard TD, Huang CC, Couch GS, Greenblatt DM, Meng EC, Ferrin TE.** 2004. UCSF Chimera--a visualization system for exploratory research and analysis. J Comput Chem **25:**1605-1612.
30. **Schrodinger, LLC.** 2010. The PyMOL Molecular Graphics System, Version 1.3r1.
31. **Galloux M, Tarus B, Blazevic I, Fix J, Duquerroy S, Eleouet JF.** 2012. Characterization of a viral phosphoprotein binding site on the surface of the respiratory syncytial nucleoprotein. J Virol **86:**8375-8387.
32. **Murray J, Loney C, Murphy LB, Graham S, Yeo RP.** 2001. Characterization of monoclonal antibodies raised against recombinant respiratory syncytial virus nucleocapsid (N) protein: identification of a region in the carboxy terminus of N involved in the interaction with P protein. Virology **289:**252-261.
33. **Zhang X, Green TJ, Tsao J, Qiu S, Luo M.** 2008. Role of intermolecular interactions of vesicular stomatitis virus nucleoprotein in RNA encapsidation. J Virol **82:**674-682.
34. **Mavrakis M, Iseni F, Mazza C, Schoehn G, Ebel C, Gentzel M, Franz T, Ruigrok RW.** 2003. Isolation and characterisation of the rabies virus N degrees-P complex produced in insect cells. Virology **305:**406-414.
35. **Mallipeddi SK, Lupiani B, Samal SK.** 1996. Mapping the domains on the phosphoprotein of bovine respiratory syncytial virus required for N-P interaction using a two-hybrid system. J Gen Virol **77 (Pt 5):**1019-1023.
36. **Green TJ, Rowse M, Tsao J, Kang J, Ge P, Zhou ZH, Luo M.** 2011. Access to RNA encapsidated in the nucleocapsid of vesicular stomatitis virus. J Virol **85:**2714-2722.
37. **Raymond DD, Piper ME, Gerrard SR, Skiniotis G, Smith JL.** 2012. Phleboviruses encapsidate their genomes by sequestering RNA bases. Proc Natl Acad Sci U S A **109:**19208-19213.

DISCUSSION

MUV NLP CHARACTERIZATION

In this thesis, I have carried out the initial characterization of the MuV NLP. Coexpression of the MuV N and P proteins in *E. coli* resulted in the production of NLP with morphology similar to those seen in other NSVs. Like the NLPs of other NSVs, the MuV NLP primarily exists as a ring structure, although a small number of helical structures was observed. Similar to the MeV NLP, the MuV NLP contains 13 N subunits (54). This implies that the MuV NLP truly mimics the assembly of the paramyxovirus NC, including at least *Rubulavirus* and *Morbillivirus* families. The MuV NLP has a number of differences from the NLP of other NSVs. The size of MuV NLP is larger than most NSV NLPs. Another interesting observation is that the MuV NLPs associated to form a helix-like structure after being subjected to pH 4.0 and then reneutralized. It seems that the rings tend to associate with each other through top-and-bottom interactions similar to what may be present in the helical structure of the paramyxovirus NC. The low pH may introduce some flexibility in the rings to allow them switch to a washer-like configuration that allows the NLP to stack on top of each other. Furthermore, unlike some other NSVs, the paramyxovirus NC can form a helical structure without the association with the matrix protein. Bends or turns can occur along the length of the paramyxovirus NC, but the overall helical structure is maintained.

This suggests that the N subunits may interact with each other through side-by-side interactions and top-and-bottom interactions in order to maintain the helical symmetry.

In addition, the MuV N ring contained RNA of different sizes, which is not clearly seen in other NSV, such as VSV (123). This suggests that the RNA in the MuV NLP is less protected. To test the effects of pH, salt, and temperature on susceptibility of N bound RNA to contaminant nucleases, the MuV NLP was exposed to a variety of different conditions. Under several conditions, the RNA contained in the MuV NLP is susceptible to digestion. This observation suggests that the association between N subunits in the MuV NLP may be weaker than those of other NSVs. Additionally, the RNA binding cavity may not provide complete protection for the RNA. The vRdRp must read the template while it is still in association with the N protein. It may seem that the RNA would be associated with the N protein more tightly if the two components are to be recognized by the vRdRp as a single unit. All the data presented here, however, indicated that the N subunits in the MuV NLP are flexible and do not encapsidate the RNA as tightly.

MUV PHOSPHOPROTEIN CHARACTERIZATION

MuV P has a modular structure comprised of several distinct functional domains. Here, I presented an experimental approach to more accurately map the functional domains of MuV P. Consistent with observations of other NSV Ps, the N-terminal region of MuV P appeared to be less stable than the region that follows (63, 124-126). However, this does not mean that the N-terminal region of MuV P does not possess any secondary or tertiary structure. A previous study determined the structure of a C-terminal portion (P343-391) of

MuV P (81). P343-391 was proposed to be MuV P_{NBD} by analogy to other NSV P proteins (81). However, P343-391 is thought to exist as a molten globule and could possibly be part of a larger C-terminal domain (81). Additionally, P proteins of other NSVs were reported to contain flexible regions between $P_{N^{\circ}D}$, P_{OD}, and P_{NBD} (61, 62, 66, 71, 74, 75, 124, 127, 128). Conversely, data did point to a possible flexible linker between P_{OD} and the P343-391 from residue 277 to 286.

MuV P is capable of binding both full length MuV NLP and truncated NLP_{379}. These observations confirm that a P binding site in the MuV NC does not require the C-terminal region of N (named as N-tail) (83). It is possible that NC binding by MuV P involves multiple regions in both N and P. His-tagged fragments of MuV P were tested for binding purified MuV NLP (51). As predicted, both full-length MuV P and P343-391 were shown to bind the NLP. Surprisingly, the N-terminal region of MuV P (P1-194) was also capable of binding the NLP. This suggests that NC binding may utilize both the N-terminal and the C-terminal regions of MuV P. This mode of NC binding is different from all other known NSV Ps. The NLP binding by the N-terminal and C-terminal regions of MuV P was confirmed and quantified by surface plasmon resonance (SPR) experiments. SPR analysis showed that the C-terminal region of P has a higher affinity for full length NLP. When the N-tail of MuV N was removed by trypsin digestion (NLP_{379}), the C-terminal region of P bound NLP_{379} with a lower affinity. The affinity of the C-terminal region of P for NLP_{379} is similar to the affinity of the N-terminal region of P binding to the full length NLP. The C-terminal region of MuV P most likely interacts with both the N-tail and additional regions of N. In contrast, there is a significant increase in binding NLP_{379} by the N-terminal region of P over full length NLP. The P1-194 NLP binding site may be more accessible after the N-tail is removed.

Interestingly, the overall affinity of the full length P for NLP is lower than that of the individual domains. The affinity values for the full length P tetramer may be underestimated since the NLP is representative of a single turn of the authentic NC, and thus, does not have the same binding sites available in comparison to the helical NC. In addition, the full length P was not very stable in solution.

Crystallization studies clearly defined that MuV P_{OD} comprises residues 213-277. The structure of MuV P_{OD} reveals a tetramer composed of one pair of long parallel α-helices and a second pair of parallel helices in the opposite orientation. The tetrameric state of P was confirmed by analytical ultracentrifugation and protein crosslinking. The MuV P_{OD} tetramer is held together by a large hydrophobic contact area between each monomer and two zippers of electrostatic interactions. This novel orientation of the MuV P tetramer positions the N-terminal and the C-terminal regions at both ends of MuV P_{OD}. The unique organization of the MuV P tetramer has not been previously reported for any other protein. Interactions between the parallel helices are different from those between the antiparallel helices. In all parallel or all antiparallel coiled coils, interactions between any neighboring pair of helices are identical.

Analysis of NSV P_{OD} structures revealed three distinct modes of P oligomerization. In the MeV P and SeV P, tetramerization results in a coiled-coil structure of four parallel helices (71, 129). On the other hand, the subunits in the VSV P dimer are parallel to each other, but a β–sheet on each side of the VSV P dimer is formed by domain swapping (69). The parallel orientation of the oligomers places the N-terminal and the C-terminal regions on opposing ends. For these NSVs, specific NC binding requires only the C-terminal region of P, so the N-terminal region of P can be positioned away from the C-terminal region. In the RABV P

dimer the N-terminal and C-terminal regions are each located at the same end (70). However, unlike MuV, there is no indication that the N-terminal region of RABV P is involved in binding NC. MuV P possesses a unique third mode of oligomerization. The MuV P subunits form a tetramer composed of parallel and antiparallel helices. The antiparallel orientation of the MuV P subunits places two N-terminal regions and two C-terminal regions on both ends of the tetramer. This organization is well suited since both the N-terminal and C-terminal regions of MuV P are involved in binding the nucleocapsid. The precise locations of both MuV P binding sites on the NC is still unclear. Our results suggest that there are P binding sites within residues 1-379 in addition to the N-tail.

AUTHENTIC MUV NUCLEOCAPSID

Currently, the only available structures of paramyxovirus NCs are low-resolution 3D reconstructions. However, atomic structures of several NSV NLPs have been solved using x-ray crystallography. These include VSV N, RABV N, and RSV N (49, 50, 130). The N monomer is composed of two core domains, NTD and CTD. The encapsidated RNA runs along a cavity formed at the NTD/CTD interface. Both NTD and CTD make lateral interactions with adjacent N subunits. Additionally, each NTD/CTD core has N- and/or C-terminal extensions, termed N-arm and C-loop (or C-arm), respectively, that stabilize NC. Strong lateral interactions between the N subunits maintain the linear integrity of NC. The extent of these interactions varies among NSVs (49). The encapsidated RNA also seems to play a role in the stability of the MuV NC, since empty MuV NC appeared considerably more flexible than NC with RNA (Figure 2d). Based on previous observations, bases in the

sequestered viral RNA could stack inside the cavity of the NTD and CTD core (130-132). It is likely that such base stacking exists in the MuV NC, which could stabilize the structure of the NC.

Similar to the NCs of other paramyxoviruses, the MuV NC exists as a left handed helical structure (54, 133, 134). The MuV NC displayed some flexibility, possibly due to a lack of significant top-bottom interactions between successive helical turns. Pitch measurements for the MuV NC varied from 55 Å to 73 Å. Similar variability in pitch was also observed for RSV, MeV and SeV NC (54, 130, 133-135). The MuV NC appears to have a larger diameter than the NC of RSV, MeV, and SeV.

Images of MuV NC incubated with P_{CTD} provided insightful details into the structural changes that accompany P_{CTD} binding to NC. With the association of P_{CTD}, the range and variability of pitch measurements increased. NC- P_{CTD} helices were significantly wider than NC alone, but NC still maintains an overall helical appearance. The C-terminus of RSV P was shown to bind the C-arm of N (136, 137). In NLP structures, the C-arm is located in what would be the space between consecutive turns of the helical NC. The interaction between P_{CTD} and NC may allow vRdRp to distort the helical conformation of the NC during RNA synthesis.

The most revealing result of this study is the observation that MuV P_{NTD} appeared to induce the helical NC to uncoil. NC uncoiling may completely expose the access to the sequestered genomic RNA. Prior to being incorporated into the NC, N exists as a monomeric protein (N^0). For VSV and RABV, N^0 is kept monomeric and RNA-free by P, forming a stable complex composed of a single N subunit and a dimer of P (52, 138). The N-terminus

of VSV P interacts with the back of the C-lobe of N and the RNA cavity (63, 124, 125). Likewise, the N-terminus of RSV P is also required for N^0-P binding (139). P binding can block the lateral contacts between N subunits to prevent NC oligomerization. Once encapsidation occurs the N^0 oligomerizes and P is free to chaperone another N^0.

In this study, I have clearly shown that significant structural changes of MuV NC occur upon P binding. These changes in NC could lead to exposure of the sequestered RNA to facilitate viral RNA synthesis. P_{NTD} and P_{CTD} as part of vRdRp appear to play an important role in altering the helical structure of the NC.

SUMMARY

How the polymerase complex assembles and gains access to the encapsidated RNA is still unresolved. The genomic RNA must be released from NC in order to be read by vRdRp. However, during viral RNA synthesis, NC does not completely disassemble to free the genomic RNA. The vRdRp must induce a conformational change in the N subunits in order to access the encapsidated RNA. Interestingly, the promoters for replication are positioned above and below each other on consecutive turns of the MuV NC, forming a "polymerase landing pad". Therefore, the helical structure of the NC may have functional implications not only in virion assembly, but also in replication (53, 54). Since the conserved sequences for initiation of replication are located in two successive turns of the NC (122) it is possible that P plays a role in recognition of the two sites by the viral RdRp. This mode of binding requires that P bind at least two or more N subunits in successive turns in the helical NC. P_{NTD} and P_{CTD} as part of vRdRp appear to play an important role in altering NC. Since both P_{NTD} and P_{CTD} are located at each end of the P tetramer, I hypothesize that the two NC binding domains of MuV P act in concert to induce changes in NC for viral RNA synthesis by vRdRp. The primary role of P_{CTD} is to allow vRdRp to specifically recognize NC, similar as P_{CTD} in other P proteins. Meanwhile, P_{NTD} primarily uncoils the MuV NC to expose the "gate" to the sequestered genomic RNA. The two functions position the vRdRp ideally at the site in NC for viral RNA synthesis. To uncoil NC, P_{NTD} binding may alter the curvature of N-N interactions within the NC so the helical symmetry is disrupted. Most likely, vRdRp

only exposes the sequestered RNA in a localized region of the NC. After vRdRp passes, the RNA template returns to its position between the NTD and CTD cores, and the helical symmetry of NC is reestablished. These changes in NC could lead to exposure of the sequestered RNA to facilitate viral RNA synthesis.

REFERENCES

1. **Johnson CD, Goodpasture EW.** 1934. AN INVESTIGATION OF THE ETIOLOGY OF MUMPS. J Exp Med **59:**1-19.
2. **Carbone K, Wolinsky J.** 2001. Mumps Virus. Fields-Virology**:**1381 - 1400.
3. **Bennett AD, Modlin J, Orenstein WA, Brandling.** 1975. Current status of mumps in the United States. J Infect Dis **132:**106-109.
4. **Enders G.** 1996. Paramyxoviruses. *In* Baron S (ed.), Medical Microbiology. The University of Texas Medical Branch at Galveston, Galveston TX.
5. **Furesz J.** 2002. Safety of live mumps virus vaccines. J Med Virol **67:**299-300.
6. **Amexis G, Rubin S, Chizhikov V, Pelloquin F, Carbone K, Chumakov K.** 2002. Sequence diversity of Jeryl Lynn strain of mumps virus: quantitative mutant analysis for vaccine quality control. Virology **300:**171 - 179.
7. **Rubin SA, Amexis G, Pletnikov M, Li Z, Vanderzanden J, Mauldin J, Sauder C, Malik T, Chumakov K, Carbone KM.** 2003. Changes in mumps virus gene sequence associated with variability in neurovirulent phenotype. J Virol **77:**11616-11624.
8. **Sauder CJ, Vandenburgh KM, Iskow RC, Malik T, Carbone KM, Rubin SA.** 2006. Changes in mumps virus neurovirulence phenotype associated with quasispecies heterogeneity. Virology **350:**48-57.
9. **Cusi MG, Santini L, Bianchi S, Valassina M, Valensin PE.** 1998. Nucleotide sequence at position 1081 of the hemagglutinin-neuraminidasegene in wild-type strains of mumps virus is the most relevant marker of virulence. J Clin Microbiol **36:**3743-3744.
10. **Ivancic J, Gulija T, Forcic D, Baricevic M, Jug R, Mesko-Prejac M, Mazuran R.** 2005. Genetic characterization of L-Zagreb mumps vaccine strain. Virus Res **109:**95 - 105.
11. **Lamb R, Kolakofsky D.** 2001. Paramyxoviridae: The Viruses and Their Replication. Fields Virology**:**1305 - 1340.
12. **Komatsu T, Takeuchi K, Yokoo J, Tanaka Y, Gotoh B.** 2000. Sendai virus blocks alpha interferon signaling to signal transducers and activators of transcription. J Virol **74:**2477-2480.
13. **Huang C, Kiyotani K, Fujii Y, Fukuhara N, Kato A, Nagai Y, Yoshida T, Sakaguchi T.** 2000. Involvement of the zinc-binding capacity of Sendai virus V protein in viral pathogenesis. J Virol **74:**7834-7841.
14. **Paterson RG, Leser GP, Shaughnessy MA, Lamb RA.** 1995. The paramyxovirus SV5 V protein binds two atoms of zinc and is a structural component of virions. Virology **208:**121-131.

15. **Steward M, Samson AC, Errington W, Emmerson PT.** 1995. The Newcastle disease virus V protein binds zinc. Arch Virol **140:**1321-1328.
16. **Andrejeva J, Poole E, Young DF, Goodbourn S, Randall RE.** 2002. The p127 subunit (DDB1) of the UV-DNA damage repair binding protein is essential for the targeted degradation of STAT1 by the V protein of the paramyxovirus simian virus 5. J Virol **76:**11379-11386.
17. **Didcock L, Young DF, Goodbourn S, Randall RE.** 1999. Sendai virus and simian virus 5 block activation of interferon-responsive genes: importance for virus pathogenesis. J Virol **73:**3125-3133.
18. **Kubota T, Yokosawa N, Yokota S, Fujii N.** 2001. C terminal CYS-RICH region of mumps virus structural V protein correlates with block of interferon alpha and gamma signal transduction pathway through decrease of STAT 1-alpha. Biochem Biophys Res Commun **283:**255-259.
19. **Nishio M, Tsurudome M, Ito M, Kawano M, Komada H, Ito Y.** 2001. High resistance of human parainfluenza type 2 virus protein-expressing cells to the antiviral and anti-cell proliferative activities of alpha/beta interferons: cysteine-rich V-specific domain is required for high resistance to the interferons. J Virol **75:**9165-9176.
20. **Park MS, Shaw ML, Munoz-Jordan J, Cros JF, Nakaya T, Bouvier N, Palese P, Garcia-Sastre A, Basler CF.** 2003. Newcastle disease virus (NDV)-based assay demonstrates interferon-antagonist activity for the NDV V protein and the Nipah virus V, W, and C proteins. J Virol **77:**1501-1511.
21. **Ulane CM, Horvath CM.** 2002. Paramyxoviruses SV5 and HPIV2 assemble STAT protein ubiquitin ligase complexes from cellular components. Virology **304:**160-166.
22. **Ulane CM, Rodriguez JJ, Parisien JP, Horvath CM.** 2003. STAT3 ubiquitylation and degradation by mumps virus suppress cytokine and oncogene signaling. J Virol **77:**6385-6393.
23. **Young DF, Didcock L, Goodbourn S, Randall RE.** 2000. Paramyxoviridae use distinct virus-specific mechanisms to circumvent the interferon response. Virology **269:**383-390.
24. **Schmitt AP, He B, Lamb RA.** 1999. Involvement of the cytoplasmic domain of the hemagglutinin-neuraminidase protein in assembly of the paramyxovirus simian virus 5. J Virol **73:**8703-8712.
25. **Schmitt AP, Leser GP, Waning DL, Lamb RA.** 2002. Requirements for budding of paramyxovirus simian virus 5 virus-like particles. J Virol **76:**3952-3964.
26. **Waning DL, Schmitt AP, Leser GP, Lamb RA.** 2002. Roles for the cytoplasmic tails of the fusion and hemagglutinin-neuraminidase proteins in budding of the paramyxovirus simian virus 5. J Virol **76:**9284-9297.
27. **Pantua HD, McGinnes LW, Peeples ME, Morrison TG.** 2006. Requirements for the assembly and release of Newcastle disease virus-like particles. J Virol **80:**11062-11073.
28. **Harrison MS, Sakaguchi T, Schmitt AP.** 2010. Paramyxovirus assembly and budding: building particles that transmit infections. Int J Biochem Cell Biol **42:**1416-1429.

29. **Ghildyal R, Mills J, Murray M, Vardaxis N, Meanger J.** 2002. Respiratory syncytial virus matrix protein associates with nucleocapsids in infected cells. J Gen Virol **83:**753-757.
30. **Schmitt PT, Ray G, Schmitt AP.** 2010. The C-terminal end of parainfluenza virus 5 NP protein is important for virus-like particle production and M-NP protein interaction. J Virol **84:**12810-12823.
31. **Liljeroos L, Huiskonen JT, Ora A, Susi P, Butcher SJ.** 2011. Electron cryotomography of measles virus reveals how matrix protein coats the ribonucleocapsid within intact virions. Proc Natl Acad Sci U S A **108:**18085-18090.
32. **Deng R, Wang Z, Mirza AM, Iorio RM.** 1995. Localization of a domain on the paramyxovirus attachment protein required for the promotion of cellular fusion by its homologous fusion protein spike. Virology **209:**457-469.
33. **Moscona A.** 1991. Defective interfering particles of human parainfluenza virus type 3 are associated with persistent infection in cell culture. Virology **183:**821-824.
34. **Moscona A, Peluso RW.** 1993. Relative affinity of the human parainfluenza virus type 3 hemagglutinin-neuraminidase for sialic acid correlates with virus-induced fusion activity. J Virol **67:**6463-6468.
35. **Bagai S, Lamb RA.** 1995. Quantitative measurement of paramyxovirus fusion: differences in requirements of glycoproteins between simian virus 5 and human parainfluenza virus 3 or Newcastle disease virus. J Virol **69:**6712-6719.
36. **Chang A, Dutch RE.** 2012. Paramyxovirus fusion and entry: multiple paths to a common end. Viruses **4:**613-636.
37. **Horvath CM, Lamb RA.** 1992. Studies on the fusion peptide of a paramyxovirus fusion glycoprotein: roles of conserved residues in cell fusion. J Virol **66:**2443-2455.
38. **Lamb RA.** 1993. Paramyxovirus fusion: a hypothesis for changes. Virology **197:**1-11.
39. **He B, Leser GP, Paterson RG, Lamb RA.** 1998. The paramyxovirus SV5 small hydrophobic (SH) protein is not essential for virus growth in tissue culture cells. Virology **250:**30-40.
40. **He B, Lin GY, Durbin JE, Durbin RK, Lamb RA.** 2001. The SH integral membrane protein of the paramyxovirus simian virus 5 is required to block apoptosis in MDBK cells. J Virol **75:**4068-4079.
41. **Hiebert SW, Lamb RA.** 1988. Cell surface expression of glycosylated, nonglycosylated, and truncated forms of a cytoplasmic protein pyruvate kinase. J Cell Biol **107:**865-876.
42. **Lin Y, Bright AC, Rothermel TA, He B.** 2003. Induction of apoptosis by paramyxovirus simian virus 5 lacking a small hydrophobic gene. J Virol **77:**3371-3383.
43. **Takeuchi K, Tanabayashi K, Hishiyama M, Yamada A, Sugiura A.** 1991. Variations of nucleotide sequences and transcription of the SH gene among mumps virus strains. Virology **181:**364-366.
44. **Takeuchi K, Tanabayashi K, Hishiyama M, Yamada A.** 1996. The mumps virus SH protein is a membrane protein and not essential for virus growth. Virology **225:**156-162.
45. **Moscona A.** 2005. Entry of parainfluenza virus into cells as a target for interrupting childhood respiratory disease. J Clin Invest **115:**1688-1698.

46. **Lamb RA, Paterson RG, Jardetzky TS.** 2006. Paramyxovirus membrane fusion: lessons from the F and HN atomic structures. Virology **344:**30-37.
47. **Lee B, Ataman ZA.** 2011. Modes of paramyxovirus fusion: a Henipavirus perspective. Trends Microbiol **19:**389-399.
48. **Smith EC, Popa A, Chang A, Masante C, Dutch RE.** 2009. Viral entry mechanisms: the increasing diversity of paramyxovirus entry. FEBS J **276:**7217-7227.
49. **Green TJ, Zhang X, Wertz GW, Luo M.** 2006. Structure of the vesicular stomatitis virus nucleoprotein-RNA complex. Science **313:**357-360.
50. **Albertini AA, Wernimont AK, Muziol T, Ravelli RB, Clapier CR, Schoehn G, Weissenhorn W, Ruigrok RW.** 2006. Crystal structure of the rabies virus nucleoprotein-RNA complex. Science **313:**360-363.
51. **Cox R, Green TJ, Qiu S, Kang J, Tsao J, Prevelige PE, He B, Luo M.** 2009. Characterization of a mumps virus nucleocapsidlike particle. J Virol **83:**11402-11406.
52. **Zhang X, Green TJ, Tsao J, Qiu S, Luo M.** 2008. Role of intermolecular interactions of vesicular stomatitis virus nucleoprotein in RNA encapsidation. J Virol **82:**674-682.
53. **Bourhis JM, Canard B, Longhi S.** 2006. Structural disorder within the replicative complex of measles virus: functional implications. Virology **344:**94-110.
54. **Bhella D, Ralph A, Yeo RP.** 2004. Conformational flexibility in recombinant measles virus nucleocapsids visualised by cryo-negative stain electron microscopy and real-space helical reconstruction. J Mol Biol **340:**319-331.
55. **Kingston RL, Hamel DJ, Gay LS, Dahlquist FW, Matthews BW.** 2004. Structural basis for the attachment of a paramyxoviral polymerase to its template. Proc Natl Acad Sci U S A **101:**8301-8306.
56. **Emerson SU, Schubert M.** 1987. Location of the binding domains for the RNA polymerase L and the ribonucleocapsid template within different halves of the NS phosphoprotein of vesicular stomatitis virus. Proc Natl Acad Sci U S A **84:**5655-5659.
57. **Chenik M, Schnell M, Conzelmann KK, Blondel D.** 1998. Mapping the interacting domains between the rabies virus polymerase and phosphoprotein. J Virol **72:**1925-1930.
58. **Mavrakis M, Mehouas S, Real E, Iseni F, Blondel D, Tordo N, Ruigrok RW.** 2006. Rabies virus chaperone: identification of the phosphoprotein peptide that keeps nucleoprotein soluble and free from non-specific RNA. Virology **349:**422-429.
59. **Chenik M, Chebli K, Gaudin Y, Blondel D.** 1994. In vivo interaction of rabies virus phosphoprotein (P) and nucleoprotein (N): existence of two N-binding sites on P protein. J Gen Virol **75 (Pt 11):**2889-2896.
60. **Masters PS, Banerjee AK.** 1988. Complex formation with vesicular stomatitis virus phosphoprotein NS prevents binding of nucleocapsid protein N to nonspecific RNA. J Virol **62:**2658-2664.
61. **Takacs AM, Das T, Banerjee AK.** 1993. Mapping of interacting domains between the nucleocapsid protein and the phosphoprotein of vesicular stomatitis virus by using a two-hybrid system. Proc Natl Acad Sci U S A **90:**10375-10379.

62. **Tarbouriech N, Curran J, Ebel C, Ruigrok RW, Burmeister WP.** 2000. On the domain structure and the polymerization state of the sendai virus P protein. Virology **266:**99-109.
63. **Chen M, Ogino T, Banerjee AK.** 2007. Interaction of vesicular stomatitis virus P and N proteins: identification of two overlapping domains at the N terminus of P that are involved in N0-P complex formation and encapsidation of viral genome RNA. J Virol **81:**13478-13485.
64. **Karlin D, Ferron F, Canard B, Longhi S.** 2003. Structural disorder and modular organization in Paramyxovirinae N and P. J Gen Virol **84:**3239-3252.
65. **Blanchard L, Tarbouriech N, Blackledge M, Timmins P, Burmeister WP, Ruigrok RW, Marion D.** 2004. Structure and dynamics of the nucleocapsid-binding domain of the Sendai virus phosphoprotein in solution. Virology **319:**201-211.
66. **Llorente MT, Garcia-Barreno B, Calero M, Camafeita E, Lopez JA, Longhi S, Ferron F, Varela PF, Melero JA.** 2006. Structural analysis of the human respiratory syncytial virus phosphoprotein: characterization of an alpha-helical domain involved in oligomerization. J Gen Virol **87:**159-169.
67. **De BP, Banerjee AK.** 1985. Requirements and functions of vesicular stomatitis virus L and NS proteins in the transcription process in vitro. Biochem Biophys Res Commun **126:**40-49.
68. **Ding H, Green TJ, Luo M.** 2004. Crystallization and preliminary X-ray analysis of a proteinase-K-resistant domain within the phosphoprotein of vesicular stomatitis virus (Indiana). Acta Crystallogr D Biol Crystallogr **60:**2087-2090.
69. **Ding H, Green TJ, Lu S, Luo M.** 2006. Crystal structure of the oligomerization domain of the phosphoprotein of vesicular stomatitis virus. J Virol **80:**2808-2814.
70. **Ivanov I, Crepin T, Jamin M, Ruigrok RW.** 2010. Structure of the dimerization domain of the rabies virus phosphoprotein. J Virol **84:**3707-3710.
71. **Tarbouriech N, Curran J, Ruigrok RW, Burmeister WP.** 2000. Tetrameric coiled coil domain of Sendai virus phosphoprotein. Nat Struct Biol **7:**777-781.
72. **Mavrakis M, McCarthy AA, Roche S, Blondel D, Ruigrok RW.** 2004. Structure and function of the C-terminal domain of the polymerase cofactor of rabies virus. J Mol Biol **343:**819-831.
73. **Curran J, Boeck R, Lin-Marq N, Lupas A, Kolakofsky D.** 1995. Paramyxovirus phosphoproteins form homotrimers as determined by an epitope dilution assay, via predicted coiled coils. Virology **214:**139 - 149.
74. **Gerard FC, Ribeiro Ede A, Jr., Leyrat C, Ivanov I, Blondel D, Longhi S, Ruigrok RW, Jamin M.** 2009. Modular organization of rabies virus phosphoprotein. J Mol Biol **388:**978-996.
75. **Gerard FC, Ribeiro Ede A, Jr., Albertini AA, Gutsche I, Zaccai G, Ruigrok RW, Jamin M.** 2007. Unphosphorylated rhabdoviridae phosphoproteins form elongated dimers in solution. Biochemistry **46:**10328-10338.
76. **Gigant B, Iseni F, Gaudin Y, Knossow M, Blondel D.** 2000. Neither phosphorylation nor the amino-terminal part of rabies virus phosphoprotein is required for its oligomerization. J Gen Virol **81:**1757-1761.
77. **Jacob Y, Real E, Tordo N.** 2001. Functional interaction map of lyssavirus phosphoprotein: identification of the minimal transcription domains. J Virol **75:**9613-9622.

78. **Johansson K, Bourhis JM, Campanacci V, Cambillau C, Canard B, Longhi S.** 2003. Crystal structure of the measles virus phosphoprotein domain responsible for the induced folding of the C-terminal domain of the nucleoprotein. J Biol Chem **278:**44567-44573.
79. **Kolakofsky D, Le Mercier P, Iseni F, Garcin D.** 2004. Viral DNA polymerase scanning and the gymnastics of Sendai virus RNA synthesis. Virology **318:**463-473.
80. **Ribeiro EA, Jr., Favier A, Gerard FC, Leyrat C, Brutscher B, Blondel D, Ruigrok RW, Blackledge M, Jamin M.** 2008. Solution structure of the C-terminal nucleoprotein-RNA binding domain of the vesicular stomatitis virus phosphoprotein. J Mol Biol **382:**525-538.
81. **Kingston RL, Gay LS, Baase WS, Matthews BW.** 2008. Structure of the nucleocapsid-binding domain from the mumps virus polymerase; an example of protein folding induced by crystallization. J Mol Biol **379:**719-731.
82. **Green TJ, Luo M.** 2009. Structure of the vesicular stomatitis virus nucleocapsid in complex with the nucleocapsid-binding domain of the small polymerase cofactor, P. Proc Natl Acad Sci U S A **106:**11713-11718.
83. **Kingston RL, Baase WA, Gay LS.** 2004. Characterization of nucleocapsid binding by the measles virus and mumps virus phosphoproteins. J Virol **78:**8630-8640.
84. **Fuentes SM, Sun D, Schmitt AP, He B.** 2010. Phosphorylation of paramyxovirus phosphoprotein and its role in viral gene expression. Future Microbiol **5:**9-13.
85. **Takacs AM, Barik S, Das T, Banerjee AK.** 1992. Phosphorylation of specific serine residues within the acidic domain of the phosphoprotein of vesicular stomatitis virus regulates transcription in vitro. J Virol **66:**5842-5848.
86. **Gao Y, Lenard J.** 1995. Multimerization and transcriptional activation of the phosphoprotein (P) of vesicular stomatitis virus by casein kinase-II. EMBO J **14:**1240-1247.
87. **Lenard J.** 1999. Host cell protein kinases in nonsegmented negative-strand virus (mononegavirales) infection. Pharmacol Ther **83:**39-48.
88. **Chattopadhyay D, Raha T.** 1997. Single serine phosphorylation within the acidic domain of Chandipura virus P protein regulates the transcription in vitro. Virology **239:**11-19.
89. **Raha T, Samal E, Majumdar A, Basak S, Chattopadhyay D, Chattopadhyay DJ.** 2000. N-terminal region of P protein of Chandipura virus is responsible for phosphorylation-mediated homodimerization. Protein Eng **13:**437-444.
90. **Gupta AK, Blondel D, Choudhary S, Banerjee AK.** 2000. The phosphoprotein of rabies virus is phosphorylated by a unique cellular protein kinase and specific isomers of protein kinase C. J Virol **74:**91-98.
91. **Byrappa S, Gupta KC.** 1999. Human parainfluenza virus type 1 phosphoprotein is constitutively phosphorylated at Ser-120 and Ser-184. J Gen Virol **80 (Pt 5):**1199-1209.
92. **Huntley CC, De BP, Banerjee AK.** 1997. Phosphorylation of Sendai virus phosphoprotein by cellular protein kinase C zeta. J Biol Chem **272:**16578-16584.
93. **Chen JL, Das T, Banerjee AK.** 1997. Phosphorylated states of vesicular stomatitis virus P protein in vitro and in vivo. Virology **228:**200-212.

94. **Hamaguchi M, Yoshida T, Nishikawa K, Naruse H, Nagai Y.** 1983. Transcriptive complex of Newcastle disease virus. I. Both L and P proteins are required to constitute an active complex. Virology **128:**105-117.
95. **Emerson SU, Yu Y.** 1975. Both NS and L proteins are required for in vitro RNA synthesis by vesicular stomatitis virus. J Virol **15:**1348-1356.
96. **Gupta AK, Mathur M, Banerjee AK.** 2002. Unique capping activity of the recombinant RNA polymerase (L) of vesicular stomatitis virus: association of cellular capping enzyme with the L protein. Biochem Biophys Res Commun **293:**264-268.
97. **Rhodes DP, Moyer SA, Banerjee AK.** 1974. In vitro synthesis of methylated messenger RNA by the virion-associated RNA polymerase of vesicular stomatitis virus. Cell **3:**327-333.
98. **Testa D, Banerjee AK.** 1977. Two methyltransferase activities in the purified virions of vesicular stomatitis virus. J Virol **24:**786-793.
99. **Ogino T, Kobayashi M, Iwama M, Mizumoto K.** 2005. Sendai virus RNA-dependent RNA polymerase L protein catalyzes cap methylation of virus-specific mRNA. J Biol Chem **280:**4429-4435.
100. **Poch O, Blumberg BM, Bougueleret L, Tordo N.** 1990. Sequence comparison of five polymerases (L proteins) of unsegmented negative-strand RNA viruses: theoretical assignment of functional domains. J Gen Virol **71 (Pt 5):**1153-1162.
101. **Poch O, Tordo N, Keith G.** 1988. Sequence of the 3386 3' nucleotides of the genome of the AVO1 strain rabies virus: structural similarities in the protein regions involved in transcription. Biochimie **70:**1019-1029.
102. **Svenda M, Berg M, Moreno-Lopez J, Linne T.** 1997. Analysis of the large (L) protein gene of the porcine rubulavirus LPMV: identification of possible functional domains. Virus Res **48:**57-70.
103. **Wertz GW, Whelan S, LeGrone A, Ball LA.** 1994. Extent of terminal complementarity modulates the balance between transcription and replication of vesicular stomatitis virus RNA. Proc Natl Acad Sci U S A **91:**8587-8591.
104. **Whelan SP, Wertz GW.** 1999. The 5' terminal trailer region of vesicular stomatitis virus contains a position-dependent cis-acting signal for assembly of RNA into infectious particles. J Virol **73:**307-315.
105. **Whelan SP, Wertz GW.** 1999. Regulation of RNA synthesis by the genomic termini of vesicular stomatitis virus: identification of distinct sequences essential for transcription but not replication. J Virol **73:**297-306.
106. **Abraham G, Rhodes DP, Banerjee AK.** 1975. Novel initiation of RNA synthesis in vitro by vesicular stomatitis virus. Nature **255:**37-40.
107. **Moyer SA, Banerjee AK.** 1975. Messenger RNA species synthesized in vitro by the virion-associated RNA polymerase of vesicular stomatitis virus. Cell **4:**37-43.
108. **Abraham G, Rhodes DP, Banerjee AK.** 1975. The 5' terminal structure of the methylated mRNA synthesized in vitro by vesicular stomatitis virus. Cell **5:**51-58.
109. **Wang JT, McElvain LE, Whelan SP.** 2007. Vesicular stomatitis virus mRNA capping machinery requires specific cis-acting signals in the RNA. J Virol **81:**11499-11506.
110. **Ogino T, Banerjee AK.** 2007. Unconventional mechanism of mRNA capping by the RNA-dependent RNA polymerase of vesicular stomatitis virus. Mol Cell **25:**85-97.

111. **Barr JN, Whelan SP, Wertz GW.** 1997. cis-Acting signals involved in termination of vesicular stomatitis virus mRNA synthesis include the conserved AUAC and the U7 signal for polyadenylation. J Virol **71:**8718-8725.
112. **Barr JN, Wertz GW.** 2001. Polymerase slippage at vesicular stomatitis virus gene junctions to generate poly(A) is regulated by the upstream 3'-AUAC-5' tetranucleotide: implications for the mechanism of transcription termination. J Virol **75:**6901-6913.
113. **Hwang LN, Englund N, Pattnaik AK.** 1998. Polyadenylation of vesicular stomatitis virus mRNA dictates efficient transcription termination at the intercistronic gene junctions. J Virol **72:**1805-1813.
114. **Stillman EA, Whitt MA.** 1997. Mutational analyses of the intergenic dinucleotide and the transcriptional start sequence of vesicular stomatitis virus (VSV) define sequences required for efficient termination and initiation of VSV transcripts. J Virol **71:**2127-2137.
115. **Iverson LE, Rose JK.** 1981. Localized attenuation and discontinuous synthesis during vesicular stomatitis virus transcription. Cell **23:**477-484.
116. **Abraham G, Banerjee AK.** 1976. The nature of the RNA products synthesized in vitro by subviral components of visicular stomatitis virus. Virology **71:**230-241.
117. **Ball LA, White CN.** 1976. Order of transcription of genes of vesicular stomatitis virus. Proc Natl Acad Sci U S A **73:**442-446.
118. **Emerson SU.** 1982. Reconstitution studies detect a single polymerase entry site on the vesicular stomatitis virus genome. Cell **31:**635-642.
119. **Iverson LE, Rose JK.** 1982. Sequential synthesis of 5'-proximal vesicular stomatitis virus mRNA sequences. J Virol **44:**356-365.
120. **Emerson SU, Wagner RR.** 1972. Dissociation and reconstitution of the transcriptase and template activities of vesicular stomatitis B and T virions. J Virol **10:**297-309.
121. **Davis NL, Wertz GW.** 1982. Synthesis of vesicular stomatitis virus negative-strand RNA in vitro: dependence on viral protein synthesis. J Virol **41:**821-832.
122. **Kolakofsky D, Roux L, Garcin D, Ruigrok RW.** 2005. Paramyxovirus mRNA editing, the "rule of six" and error catastrophe: a hypothesis. J Gen Virol **86:**1869-1877.
123. **Green TJ, Macpherson S, Qiu S, Lebowitz J, Wertz GW, Luo M.** 2000. Study of the assembly of vesicular stomatitis virus N protein: role of the P protein. J Virol **74:**9515-9524.
124. **Karlin D, Longhi S, Receveur V, Canard B.** 2002. The N-terminal domain of the phosphoprotein of Morbilliviruses belongs to the natively unfolded class of proteins. Virology **296:**251-262.
125. **Leyrat C, Jensen MR, Ribeiro EA, Jr., Gerard FC, Ruigrok RW, Blackledge M, Jamin M.** 2011. The N(0)-binding region of the vesicular stomatitis virus phosphoprotein is globally disordered but contains transient alpha-helices. Protein Sci **20:**542-556.
126. **Longhi S, Receveur-Brechot V, Karlin D, Johansson K, Darbon H, Bhella D, Yeo R, Finet S, Canard B.** 2003. The C-terminal domain of the measles virus nucleoprotein is intrinsically disordered and folds upon binding to the C-terminal moiety of the phosphoprotein. J Biol Chem **278:**18638-18648.

127. **Choudhary SK, Malur AG, Huo Y, De BP, Banerjee AK.** 2002. Characterization of the oligomerization domain of the phosphoprotein of human parainfluenza virus type 3. Virology **302:**373-382.
128. **Rahaman A, Srinivasan N, Shamala N, Shaila MS.** 2004. Phosphoprotein of the rinderpest virus forms a tetramer through a coiled coil region important for biological function. A structural insight. J Biol Chem **279:**23606-23614.
129. **Communie G, Crepin T, Maurin D, Jensen MR, Blackledge M, Ruigrok RW.** 2013. Structure of the tetramerization domain of measles virus phosphoprotein. J Virol **87:**7166-7169.
130. **Tawar RG, Duquerroy S, Vonrhein C, Varela PF, Damier-Piolle L, Castagne N, MacLellan K, Bedouelle H, Bricogne G, Bhella D, Eleouet JF, Rey FA.** 2009. Crystal structure of a nucleocapsid-like nucleoprotein-RNA complex of respiratory syncytial virus. Science **326:**1279-1283.
131. **Green TJ, Rowse M, Tsao J, Kang J, Ge P, Zhou ZH, Luo M.** 2011. Access to RNA encapsidated in the nucleocapsid of vesicular stomatitis virus. J Virol **85:**2714-2722.
132. **Raymond DD, Piper ME, Gerrard SR, Skiniotis G, Smith JL.** 2012. Phleboviruses encapsidate their genomes by sequestering RNA bases. Proc Natl Acad Sci U S A **109:**19208-19213.
133. **Egelman EH, Wu SS, Amrein M, Portner A, Murti G.** 1989. The Sendai virus nucleocapsid exists in at least four different helical states. J Virol **63:**2233-2243.
134. **Schoehn G, Mavrakis M, Albertini A, Wade R, Hoenger A, Ruigrok RW.** 2004. The 12 A structure of trypsin-treated measles virus N-RNA. J Mol Biol **339:**301-312.
135. **Bakker SE, Duquerroy S, Galloux M, Loney C, Conner E, Eleouet JF, Rey FA, Bhella D.** 2013. The respiratory syncytial virus nucleoprotein-RNA complex forms a left-handed helical nucleocapsid. J Gen Virol **94:**1734-1738.
136. **Galloux M, Tarus B, Blazevic I, Fix J, Duquerroy S, Eleouet JF.** 2012. Characterization of a viral phosphoprotein binding site on the surface of the respiratory syncytial nucleoprotein. J Virol **86:**8375-8387.
137. **Murray J, Loney C, Murphy LB, Graham S, Yeo RP.** 2001. Characterization of monoclonal antibodies raised against recombinant respiratory syncytial virus nucleocapsid (N) protein: identification of a region in the carboxy terminus of N involved in the interaction with P protein. Virology **289:**252-261.
138. **Mavrakis M, Iseni F, Mazza C, Schoehn G, Ebel C, Gentzel M, Franz T, Ruigrok RW.** 2003. Isolation and characterisation of the rabies virus N degrees-P complex produced in insect cells. Virology **305:**406-414.
139. **Mallipeddi SK, Lupiani B, Samal SK.** 1996. Mapping the domains on the phosphoprotein of bovine respiratory syncytial virus required for N-P interaction using a two-hybrid system. J Gen Virol **77 (Pt 5):**1019-1023.